Motion Tracking of Highly Dynamic Multi-link Systems in Unconstrained Space

---

A

Thesis

Presented to

the faculty of the School of Engineering and Applied Science

University of Virginia

---

in partial fulfillment

of the requirements for the degree

Master of Science

by

Jeronimo Cox Jr

August 2023

APPROVAL SHEET

This

Thesis

is submitted in partial fulfillment of the requirements
for the degree of

Master of Science

Author: Jeronimo Cox Jr

This Thesis has been read and approved by the examing committee:

Advisor: Dr. Tomonari Furukawa

Advisor:

Committee Member: Dr. Richard Kent

Committee Member: Dr. Shawn Russell

Committee Member:

Committee Member:

Committee Member:

Committee Member:

Accepted for the School of Engineering and Applied Science:

Jennifer L. West, School of Engineering and Applied Science

August 2023

MOTION TRACKING OF HIGHLY DYNAMIC MULTI-LINK SYSTEMS IN UNCONSTRAINED SPACE

Jeronimo Cox Jr

Bristow, Virginia

Bachelor of Science in Mechanical Engineering, Virginia Tech, 2019

A Thesis submitted to the Graduate Faculty

of the University of Virginia in Candidacy for the Degree of

Master of Science

Department of Mechanical and Aerospace Engineering

University of Virginia

May 2022

Richard Kent, Chair

Tomonari Furukawa(Advisor)

Shawn Russell

Motion Tracking of Highly Dynamic Multi-link Systems in Unconstrained Space

Jeronimo Cox Jr

(ABSTRACT)

This thesis presents a motion tracking methodology for highly-dynamic, multi-link systems unconstrained by space due to visual obstruction or magnetic distortion. The proposed technique of dynamic measurement fusion changes the role of the accelerometer from correcting inclination with the gravity vector only in quasi-static motion, to measuring centrifugal forces of links. This allows measuring angular rate of links not only with gyroscopes embedded to Inertial Measurement Unit (IMU)s, but also accelerometers, making more use of the inertial sensors. Headings of links are corrected with magnetometers. As local distortion is inconsistent at every position in some space, a method is proposed to measure local hard iron distortion, allowing heading correction to be more effective in nonuniform magnetic fields. In validating the techniques using an experimentally induced two degree of freedom motion, error in estimated state has improved by half an order of magnitude. While the methods have worked to track highly dynamic humanoid motion, the proposed technique has difficulty estimating quasi-static 3D motions.

Dedication

To my family and friends, and those who never once had any doubts.

Acknowledgments

None of this would have been possible without Professor Tomonari Furukawa, thank you for giving me chances to prove myself throughout my career. You have supported me and guided me towards a career I am happier with. Thank you for allowing me to show my skills in the field that most excites me. I'll never forget the roots of working up to more complex land vehicles to make autonomous, and using my crash experience to make an impact. It has been an honor working with you throughout the years and I look forward to our future friendship.

I'd like to thank Honda for the opportunity of working towards a safer tomorrow. It has been a dream to work with the automotive industry at all, and I am glad I was able to experience such a professional environment first hand. It has further inspired me with my career and endeavors.

I'd like to also thank my lab members and friends who have guided me and have helped achieve this goal of mine. I wouldn't have been able to achieve any of this without their advice, input, and suggestions, and I am very thankful to have worked with such talented people.

Contents

List of Figures

List of Tables

Chapter 1

Introduction

1.1 Background

For years, motion tracking of multi-link systems has been a subject of interest in robotics, biomechanical analysis, education, games, films, and more. Tracking the motion of these systems is essential to controlling the motion efficiently and optimally. Whether attempting to design a constrained motion, such as the limited motion targeted by an occupant in a crash, or improving the performance of a motion, such as improving the gait and posture of someone in athletics or rehabilitation, accurately tracking these motions is crucial to best understand the measured motions.

Joint encoders are one form of embedded sensors used for excellent motion tracking for robotic manipulation [1]. Though manipulators with positional feedback using encoders currently work in industry, encoders eventually suffer from error, as actuation over time leads to warped shafts and misaligned bearings [2]. They're also generally hard to install to track the complex degrees of freedom of humanoid joints.

In the event that tracking of an advanced motion movement without joint encoders is required, an active optical system is the usual choice as it provides high reliability and accuracy. Using multiple cameras for depth measurements of observable targets has been a common practice for motion tracking, providing more information than

possible with a monocular camera. An example of a visual motion tracking system is the OptiTrack Motion Capture System, which uses cameras and reflective ball markers to estimate positions of multi-link bodies with tenths of a millimeter of error, allowing for accurate measurements for more complex motions. For this reason, the visual motion capture system is used for ground truth measurements in the performance analysis of methods proposed in this thesis. As long as multiple cameras can catch all markers of interest for the duration of the motion being measured, camera-based tracking provides accurate pose measurements; however, optical tracking suffers when targets are not observable by multiple cameras.

Between replacing encoders that break with high torque loads, and purchasing camera equipment capable of tracking at sufficiently high frame rates and accuracy, the required technologies can be costly. In some cases, many multi-link systems are neither equipped with joint encoders nor fully observable by cameras, which are the conditions of concern in this paper. One example of motion tracking in the described conditions is motion tracking of people in manufacturing plants and facilities with machinery and equipment in the way, a use case targeted by auto companies recently. Highly dynamic systems, or systems that experience high torque or changing accelerations exceeding 2 G, are the systems targeted for motion tracking of concern in this thesis. In crash test applications, the motions of some parts of the dummy are unobservable because the material of vehicles obstructs the view. Unobserved with joint encoders and cameras, these motions must be tracked with external dead-reckoning [3]. This gives rise to the need for externally mounted IMU-based motion tracking, where the IMU most typically consists of accelerometers, gyroscopes, and magnetometers. Accelerometers are instruments used to measure linear acceleration and are observant of the gravity vector, the constant force everyone and everything experiences on Earth.

Gyroscopes are instruments used to measure the rate of angular rotation. A magnetometer is an instrument used to measure the strength and direction of the magnetic field in the vicinity of the instrument as an electric compass [4]. The utilization of sensor packages also increases the range of usable sampling rates compared to that of high-quality visual motion tracking systems, allowing for more saturation of measurements for the duration of a motion. Similar to how a gyroscope might be used to measure current orientation from an initial reference direction, magnetometers can be used to measure orientation with respect to Earth's magnetic field. Commonly, the gyroscope uses measurements to estimate the accumulated change in orientation from a reference heading, but may accumulate error due to drift as a dead reckoning sensor [5].

1.2 Challenges

The intended solution for motion tracking is the use of strap-down IMUs in combination with state estimation methods that compensate for the error accumulated with the integration of noisy sensor signals known as drift [3]. Drift can be compensated for with global correction, or the usage of a measurement that does not change over different variants. Methods of global correction include positional correction with GPS [6] using the global coordinate system as reference, however, GPS devices do not work well in indoor environments and aren't meant for precision positioning. For more focused positional correction, IMU-based motion estimations have been corrected with cameras [7] commonly static to global frames for correction, however, fail in the scenario of concern in this paper. The reference direction used initially is observed throughout the duration of tracking a motion in a uniform field, making

magnetometers global correctors.

Magnetometers embedded in IMUs are used for global correction of heading direction using the reference direction of magnetic north [8]. Some methods of heading correction with magnetometers assume that the magnetic field within the space of interest is uniform, however, the direction of magnetic north changes in scenarios with sources of distortion. For example, the expected direction of magnetic north changes based on where a measurement is taken around the world due to the poles of the Earth [9]. By taking measurements with a magnetometer near sources of distortion, measurements reflect geomagnetic north, as well as the vector of the local magnetic field due to distortion. As the position of the magnetometer changes in the described spaces, the proximity to structures also changes, causing the distortion to each position to fluctuate, and altering the direction of the measured magnetic north. To prove the advantages of orientation correction with magnetic north, experimental spaces were designed with caution of the effects of iron structures and electrical equipment on the local magnetic field. Objects of those materials are removed from the proximity of the experimental space. As IMUs are crucial to measuring the reference north to correct for drift, understanding the consistency of the measured reference direction is required. Important to robotics applications is the consideration of environmental factors such as the inconsistency of the referenced vector relied upon for correction that could play a role in aiding or harming the performance of a system.

To better understand the consistency of magnetic north within spaces inside iron structures, magnetometers were used to collect data in a naval ship, and observe magnetic field consistency as seen in Fig. 1.1. While trying to keep a constant heading with the measurement device moved without orientation change in proximity to power systems, electrical components, and structures of the ship, the signals of

(a) USS Wisconsin in Norfolk, VA

(b) Data collection in boat

Figure 1.1: Lab visit to potential environment of robotics applications.

the magnetometer were inconsistent as seen in Fig. 1.2. Without considering the consistency of the magnetic north measured, the amount of distortion throughout these spaces is unique from position to position. What was also clear when recording the data is how clear distortion increases with proximity to metals and devices. If magnetometers are to be used for orientation correction in environments within ferrite structures, the distortion to the reference direction being measured must be considered and accounted for.

One method of removing the effects of distortion so that Earth's magnetic field can be better observed throughout a space is the application of magnetic shielding. Similar to the goal of a Faraday cage, shielding can be used to remove the effects of exterior electromagnetic fields. To understand the effects of different methods of shielding, experimentation was designed to see at what proximity to an inductor, in constant conditions with two inductor orientations, do magnetometers begin to observe distortion. The prototype setup used to maintain the orientation of the sensor while it is

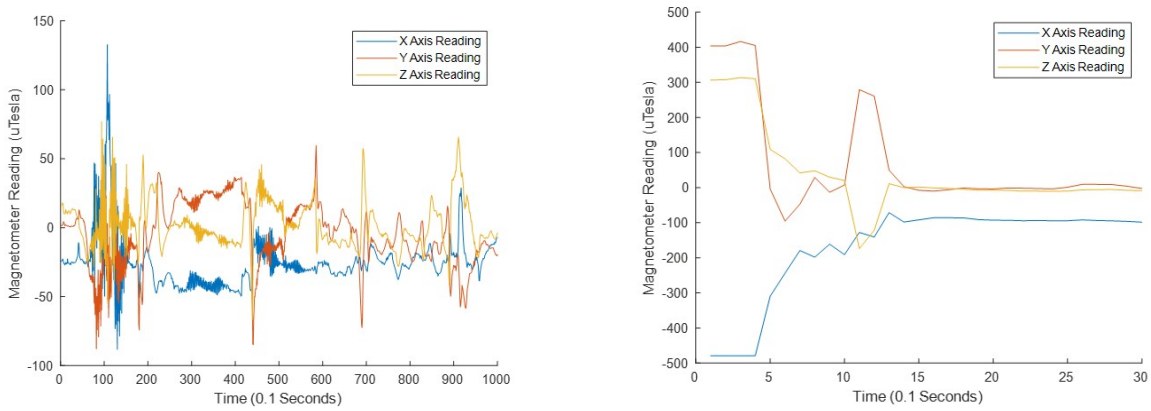

(a) Data collected while walking through electrical room with constant heading

(b) Data collected while walking by power transformer with constant heading

Figure 1.2: Plotted magnetometer measurements taken while moved by iron structures and electrical components without orientation change.

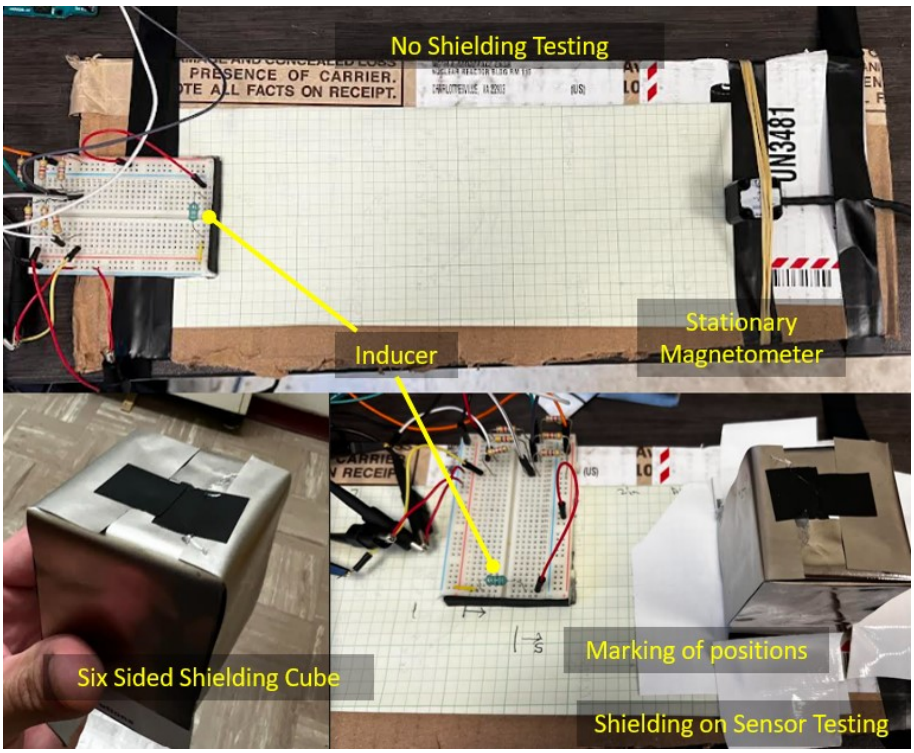

Figure 1.3: Experimentation detecting proximity to an inducer that distortion can be detected in magnetometer measurement, along with the effects of magnetic shielding MCF5.

translated can be seen in Fig. 1.3.

Two layers of MCF5 magnetic shielding covering a cube were placed over any desired location, for example, over the sensor or over the inducer. These conditions were compared to the same but without shielding, assuming the usual conditions of magnetometers in locations with materials that have distorting properties. The results, measured by the proximity of the inducer before distortion to the signal was observed, can be seen in Table 1.1. The distortion measured with no use of shielding was measured fairly close to the magnetometer. The effects of shielding were fairly similar for both placement on the inducer and sensor, however, shielding around the sensor removed the observability of Earth's magnetic field in any direction.

The non-uniformity of magnetic signals in proximity to iron structures poses the largest challenge for orientation correction with magnetometers with externally mounted IMU-based tracking. The aid from shielding is limited when encasing the sensors, as the observability of Earth's magnetic field only worsens. The non-uniformity of magnetic fields has been used for mapping and localization of magnetometers in different spaces, however, mapping of magnetic fields can be costly and inefficient. For this reason, this thesis is only targeting motion tracking in nonuniform magnetic fields

Table 1.1: Results of shielding testing to observe effects of magnetometer signal with proximity to an inducer.

Inductor Pose	Shielding Usage	Proximity Before Distortion
Parallel	No Shielding	13.2 [cm]
	Shielding on Inducer	10.3 [cm]
	Shielding on Sensor	9.9[cm]
Perpendicular	No Shielding	12.5 [cm]
	Shielding on Inducer	9.5 [cm]
	Shielding on Sensor	8.6 [cm]

without *a priori* mappings of magnetic fields.

1.3 Objectives

The goal of this research is to provide a motion-tracking solution for a highly dynamic system, that works in environments or situations with magnetic distortion, unobservable by cameras or joint encoders. The externally mountable sensor package selected to achieve the goal is an IMU. As sensor drift leads to accumulated error, the approach utilizes magnetometers as global correctors to the orientations of the links of the system, using measured magnetic north. The challenge with using magnetometers is that the ferrous materials obstructing the sight of the system may also be causing nonuniformity of the magnetic field throughout the space. As the end goal application is to be able to track a test dummy inside of a crashing vehicle, the intention is to develop a motion-tracking technique that works sufficiently even with magnetic field inconsistency.

First is the validation of the use of dynamic measurement fusion for tracking a highly dynamic motion of a complexity-reduced two-link system. Prior to using any of this technology with crash test dummies, the proposed technique must be proven to provide better estimations than conventional IMU usage. With completed validation of the use of gyroscopes and accelerometers measuring centrifugal forces to measure angular rotation, and correcting orientation with magnetometers in a space with magnetic uniformity, the method is prepared to be used for more complex motion to prove the efficacy of the method.

Work continued to understand the performance of dynamic measurement fusion in the intended environment, a space with inconsistent magnetic north. State estimation

with IMUs equipped with magnetometers has mostly been modeled for environments with homogeneous magnetic fields, spaces where calibration parameters are consistent throughout spaces. As single magnetometers have difficulty with real-time calibration for orientation estimation in distorted environments, a methodology is proposed to better understand the magnetic field conditions from position to position. In this thesis, the proposed approach is to measure distortion for real-time calibration to provide better estimates of orientation. As an extension of dynamic measurement fusion, measuring orientation with respect to local magnetic field, along with calibration, is achieved with an array of two, closely positioned, oppositely facing 3-axis magnetometers. With this approach, local hard iron distortion is compensated for by real-time measurement. Correcting orientations with dynamic measurement fusion by using the most recent prior magnetic north vector direction rather than referencing the initial direction, along with local calibration, is used for better pose estimation of a multi-link system in nonuniform magnetic fields.

Sensor mounts, including the IMU packages used to estimate the motion, as well as visual motion tracking markers for ground truth measurement, are prepared for validation of the proposed methods of tracking motion with increased complexity. The design for experimentation with coupled magnetometers is planned and conducted with more accessible sensors in less intense motion to compensate for limited sampling rates. Using arm movement as a two link system with increased degrees of freedom, use of coupled magnetometers for distortion compensation. In preparing for the use of dynamic measurement fusion to track the motion of a dummy for analysis of the proposed method, the magnetometers at the quality required for experimentation were damaged, and the team was left with an extensive lead time until they can be replaced. For this reason, validation of dynamic measurement fusion using pseudo-

magnetometer data generated with OptiTrack data targeted as the goal of proving the developed method at Honda ADC. With the validation of the proposed sensor method utilizing the complexity-reduced two-link system with scalability of degrees of freedom in an environment with magnetic nonuniformity, the intended future work of this research is to validate coupled magnetometers in the same test previously conducted with the dummies.

1.4 Contributions

This thesis presents a technique of motion tracking highly dynamic systems with externally mounted IMUs. Orientation correction is achieved in nonuniform magnetic fields with coupled magnetometers capable of reducing error by consideration of local distortion. To better compensate for distortion, hard iron distortion is measured with the positioning of two oppositely facing magnetometers. As the magnetic north vector is inconsistent in spaces of interest, a new sensor model for magnetometers is introduced using a magnetometers' most recent previous measurement as a reference direction, rather than the initially observed magnetic north. As the main concern of this paper, highly dynamic systems that experience more intense transformations of sensor frame than the transformation of magnetic north in a nonuniform field, usage of magnetometers can be useful as an additional dead-reckoning measurement correcting states in an extended Kalman filter (EKF) framework. The contributions go as follows,

- Application of dynamic measurement fusion to measure highly dynamic motion of physical systems.

- Coupled oppositely-faced magnetometers for real-time hard iron distortion measurement for motion tracking
- Dead-reckoning sensor model for magnetometer to compensate for the inconsistency of direction of referenced magnetic north within proximity to iron structures

1.5 Outline

This thesis is organized as follows. Chapter 2 reviews literature on motion tracking with externally mounted IMUs. It also reviews literature on magnetic field distortion compensation and utilizations of magnetometer arrays. Chapter 3 formulates the application of Dynamic Measurement Fusion to track a highly dynamic multi-link system. Chapter 4 explains the proposed usage of two oppositely facing magnetometers for real-time calibration in nonuniform magnetic fields. Chapter 5 presents the design for the application and validation of Dynamic Measurement Fusion to track the motion of humanoid systems. Experimental validation of the proposed approaches is conducted in Chapter 6, and the final chapter summarizes the results and conclusions.

Chapter 2

Review of Literature

2.1 Motion Tracking with IMUs

Past work on motion tracking of multi-link systems incorporating IMUs can be classified into two approaches. In the most common approach, a 6DOF IMU, an embedded combination of a three-axis gyroscope and a three-axis accelerometer, is attached to the center of each link measuring the angular velocity and the linear acceleration, respectively. While both are dead-reckoning sensors, methods have been introduced to globally correct heading using the gravity vector measured with linear accelerometers. Taetz et al. [10], Kok et al. [11], and Ahmadi et al. [12] developed computationally efficient multi-link motion capture systems with this approach and tracked the linear and angular motions correspondingly, using only accelerometers and gyroscopes. [13]

Various frameworks of attitude estimation have been developed using global correction with this arrangement. Cantelli et al [14] and Euston et al [15] used IMUs with inclination correction using the gravity vector for joint angle estimation of manipulators and attitude estimation of unmanned air vehicles, respectively. These cases for motion tracking involve sensor suites in proximity to motors and electrical components, which cause excessive distortion for heading correction with magnetometers. Wang et al [16] optimized Cantelli's approach for walking motion capture by correcting inclination only in states with zero acceleration or velocity, known as zero velocity

updates (ZUPT). While ZUPT allows for cleaner observation of the gravity vector in quasi-static motion, the method fails for highly dynamic systems. Angermann et al [17] introduced the use of SLAM with inertial sensors containing just gyroscopes and accelerometers mounted to users' feet for tracking motions of pedestrians, while also constructing maps of walking paths in indoor and outdoor environments. Garcia Puyol et al [18] introduced H-tree data structures to reduce the storage size of maps and reduce computation time as maps progress in size. Ample work has been done to track motion with 6DOF IMUs, however, this only performs well when motion is quasi-static with minimal acceleration to impede the observability of the gravity vector.

The second kind of approach uses nine degree of freedom (9DOF) IMUs, similar to a six degree of freedom (6DOF) but inclusive of the three-axis magnetometer which measures geomagnetism and provides the direction of magnetic north. As accelerometer-based gravity measurement for correction has only been accurate at quasi-static motion [19], correction of joint angle estimations using magnetometers was investigated as a viable global correction technique.

The QUEST method [8] was the pioneered usage of inclination correction with accelerometers and heading correction with magnetometers. Yun et al [20] integrated this method into motion tracking with external IMUs of humanoid poses. Mahony et all [21] and Valenti et al [22] used correction of inclination using accelerometers and heading with magnetometer measurement using stability analysis of measured vectors. Laidig et al [23] used a similar approach applying a low pass filter to measurement signals using estimation in quarternion. Local magnetic fields have an expected dip angle based on positioning on the earth's surface [9]. Inclination correction using local dip angle has been used, similar to correction with the gravity vector. Magdwick

et al [24] and Yadav et al [19] used the gravity vector as well as local magnetic dip angle for inclination correction, using gradient descent and a particle filter for optimization, respectively. Li et al [25] compared how ZUPT works with gyroscope measurement integration, an EKF framework using yaw correction with magnetometers, and a method with heuristic drift reduction to compensate for heading error in walking motions. In some sensor models for orientation estimation, reliance on the magnetometer decreases when distortion is detected. Rotenberg et al [26] used deviation in measured magnetic dip angle and magnitude to detect distortion and increase covariance in a Kalman filter framework.

While existing IMU-based techniques have been successfully applied to the motion tracking of multi-link systems, the targeted multi-link systems experience relatively low linear accelerations. These techniques estimate attitude using magnetic fields and gravity, while accelerometer-based gravity measurement is accurate only at near-constant velocities in inertial reference frames. When the system is highly dynamic, accelerometer measurements deliver not only information about the gravity vector but also information coming from the system motion (i.e. linear and centrifugal accelerations). Since high-speed motion is important to accurately quantify in many applications, linear and angular accelerations must be modeled and handled properly such that motion is accurately tracked.

2.2 Calibration of Magnetometers

With all sensors come unintended error in different usage conditions. Measurement error models are used to compensate for known potential sources of error in magnetic fields measured. Common sources are non-orthogonality of the physical sensor axes

and the axes scaling between different channels, information typically provided for individual sensors by manufacturers. To better observe magnetic north, error models are used to map distortion and are compensated for with calibration. Substantial work has been done to characterize distortion in magnetometer measurements. Tolles and Lawson [27] identified distortion of the magnetic field measured with magnetometers onboard an aircraft proportional to the angular rate of the aircraft, identified as eddy current effects. Bickel et al [28] worked to produce an error model inclusive of the effects of eddy currents. The most commonly used complete measurement error model includes consideration of soft iron, hard iron, scale factor, and misalignment errors [29]. With more detailed error models came more robust calibration methods for magnetometers. Caruso et al [30] explained calibration for planar applications correcting for hard iron and soft iron distortion. Conventional calibration methods successful at finding calibration parameters are normally used prior to measurement of

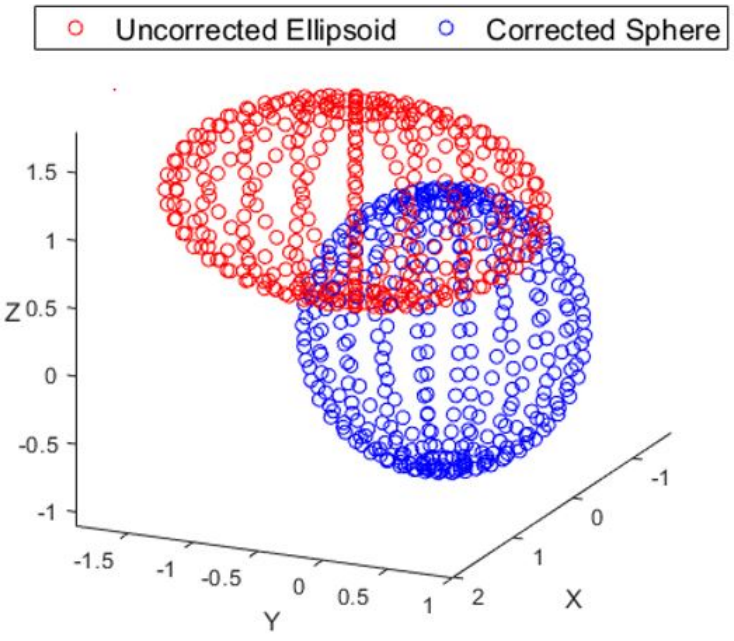

Figure 2.1: A visualization of the goal achieved with calibration of a magnetometer, transformation of an ellipsoid to a sphere around the origin.

a motion, working only in homogeneous magnetic fields, or most often static positions. Calibration requires a dataset produced with coverage of all possible orientations in mind, rotating the sensor for its measured points at all possible orientations. Dataset collection and calibration is normally completed prior to the measurement of a motion. When a dataset is well produced, measured points from all rotations form an ellipsoid. An example of the ellipsoid and the required transformation of the data set so that orientation can be measured within those distortion conditions can be seen in Fig. 2.1. All transformations of data to remove error and fit data as a centered sphere are calibration parameters used to compensate for distortion. Caruso et al [31] suggested finding the average of the maximums and minimums of the dataset in each degree of freedom, along with scaling the ellipse by the major axis to fit a sphere. Kok et al [32] achieved fitting of a function to map the ellipse with maximum likelihood formulation. Riwanto et al [33] achieved rotation axis fitting using particle swarm optimization to calibrate magnetometers, requiring less coverage of the ellipsoid formed with measured points. Tahir et al [34] incorporated solving the calibration model into a stochastic optimization problem, using simultaneous perturbation stochastic approximation to reduce complexity compared to particle filter approaches. All of the approaches listed are processes for calibration prior to measuring a motion, however, they don't account for the additional required calibration when an object travels through a nonuniform magnetic field.

Methods to estimate new calibration parameters as a body moves through a nonuniform field, or real-time calibration, have also been developed. Alonso et al [35] developed the TWOSTEP approach where calibration parameters are initially predicted using a centering approximation method, and are corrected using weighted sums of all measurements up to any point. The method requires more computation time

to estimate calibration parameters as more measurements are collected, leaving it more useful for post-processing data collected during a motion. Crassidis et al [36] compared the TWOSTEP method with both an EKF and an unscented Kalman filter (UKF) framework for estimating calibration parameters in real-time applications. The UKF framework performed the best in terms of accuracy and convergence properties as it works best with non-linearity.

2.3 Localization with Magnetometers

With the difficulty of global correction of orientation due to inconsistent magnetic north, efforts to refine localization with magnetometers did not stop. Suksakulchai et al [37] provided foundational work introducing the matching of distortion of heading direction to predetermined distortion signatures matched to locations. Matching heading deviation by position, durations of freshly measured signals are matched to distortion signatures with the least squares method. This work suggested that the inconsistency of magnetic fields in spaces can be used for localization, despite failure to correct orientation with inconsistent magnetic north. Methods of mapping magnetic fields in spaces to be used for localization came as result. Gozick et al [38] localized with known locations of ferrites within a corridor and a function of residual magnetism based on proximity to ferrite structures. Navarro et al [39] suggested an approach for heading correction using magnetic components at the correct position of the robot, prerecorded on a planar map. In the case of trying to motion track with just IMUs, the position of the system is estimated rather than collecting information on the actual position, making it difficult to properly correct heading with any error to the estimated position. Despite Navarro not including a way to map the magnetic

field direction for every position in a map approach, the work introduced a need for magnetic field mapping. Le Grand et al [40] produced a detailed method to map the magnetic field vector and intensity to be used for localization. Akai et al [41] mapped magnetic field using a magnetometer array on a robot to be used for future localization. Solin et al [42] mapped the interpolated vector field of ambient magnetic field using Gaussian processes. Kuevor et al [43] used Guassian process regression (GPR) to efficiently map magnetic fields in a space to use as *a priori* for motion tracking, and a method to improve roll and pitch estimation with GPR maps.

As methods for spatially mapping magnetic fields became more diverse, implementations of SLAM with magnetometers for navigation in robotics applications have become a field of interest. Akai et al [44] localized a robot with SLAM of geometric and magnetic landmarks using lidar and magnetometer, respectively. Robertson et al [45] extended FootSLAM to include mapping of local magnetic field intensities to help localize with returns to different positions known as MagSLAM.

2.4 Mounted Motion and Magnetic Sensor Arrays

Work in the automotive industry has introduced redundant measurements to better measure the motions of systems using sensor arrays. Alem et al [46] introduced usage of six accelerometers to measure angular acceleration of a head motion, but found that results were not reliable enough. Padgaonkar et al [47] compared the usage of six linear accelerometer arrays to the proposed usage of nine linear accelerometers, or nine accelerometer array package (NAAP), measuring tangential accelerations to measure the angular rotation of a body as depicted in Fig. 2.2. DiMasi et al [48] used the developed NAAP methodology to track the motion of the head of a test dummy

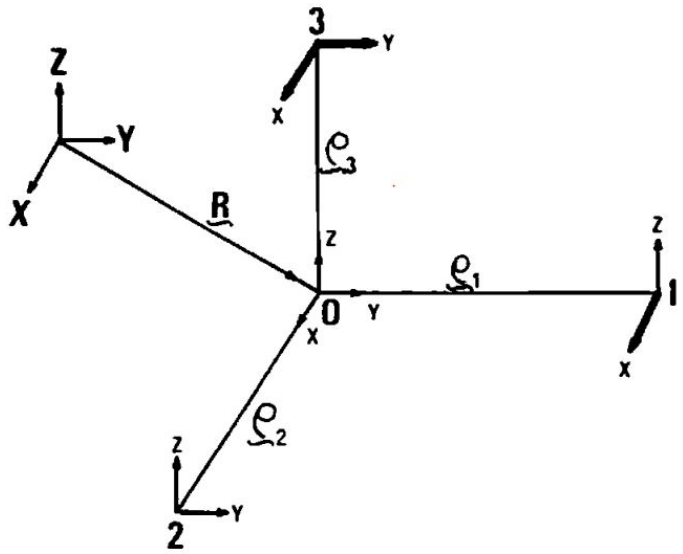

Figure 2.2: An figure depicting the directions and positions of linear accelerometers within a 6 sensor array with lighter arrows, and the 9 sensor array including the darker arrows. [47]

where sensors can be mounted internally. While useful for measuring relative motion, integration error accumulated over time. Takhounts et al [49] worked to investigate whether or not accumulated error was due to the integration of noisy signals, or missing considerations to the kinematics used to estimate motion, using the NAAP. With a developed consistency check for measurements, a better kinematics model with more defined constraint equations was developed accounting for dependency between degrees of freedom. The utilization of accelerometer and gyroscope arrays has proven useful in measuring relative motion for cases like impacts and crashes. The methods have, however, had difficulties measuring absolute motion with the issues of sensor drift. The usage of multiple magnetometers as a sensor suite has not been an uncommon practice for understanding local magnetic fields. Measuring changes in magnetic field reference direction between multiple sensors has been one way magnetometers have proved effective for positional tracking of metallic anomalies [50]. For the past decade, arrays of magnetometers have been used for magnetic gradient mapping to

detect anomalies [51]. Kozick et al [52] improved the usage of magnetometers for tracking the motion of magnetic dipoles, a technique that can be used with several magnetometers. Anomaly detection has led to calibration techniques for magnetometer arrays serving as gradiometers. Calibration methods for magnetometer arrays have been developed for both uniform [53] and non-uniform magnetic fields [54]. While magnetometer arrays have been commonly used for anomaly detection and finding metallic materials, magnetometer arrays can also potentially provide more information about the environment in motion tracking cases.

2.5 Summary

Motion tracking using externally mounted IMUs has been a well-studied topic for quite some time. Usage of IMU measurements have been used to track motions and even the mapping of paths traveled in urban settings. Methods to correct heading estimations of systems being tracked with measurement of the gravity vector have proven successful for tracking systems remaining in quasi-static conditions. Work to develop methods capable of tracking highly dynamic motion with external IMUs has plateaued with the capabilities of visual motion capture systems. The QUEST method uses gravity vector inclination correction in conjunction with heading correction using measurements from magnetometers, assuming a uniform magnetic field. Dynamic Measurement Fusion is proposed to allow for the redundancy of measurements of the angular rotation occurring on links in a system. With measurement redundancy, the motion is better observed, and the multiple beliefs based on measurements of the same state from different sensors can be fused to increase the accuracy of estimations. This method is employed to better handle highly dynamic motions of

multi-link systems.

Global correction with magnetometers is well-studied and useful, especially in spaces with uniform magnetic fields. With the nonuniformity of magnetic fields leading to difficulties correcting orientations of estimations in some locations and environments, work has aimed to compensate for the distortion of measured fields. Measurement error models accounting for the sources of error that cause variation in the measurement of local magnetic field vectors have been developed to compensate for local distortion and better observe magnetic north. As distortion varies by position in some spaces, calibration for distortion at one position may not work for others. Calibrating each step of the motion using the accumulated dataset of measurements to estimate calibration parameters has been one method aimed at solving magnetometer usage in nonuniform fields, however, takes too much computation time as the duration of the motion being measured increases. Different methods of estimating calibration parameters, along with the state of the system being tracked, have been used, and only have found more success using methods better at handling non-linearity.

Sensor arrays of accelerometers and gyroscopes have commonly used measurement redundancy to better measure motions. While sufficient for measuring relative motions, drift still accumulates with dead-reckoning sensors, leaving measuring absolute motions difficult. Magnetometer arrays have been found useful for measuring changes in magnetic field gradients. The most common use case for detecting changes in magnetic field gradient is magnetic anomaly detection. Although calibration procedures exist for magnetometer arrays, the sensor configurations have not been used for orientation measurement.

Relative calibration has not been achieved without processing a collected dataset. With just an additional sensor per link, measurements of an environment become rich

in information that can be used to better reduce error. Using coupled oppositely-faced magnetometers, the inconsistency of the magnetic north vector measured throughout a space can be better understood, and hard iron distortion can be observed and compensated for regardless of initial calibration.

Chapter 3

Conventional Motion Tracking with IMU

3.1 Conventional Tracking of Multi-Link Systems with External IMUs

3.1.1 Objective and Configuration

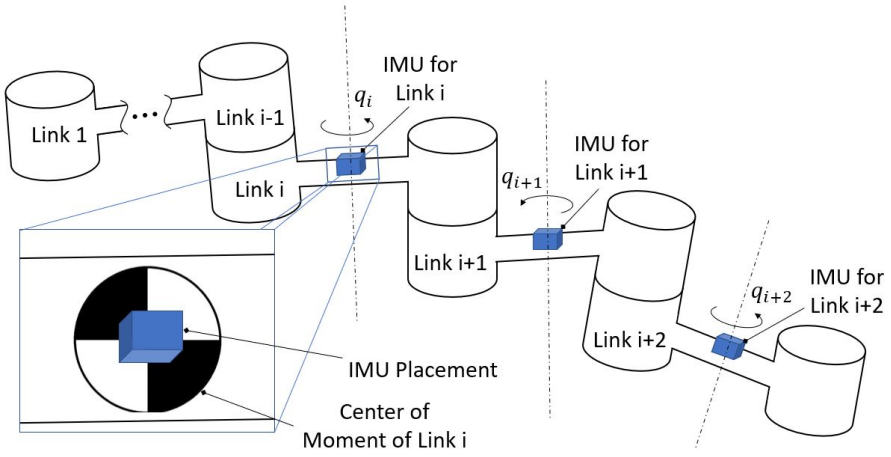

Figure 3.1: A model motion tracking problem of a multi-link system with conventional sensor placement.

Figure 3.1 shows the conventional usage of IMUs for motion tracking on the problem of concern in this chapter. The objective is to track the rotations of links of

a multi-link body using only externally mounted IMUs, which are installed on each link. Without loss of generosity, it is assumed that each link has a one degree of freedom (DOF) revolute joint, and the links are moving in one plane perpendicular to gravity. With motion tracking of a multi-link system, the translational and rotational motions of each link are considered. While gyroscopes measure the angular rotation of a link consistently from any position on its surface, different positions on the link may experience different linear accelerations. For this reason, accelerometers are usually positioned at the center of moment of a link as pictured in the figure, unless specific positioning with reliance on quasi-static motion [55, 56] is required. With this configuration, measured linear acceleration can be used to estimate translational motion of each link, leaving gyroscopes responsible for measuring rotational motion of a link, with correction from a magnetometer.

3.1.2 State Measurement

When the acceleration of a link is negligible, the orientation of each link in the global frame can be computed using magnetometers and accelerometers as follows. The accelerometer and magnetometer attached to a link measure the gravity vector $\mathbf{g}^b = \left[g_x^b, g_y^b, g_z^b\right]^\top$ (when static) and magnetic field vector $\mathbf{m}^b = \left[m_x^b, m_y^b, m_z^b\right]^\top$ in the body frame b, which are assumed to be constant. The following equations govern the transformation of the gravity and magnetometer vectors from the global frame into the body frame:

$$\mathbf{g}^b = \mathbf{R}(\phi, \psi, \theta)\mathbf{g}, \tag{3.1}$$

$$\mathbf{m}^b = \mathbf{R}(\phi, \psi, \theta)\mathbf{m}, \tag{3.2}$$

where ϕ, θ, and ψ are the roll, pitch, and yaw angles, respectively, with respect to the global east-north-up (ENU) coordinate frame, and $\mathbf{g} = [0, 0, -g]^\top$ and $\mathbf{m} = [0, m_y, m_z]^\top$ are the corresponding gravity and the earth's magnetic field vector in the ENU frame, respectively. $\mathbf{R}$ denotes the direction cosine matrix (DCM)

$$\mathbf{R}(\phi, \theta, \psi) = \begin{bmatrix} c_\theta c_\psi & c_\theta s_\psi & -s_\theta \\ s_\phi s_\theta c_\psi - c_\phi s_\psi & s_\phi s_\theta s_\psi + c_\phi c_\psi & c_\theta s_\phi \\ c_\phi s_\theta c_\psi + s_\phi s_\psi & c_\phi s_\theta s_\psi - s_\phi c_\psi & c_\theta c_\phi \end{bmatrix}, \tag{3.3}$$

where $c_{(\cdot)} = \cos(\cdot)$ and $s_{(\cdot)} = \sin(\cdot)$.

The rotation matrix $\mathbf{R}$ is often solved through the QUEST algorithm [8] to obtain the orientation of each link in the global frame. This algorithm provides a robust solution of orientation in the presence of measurement noises by solving the following optimization problem

$$\min_{\mathbf{v}^g} \frac{1}{2} \sum_i a_i \|\mathbf{v}_i^b - \mathbf{R}\,\mathbf{v}^g\|^2, \tag{3.4}$$

where $\mathbf{v}_i^b$ is the measured gravity and magnetic field in the body frame, $\mathbf{v}^g$ is the corresponding value in the global frame to estimate, and a_i is the corresponding weight for each measurement. Multiple measurements can be taken for accurate orientation during the measurement of the motion with negligible acceleration.

The fundamental problem of conventional motion tracking is that the computed orientation is accurate only when the multi-link system moves at a fairly constant, slow velocity. When the motion speed is high, linear acceleration due to centrifugal motion can be relatively large compared to the gravity. In this case, one cannot rely on the accelerometer to measure the gravity; otherwise, an erroneous gravity measurement leads to the wrong usage of Eqn. (3.1) and subsequent Eqn. (3.4). Since the links are connected, these inaccuracies compound from one link to the next. The next section presents the proposed technique which alters the conventional usage of IMU sensors and incorporates the accelerations caused by the high-speed motion of the links to track their movement.

3.2 Magnetic Field Distortion

3.2.1 Nonuniformity of Referenced Magnetic North

Hard iron distortion is the distortion to Earth's magnetic field by other objects that produce permanent magnetic fields. This kind of distortion is often observed as offset from the origin of the center of data points when a magnetometer is rotated. The magnitude of hard iron distortion is dependent on its proximity to distortion sources. Metals such as nickel and iron could cause a soft iron effect, which distorts the sphere into an ellipsoid as seen in Figure 2.1[57]. Since soft iron distortion is more related to the scaling of axes of magnetometer sensors, positional inconsistency of hard iron distortion is more of a contributor to error of attitude estimation with magnetometers. To observe the inconsistency of the magnetic field throughout a space away from and through the inside of a vehicle with an iron structure, the measurement signals of a

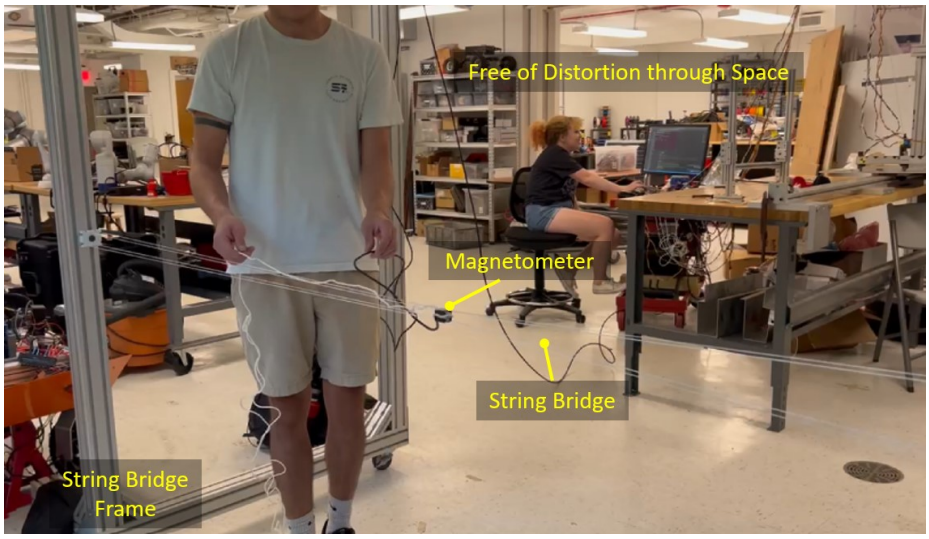

(a) Linear translation of magnetometer through unimpeded space.

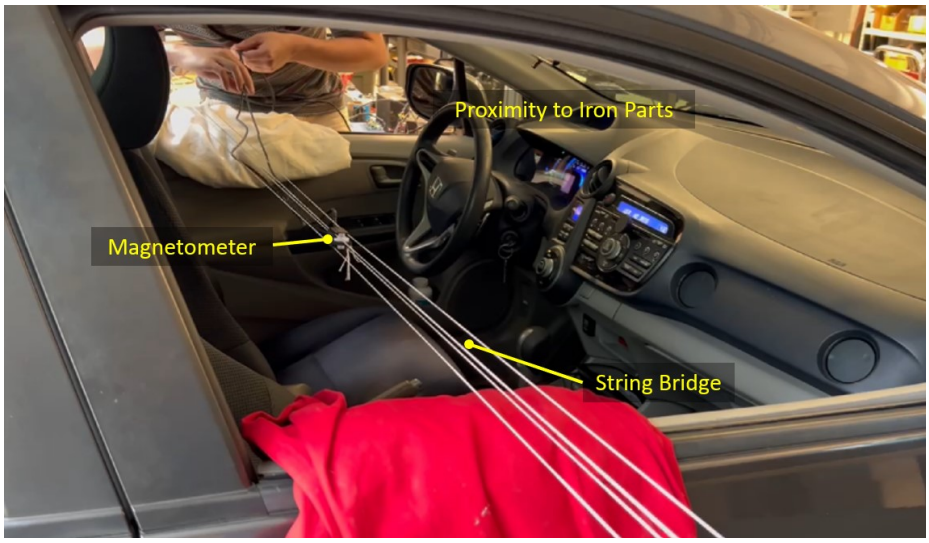

(b) Linear translation of magnetometer through vehicle structure.

Figure 3.2: Translation of a magnetometer recording data to observe the effects of magnetic distortion through the ferrite structure of a car.

triaxial magnetometer linearly translated through these environments are compared. Linear translation was achieved using a sensor module with four holes and taught strings with minimum pressure to pull the sensor along the string bridge, as seen in Fig. 3.2, to minimize the effects of extraneous magnetic effects that might have been the result of translating the magnetometer with a manipulator arm. The signals

recorded throughout the duration of the linear translation in both environments are plotted in Fig. 3.3, where the change in signals with changing proximity to ferrites of the construction of the vehicle structure is apparent. The similar shape of the output through the vehicle can be expected when translating a magnet without changing orientation by a stable magnetometer, indicating the local effects on the magnetic field of the vehicle structure can be understood as similar to that of an electromagnet.

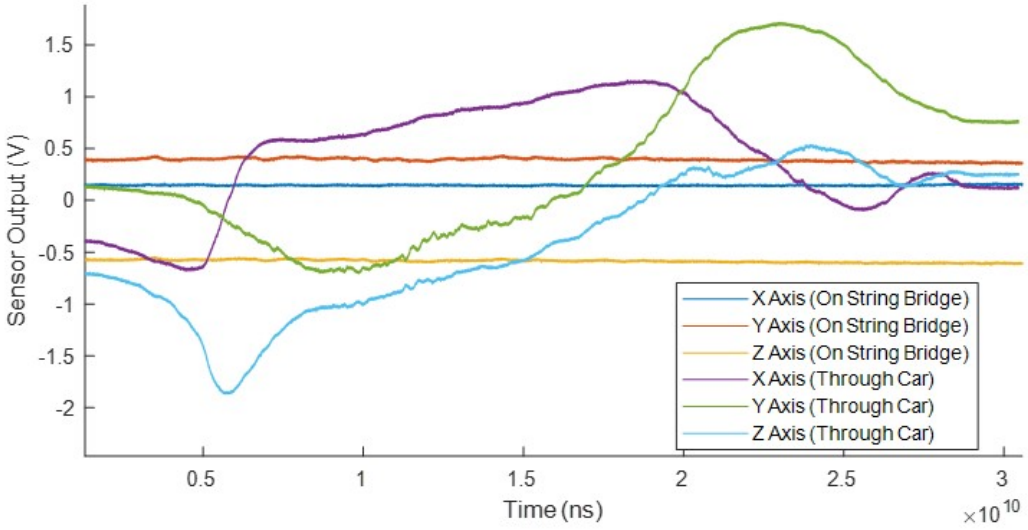

Figure 3.3: The signals of the magnetometer channels over the duration of being translated on a string bridge

With observed distortion to magnetic north measurements, compensation for distortion in magnetometer measurements needed to be considered. Calibration methods presented in the literature discussed in Section 2.2 only compensate for local distortion at the position of calibration in spaces with nonuniform magnetic fields. The proposed magnetometer usage was developed, first considering the error model of measurements from the magnetometer.

3.2.2 Measurement Error Model

An ideal calibration removes the effects of surrounding material on the magnetometer measurements. The calibration can be considered as a function that maps the measurement vector from the magnetometer $\mathbf{z}_b \in \mathbb{R}^3$, to the local magnetic field vector $\mathbf{z}_m \in \mathbb{R}^3$ that is used to estimate orientation. The effects causing error to magnetic field readings can be categorized as magnetic field distortion and sensor hardware imperfection. The two distortions caused by the proximity of the sensor to ferrite material are hard iron effects that introduce an offset to local magnetization, and soft iron effects that rotate and scale measured fields. The complete error model of a three axes magnetometer is expressed as [29]

$$\mathbf{z}_b = \mathbf{M}_{sc}\mathbf{M}_{no}\mathbf{M}_{so}\mathbf{R}_m^b(k)(\mathbf{z}_m + \mathbf{b}_{hard}) + \mathbf{b}_o + \mathbf{v}_m \tag{3.5}$$

Where $\mathbf{z}_b$ is the measurement from the magnetometer and $\mathbf{z}_m$ is the local magnetic field vector. Accounting for the effects and transformations between the two frames are $\mathbf{M}_{sc}$, $\mathbf{M}_{no}$, $\mathbf{M}_{so}$, and $\mathbf{R}_m^b(k)$ which are the scaling and non-orthogonality of the sensor axes, the axes scaling due to soft iron distortion, the time-variant rotation between the sensor frame, and the local magnetic field. The vectors b_{hard} and b_o are offsets due to hard iron distortion and sensor bias. The last term $\mathbf{v}_m$ is measurement noise which is assumed Gaussian with a high-frequency sample rate. For calibration, the error model is generalized to

$$\mathbf{z}_b = \mathbf{C}(\mathbf{z}_m + \mathbf{b}) + \mathbf{v}_m \tag{3.6}$$

where $\mathbf{C}$ is the scaling of the axes and $\mathbf{b}$ is the offset of measurements to the origin.

3.3 Summary

Normal motion tracking for humanoids using IMUs uses the gravity vector for inclination correction and magnetometers to correct heading with magnetic north. The QUEST Algorithm relies on quasi-static motion to properly observe the gravity vector for inclination correction. With greater accelerations of the system, the gravity vector is harder to tell apart from acceleration of the system. This technique has does not consider distortion that comes in different spaces.

Distortion to measured magnetic fields are compensated for with calibration. A sensor error model is solved for with data collected while the magnetometer is rotated in uniform magnetic field conditions. This technique works to consistently measure magnetic north only in spaces with uniform magnetic fields. After data collection in environments of concern, spaces with proximity to iron structures, inconsistency of the direction of magnetic north makes calibration in spaces with nonuniform magnetic fields difficult. Methods of real-time calibration are reliant on methods most capable of estimation of states of highly nonlinear systems, such as the UKF. Even with calibration using estimation methods most capable for nonlinear systems for calibration parameters, calibration fails over time.

Chapter 4

Application of Dynamic Measurement Fusion

4.1 Dynamic IMU Measurement Fusion Motion Tracking

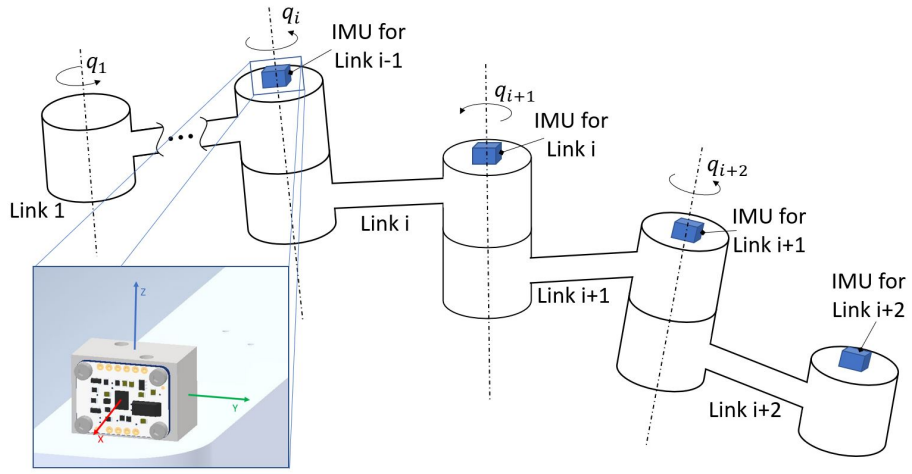

Figure 4.1: The proposed configuration of sensors for motion tracking of a highly dynamic multi-link system.

Figure 4.1 shows the developed motion tracker and the proposed positioning of the physical unit. Unlike the conventional layout, each IMU is mounted to the end of a link with a secured prototype mount. Every sensor in the body of links is wired to a central data acquisition system, recording outputs simultaneously for post processing,

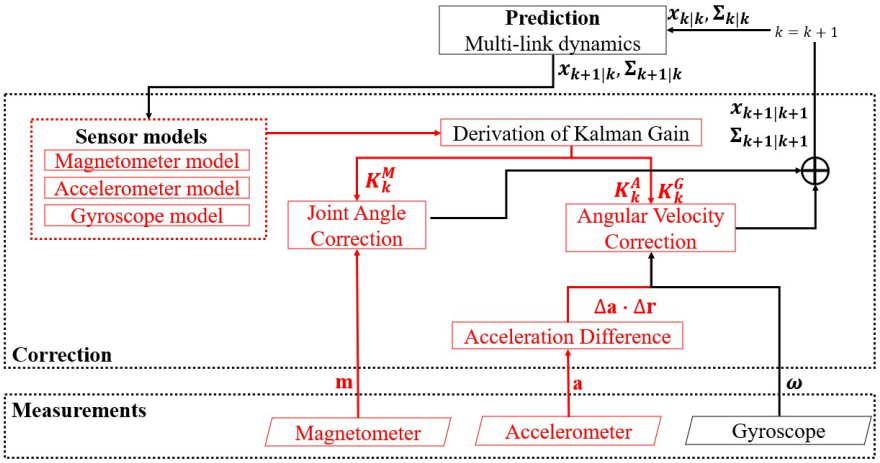

Figure 4.2: The proposed approach for motion tracking.

as real-time estimation is not the concern of this paper.

Figure 4.2 shows the approach proposed in this chapter for motion tracking. The proposed approach changes the role of accelerometer from inclination correction with gravity to correction of the angular velocity estimation, along with orientation correction with magnetometer. Under the given working condition, the angular velocity ω yields high acceleration on the multi-link system, as the centrifugal acceleration is proportional to $\omega^2 L$, where L is the length of the arm. Since the length of L increases, the angular velocity is better observed with linear accelerometers. The change removes the attitude estimation error due to high-speed motion and increases the accuracy of estimated angular velocity.

Aside from the new sensor usage, this work adopts the framework of an EKF to track the motion of the dynamic system with enhanced accuracy. The framework contains a two-step process: a prediction step and a correction step. In the prediction step, a probabilistic motion model is derived from Lagrangian analysis of the link system to predict the states through dynamics. Probabilistic sensor models then correct the states with the new arrangement. It is to be noted that the probabilistic motion and

sensor models described in the next two subsections are applicable to systems of an arbitrary number of links, although specifics for a two-link system are included in the subsections.

4.1.1 Probabilistic Motion Model

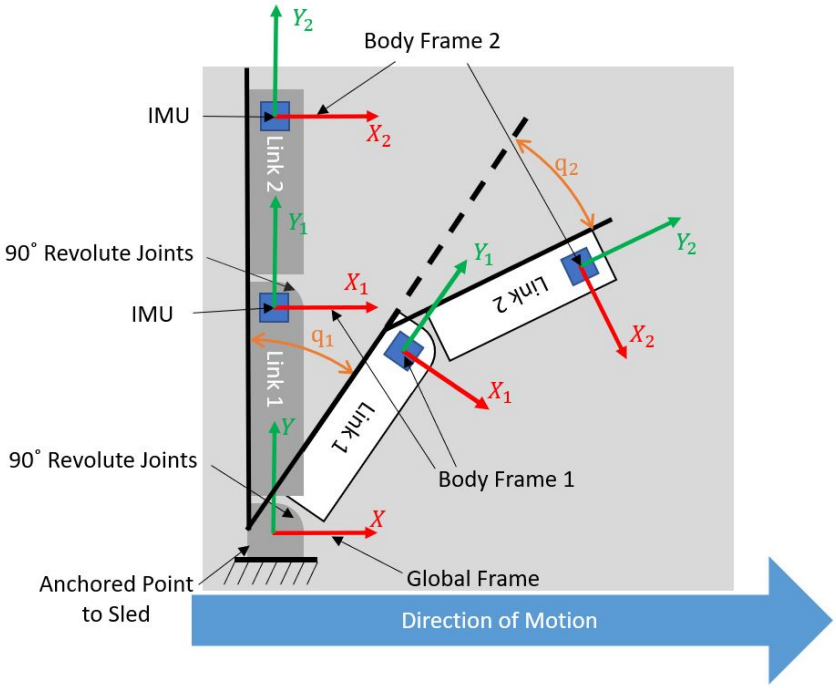

Figure 4.3: The global and body frames for state estimation.

To construct a probabilistic motion model, let the link angles $\mathbf{x}_1 = [q_1, q_2]^T$ and the angular rates $\mathbf{x}_2 = [\dot{q}_1, \dot{q}_2]^T$ where q_1 is the angular displacement of link 1, and q_2 is the angular displacement of link 2 relative to link 1, as shown in Fig. 4.3. The Lagrangian for a mechanical system constitutes the kinetic energy T and the potential energy V

$$\mathcal{L} = T - V, \tag{4.1}$$

where the kinetic energy includes the linear motion and rotational motion

$$\begin{aligned} T &= \sum_{i=1}^{2} (\frac{1}{2}\mathbf{m}_i\mathbf{v}_i^T\mathbf{v}_i + \frac{1}{2}\boldsymbol{\omega}_i^T\mathbf{I}_i\boldsymbol{\omega}_i) \\ &= \sum_{i=1}^{2} [\frac{1}{2}\mathbf{m}_i\mathbf{v}_i^T\mathbf{v}_i + \frac{1}{2}\boldsymbol{\omega}_i^T\mathbf{R}_b^i\mathbf{I}_i(\mathbf{R}_b^i)^T\boldsymbol{\omega}_i] \end{aligned} \tag{4.2}$$

and for the the two-link system working on the horizontal plane $V = 0$.

$$\frac{\partial}{\partial t}(\frac{\partial \mathcal{L}}{\partial \dot{q}_i}) - \frac{\partial \mathcal{L}}{\partial q_i} = \boldsymbol{\tau}_i \tag{4.3}$$

In the systems of interest in this paper, the torques are neglected as no active control is applied, and the friction forces and torques on the joint are also assumed to be negligible. Derived from Lagrangian mechanics, the dynamics of the system are given by

$$\begin{aligned} \mathbf{0} &= \mathbf{M}\left(\mathbf{x}_1\right)\dot{\mathbf{x}}_2 + \mathbf{V}\left(\mathbf{x}_1, \mathbf{x}_2\right) + \mathbf{F}\left(\mathbf{x}_1, \mathbf{x}_2\right) + \mathbf{G}\left(\mathbf{x}_1\right) + \mathbf{w}, \\ \mathbf{0} &= \dot{\mathbf{x}}_1 - \mathbf{x}_2 \end{aligned} \tag{4.4}$$

where the inertial, gravity, and Coriolis matrices of the dynamic equation are given by

$$\begin{aligned} \mathbf{M}(\mathbf{x}_1) &= \begin{bmatrix} m_2 + \frac{m_1}{s_2^2} & 0 \\ 0 & m_2 \end{bmatrix}, \\ \mathbf{G}(\mathbf{x}_1) &= \begin{bmatrix} m_1 g\frac{c_1}{s_2} + m_2 g s_{12} \\ m_2 g c_{12} \end{bmatrix}, \\ \mathbf{V}(\mathbf{x}_1, \mathbf{x}_2) &= \begin{bmatrix} -(m_2 l_1 c_2 + m_2 l_2)\dot{q}_1^2 - m_2 l_2 \dot{q}_2^2 - (2m_2 l_2 \\ \quad + m_2 l_1 c_2 + m_1 l_1 \frac{c_2}{s_2^2})\dot{q}_1\dot{q}_2 \\ m_2 l_1 s_2 \dot{q}_1^2 + l_1 m_2 s_2 \dot{q}_1 \dot{q}_2 \end{bmatrix}, \end{aligned} \tag{4.5}$$

where m_1 and m_2 are the masses of two links, and l_1 and l_2 are the corresponding

lengths. Variables with c and s are

$$\begin{aligned} c_1 &= \cos(q_1),\ s_1 = \sin(q_1), \\ c_2 &= \cos(q_2),\ s_2 = \sin(q_2), \\ c_{12} &= \cos(q_1 + q_2), \quad s_{12} = \sin(q_1 + q_2). \end{aligned} \tag{4.6}$$

$\mathbf{w} \sim \mathcal{N}(\mathbf{0}, \mathbf{\Sigma}_{\boldsymbol{v}})$ is a vector of motion noise with mean $\mathbf{0}$ and covariance $\mathbf{\Sigma}_{\boldsymbol{v}}$. The Gaussian assumption is valid since sensor measurements take place at a sufficiently high frequency.

4.1.2 Probabilistic Sensor Models

Sensor model for accelerometers

The proposed technique uniquely measures angular velocities from accelerometers using the relation of accelerations at differential positions on a rigid link, that is

$$\mathbf{a}_{p2} = \mathbf{a}_{p1} + \dot{\boldsymbol{\omega}} \times \mathbf{r} + \boldsymbol{\omega} \times (\boldsymbol{\omega} \times \mathbf{r}), \tag{4.7}$$

where $\mathbf{a}_{p1}$ and $\mathbf{a}_{p2}$ are the accelerations at point $p1$ and point $p2$ on the same link, respectively, and $\mathbf{r}$ is the vector from $p1$ to $p2$. $\boldsymbol{\omega}$ and $\dot{\boldsymbol{\omega}}$ are the rigid body's angular velocity and angular acceleration, respectively. The multiplication of Eqn. (4.7) by $\mathbf{r}$ and its rearrangement yield a relationship between accelerations at different positions and angular velocity as

$$(\mathbf{a}_{p2} - \mathbf{a}_{p1}) \cdot \mathbf{r} = (\boldsymbol{\omega} \times (\boldsymbol{\omega} \times \mathbf{r})) \cdot \mathbf{r} = (\boldsymbol{\omega} \cdot \mathbf{r})^2 - ||\mathbf{r}||^2 ||\boldsymbol{\omega}||^2. \tag{4.8}$$

The sensor model for accelerometers can be further simplified for the planar manipulator. Firstly, $\boldsymbol{\omega} \cdot \mathbf{r}$ can be removed from the right hand side, as $\boldsymbol{\omega} \cdot \mathbf{r} = 0$. Secondly, the accelerometers are installed on the joints to minimize the usage of sensors. As the dot product is invariant when performing frame rotation, the left hand side of the Eqn. (4.8) can be rewritten in the body frame, and this writes the probabilistic sensor model of the accelerometer as

$$\begin{aligned} \mathbf{z}_a &\equiv \begin{bmatrix} a_{1,x} \\ a_{2,x} - (c_2 a_{1,x} - s_2 a_{1,y}) \end{bmatrix} \\ &= \begin{bmatrix} l_1 \dot{q}_1^2 \\ l_2 \left(\dot{q}_1 + \dot{q}_2\right)^2 \end{bmatrix} + \begin{bmatrix} v_{1,x} \\ (c_2 v_{1,x} - s_2 v_{1,y}) \end{bmatrix}. \end{aligned} \tag{4.9}$$

where $a_{1,\cdot}$ and $a_{2,\cdot}$ are the accelerometer measurements in the body frame, respectively, as referenced in Fig. (4.3), and v is the corresponding measurement noise. l_1 and l_2 are the length of the manipulator arms, respectively. Since this is nonlinear with respect to $\mathbf{x}_2$, the Jacobian of the sensor model is computed by taking the derivative of Eqn. (4.9) with respect to the state variable $\mathbf{x}$, that is

$$\mathbf{H}^A = \begin{bmatrix} 0 & 0 & 2l_1\dot{q}_1 & 0 \\ 0 & 0 & 2l_2(\dot{q}_1 + \dot{q}_2)\dot{q}_1 & 2l_2(\dot{q}_1 + \dot{q}_2)\dot{q}_1 \end{bmatrix}. \tag{4.10}$$

Sensor model for magnetometers

The magnetometer fully observes the orientation of each link. Assuming the magnetic field is homogeneous in the global frame, the orientation of each link is observed by

the magnetometers by

$$\mathbf{Q}(x_{1,k})^{\top}(\mathbf{z}_{m,k} - \mathbf{v}_{m,k}) = \mathbf{Q}(\mathbf{x}_{1,0})^{\top}(\mathbf{z}_{m,0} - \mathbf{v}_{m,0}), \tag{4.11}$$

where $\mathbf{z}_{m,k}$ and $\mathbf{v}_{m,k}$ are the magnetometer measurement and its noise at step k, respectively, and for the two-link system, the block diagonal matrix $\mathbf{Q}(\mathbf{x}_{1,k})$ is given by

$$\mathbf{Q}(\mathbf{x}_{1,k}) = \begin{bmatrix} c_1 & s_1 & 0 & 0 \\ -s_1 & c_1 & 0 & 0 \\ 0 & 0 & c_{12} & s_{12} \\ 0 & 0 & -s_{12} & c_{12} \end{bmatrix}. \tag{4.12}$$

The multiplication of $\mathbf{Q}(x_{1,k})$ on both sides and the rearrangement of $\mathbf{v}_{m,k}$ to the right side yield the sensor model for the magnetometers as

$$\begin{aligned} \mathbf{z}_{m,k} = \mathbf{h}_m(\mathbf{x}_{1,k}) + \mathbf{v}'_{m,k} = \mathbf{Q}(\mathbf{x}_{1,k})\mathbf{Q}(\mathbf{x}_{1,0})^T\mathbf{z}_{m,0} \\ + (\mathbf{v}_{m,k} - \mathbf{Q}(\mathbf{x}_{1,k})\mathbf{Q}(\mathbf{x}_{1,0})^T\mathbf{v}_{m,0}), \end{aligned} \tag{4.13}$$

where $\mathbf{h}_m(\mathbf{x}_{1,k}) \equiv \mathbf{Q}(\mathbf{x}_{1,k})\mathbf{Q}(\mathbf{x}_{1,0})^T\mathbf{z}_{m,0}$ and $\mathbf{v}'_{m,k} \equiv \mathbf{v}_{m,k} - \mathbf{Q}(\mathbf{x}_{1,k})\mathbf{Q}(\mathbf{x}_{1,0})^T\mathbf{v}_{m,0}$ are the sensor model and the noise of which the covariance is updated at every time step k, respectively. The formula has the advantage that no exact magnetic north vector is measured. Since this is also nonlinear with respect to $\mathbf{x}_{1,k}$, the Jacobian of the sensor model $\mathbf{H}^M$ is derived by taking the derivative with respect to the state variable as

$$\mathbf{H}^M = \begin{bmatrix} \frac{\partial \mathbf{h}_m(\mathbf{x}_{1,k})}{\partial \mathbf{x}_1}\Big|_{\mathbf{x}_{1,k}} & \mathbf{0}_{4\times 2} \end{bmatrix}. \tag{4.14}$$

Sensor model for gyroscopes

As the gyroscope measures the angular velocity directly, the sensor model of the gyroscope can be derived straightforwardly. By equating the angular velocity measured by the gyroscope to the system state, the sensor model is obtained linearly as

$$\mathbf{z}_g = \mathbf{C_g x} + \mathbf{v}_g, \tag{4.15}$$

where $\mathbf{z}_g$ and $\mathbf{v}_g \in \mathbb{R}^2$ are the angular velocity measurements and its noise, respectively, and where the measurement matrix $\mathbf{C_g}$ for the two-link case is given by

$$\mathbf{C_g} = \begin{bmatrix} 0 & 0 & 1 & 0 \\ 0 & 0 & 1 & 1 \end{bmatrix}. \tag{4.16}$$

4.1.3 EKF Based State Estimation

After the construction of the motion model (4.4) and the sensor models of Eqn. (4.9), Eqn. (4.13), and Eqn. (4.15), the EKF can correct the prediction through the sensor measurements [58]. Since the magnetometers correct the joint angles, whereas the gyroscopes and accelerometers correct the joint angular velocities, the means of the joint angles and the joint angular velocities are predicted, respectively, by

$$\hat{\mathbf{x}}_{1,k|k} = \hat{\mathbf{x}}_{1,k|k-1} + \mathbf{K}_k^M \left[\mathbf{z}_{m,k} - \mathbf{h}_m\left(\hat{\mathbf{x}}_{1,k|k-1}\right)\right], \tag{4.17a}$$

$$\begin{aligned}\hat{\mathbf{x}}_{2,k|k} = \hat{\mathbf{x}}_{2,k|k-1} &+ \mathbf{K}_k^G \left[\mathbf{z}_{g,k} - \mathbf{C_g}\left[\hat{\mathbf{x}}_{1,k|k-1}, \hat{\mathbf{x}}_{2,k|k-1}\right]^\top\right] \\ &+ \mathbf{K}_k^A \left[\mathbf{z}_{a,k} - \mathbf{h}_a\left(\hat{\mathbf{x}}_{1,k|k-1}, \hat{\mathbf{x}}_{2,k|k-1}\right)\right],\end{aligned} \tag{4.17b}$$

where $\mathbf{K}_k^M$, $\mathbf{K}_k^G$, and $\mathbf{K}_k^A$ are the Kalman gains for the magnetometer, gyroscope, and accelerometer given by

$$\mathbf{K}_k^M = \mathbf{\Sigma}_{k|k} \left(\mathbf{H}_k^M\right)^\top \left(\mathbf{\Sigma}_k^M\right)^{-1}, \tag{4.18a}$$

$$\mathbf{K}_k^G = \mathbf{\Sigma}_{k|k} \left(\mathbf{C}_\mathbf{g}\right)^\top \left(\mathbf{\Sigma}_k^G\right)^{-1}, \tag{4.18b}$$

$$\mathbf{K}_k^A = \mathbf{\Sigma}_{k|k} \left(\mathbf{H}_k^A\right)^\top \left(\mathbf{\Sigma}_k^A\right)^{-1}. \tag{4.18c}$$

Here $\mathbf{\Sigma}_{k|k}$ is the covariance of the state estimation and is updated by

$$\mathbf{\Sigma}_{k|k}^{-1} = \mathbf{\Sigma}_{k|k-1}^{-1} + \sum_i \left(\mathbf{H}_k^i\right)^\top \left(\mathbf{\Sigma}_k^i\right)^{-1} \mathbf{H}_k^i, \tag{4.19}$$

where $\mathbf{\Sigma}_k^{(\cdot)}$ represents the covariance of sensor noises in Eqn. (4.9), (4.13), and (4.15).

4.2 Summary

In this chapter, the methodology behind the application of dynamic measurement fusion is explained. Linear accelerometers are used to measure centrifugal forces experienced by links to correct the angular rate of links along with gyroscopes. Better measurement of centrifugal forces can be achieved by targeting mounting points to the ends of links. The farther the mounted accelerometers, the better the resolution of a data acquisition can measure centrifugal forces. Joint angles are globally corrected with magnetometers, diminishing the effects of sensor drift, however, assuming the magnetic field throughout the space the system travels is consistent and uniform. Using the proposed motion model of the two-link system, the sensor models, and the

EKF framework to fuse the measurements together, the estimation between using both gyroscopes and an accelerometer to measure the angular rate, and using just gyroscopes, both with correction from magnetometer, are compared. Figure 4.4 shows the prototype motion tracker mounted to the end of a link used for experimental validation.

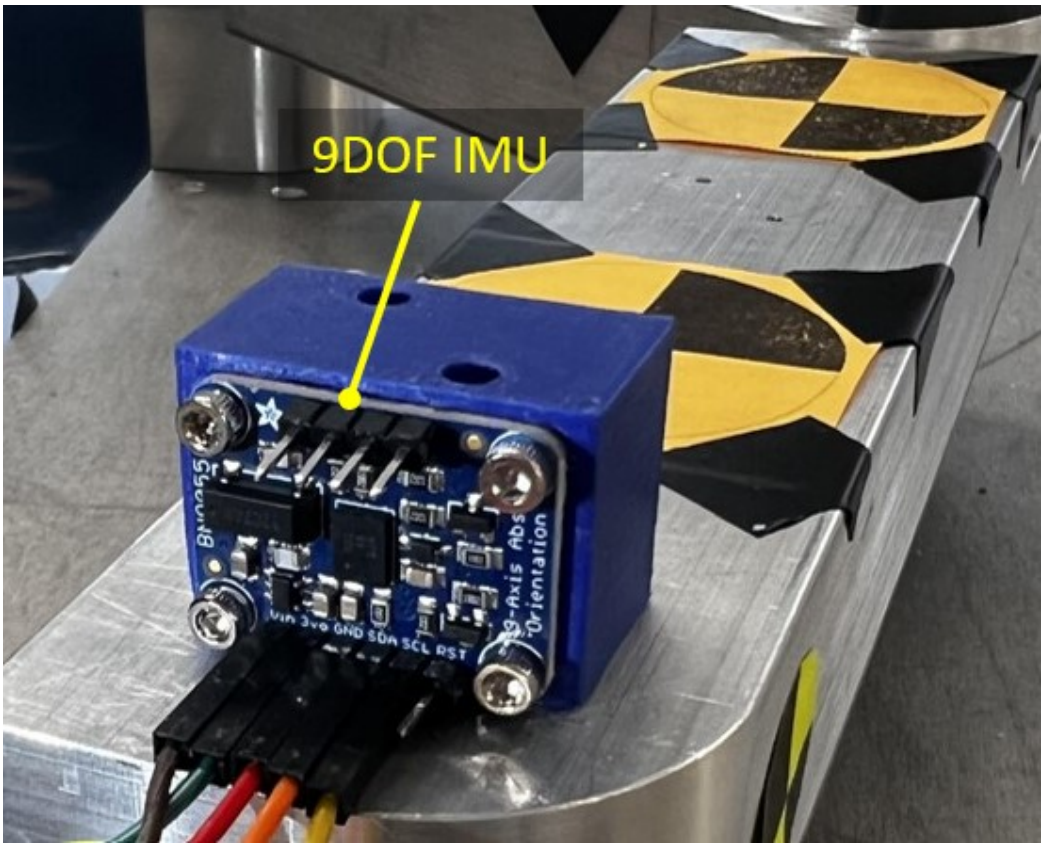

Figure 4.4: The experimental setup used to induce and measure a highly dynamic swinging motion.

Chapter 5

Coupled Magnetometers in Nonuniform Fields

5.1 Usage of Coupled Magnetometers

5.1.1 Development of Sensor Configuration

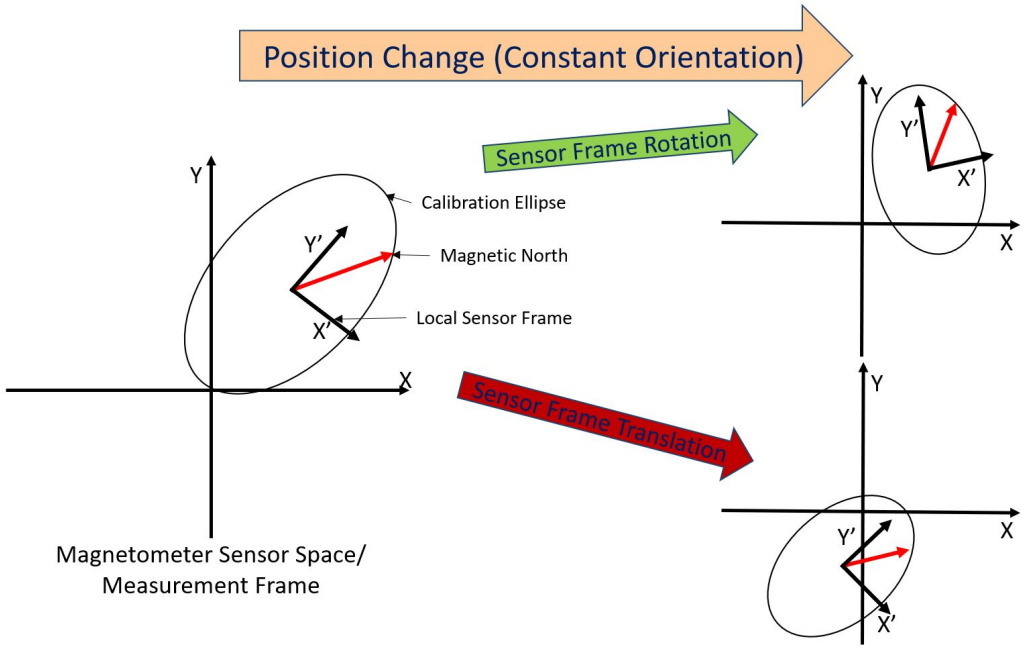

Figure 5.1: A diagram illustrating the issue faced using magnetometer measurements with change of position in nonuniform magnetic field.

The concern with using magnetometers in nonuniform magnetic fields is visualized in Fig. 5.1. With any change to the position of a magnetometer without rotation in a space with a nonuniform magnetic field, there are two expected transformations of the sensor frame within the magnetometer sensor space or measurement frame. If the sensor frame is rotated in the sensor space, then either a change in orientation has occurred, or a change in the magnetic north vector measured was the cause. Inconsistency of the direction of magnetic north is expected in proximity to sources of distortion and is difficult to account for with a system that changes orientation as it is translated through a nonuniform field. The sensor frame may also translate through the sensor space, indicating a change in hard iron distortion. The transformations of the sensor frame can be thought of as transformations of the ellipse used for calibration from position to position in the space of the nonuniform magnetic field. While

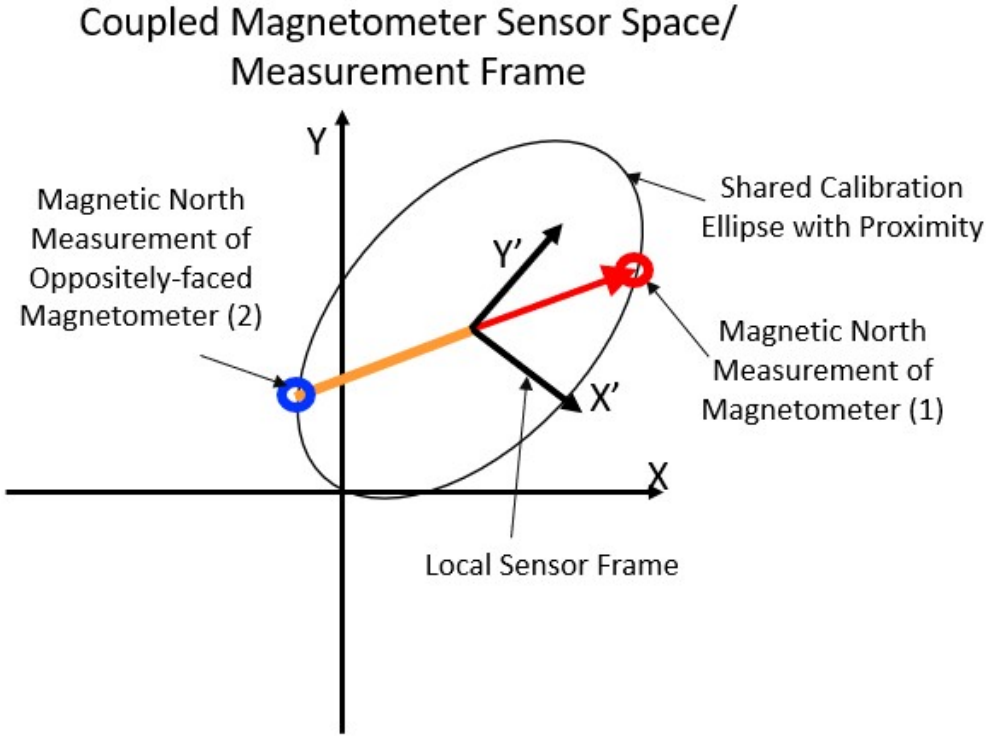

Figure 5.2: A diagram illustrating the intended usage of coupled magnetometers for orientation correction, measuring opposite sides of a calibration ellipsoid.

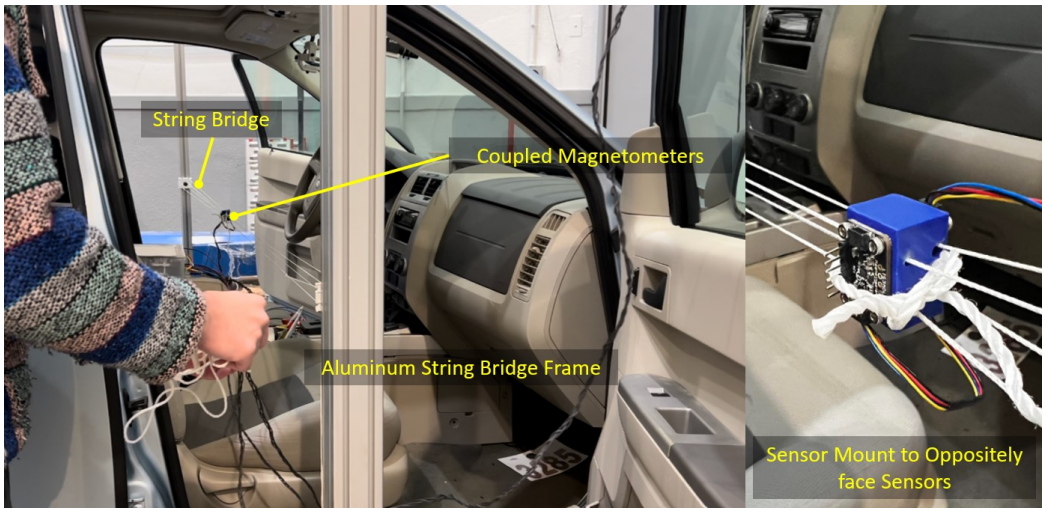

Figure 5.3: The translation of coupled, oppositely-facing magnetometers along string bridge previously used to make insights about magnetic field nonuniformity.

tracking changes of magnetic north remains difficult, the proposed use case of coupled magnetometers compensates for hard iron distortion by making two measurements of oppositely facing magnetometers. Similarly illustrated with a planar example in Fig. 5.2, the oppositely facing magnetometers make measurements on opposite sides of an ellipsoid measuring the local magnetic north vector. With each new position in the nonuniform magnetic field, a transformation of the local sensor frame within the magnetometer's sensor space or measurement frame occurs.

Using the approach of having two oppositely facing magnetometers, the magnetic field throughout the space of a vehicle frame is measured, as seen in Fig. 5.3. The measurements of each magnetometer are in blue and red, with a colored line between the measured points for each time step, as seen in Fig. 5.4. The line starts in black and changes to red throughout the duration of the data recorded to clarify the results as the magnetometer is translated through a vehicle. The inconsistency of magnetic north is observable with the changing orientation of the vector between the two measured points.

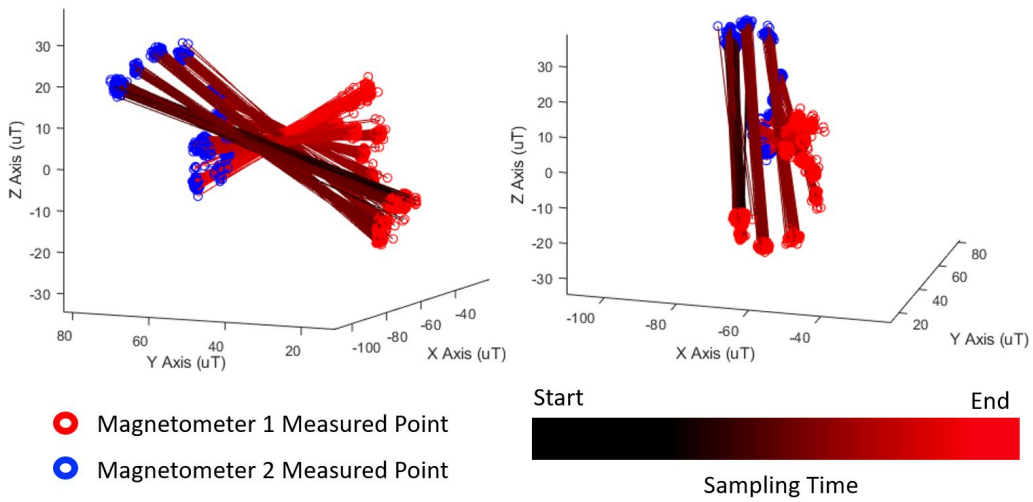

Figure 5.4: Measurements with coupled, oppositely-facing magnetometers through a nonuniform magnetic field, visualizing the nonuniformity of distortion and magnetic north.

This effect is intended on being recreated for testing the estimation method and coupled magnetometer configuration. Compared to using a single magnetometer, measurements require far less processing to be able to visualize the measured magnetic north direction. Using the coupled magnetometers, two things are made obvious with the visualization of data measured during the translation through a nonuniform magnetic field. Firstly, the consistency of hard iron distortion throughout the space could be assumed if the center points of all the magnetic north lines converged at one point. Rather, there is a visible transformation of the location and orientation of magnetic north in the measurement space as the magnetometer is translated. Secondly, visible with the changing orientation of the lines over the duration of the measured times is the inconsistency of magnetic north throughout the space in the vehicle.

5.1.2 Measurement of Hard Iron Distortion

In a space within a nonuniform field, a variation to distortion, or transformation to the ellipse formed in calibration, occurs at every position. The two magnetometers are posed to measure two points on opposite sides of the ellipse as $X \sim \mathcal{N}(\mu_X, \sigma_X)$ in each degree of freedom, where μ_X is the mean of the measurement and σ_X is the variance based on the sensor. The hard iron distortion offset is produced by finding the mean of the Gaussians. The mean of the Gaussians is $X \sim \mathcal{N}(\alpha\mu_{X_1} + (1-\alpha)\mu_{X_2}, \alpha^2\sigma_{X_1}^2 + (1-\alpha)^2\sigma_{X_2}^2)$ where α can be calculated with the variance of each measurement with

$$\alpha = \frac{\sigma_{X_2}^2}{\sigma_{X_1}^2 + \sigma_{X_2}^2}. \tag{5.1}$$

The measured orientation is the angle of rotation of the mean of a measured point around the mean of the calculated center point. For the two-dimensional case of concern in this paper, using the covariance of the Gaussians as a radius to make a circle around the means of the measured points and one of the measured distributions,

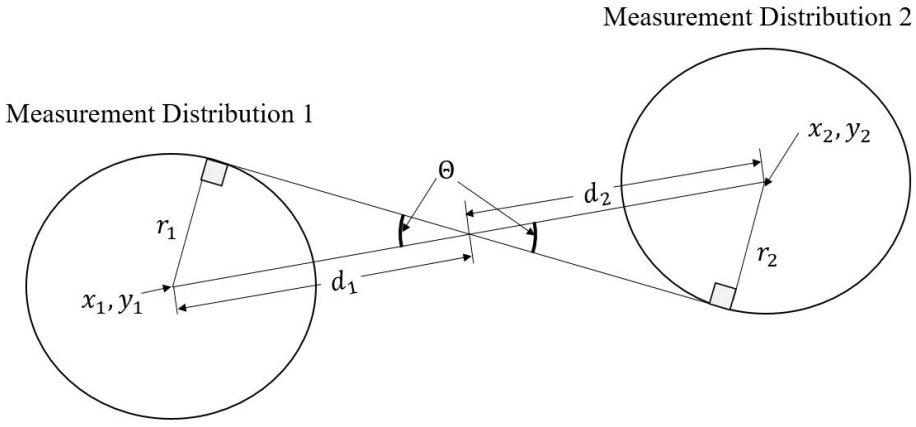

Figure 5.5: The geometry of determining the error of the orientation measured with coupled magnetometers using the mean of the measured points and one of the measured points.

the error of measured orientation can be calculated. The angle between the inner tangent lines from the center distribution to a measurement distribution is the error of measured orientation. Figure 5.5 illustrates how two triangles can be formed using one of the inner tangent lines, and a line between the centers of the two measured points. Using Triangle Proportionality Theorem, the angle between the two lines can be calculated by solving for d_1 and d_2 with

$$\frac{r_1}{r_2} = \frac{d_1}{d_2},\ d_1 + d_2 = \sqrt{(x_2 - x_1)^2 + (y_2 - y_1)^2} \tag{5.2}$$

where r and (x, y) are the radius and coordinates of the center point of a measurement distribution, respectively. The error can be calculated as 2Θ, where Θ is $\arcsin\left(\frac{r_1}{d_1}\right)$.

The estimated offset can be used to more accurately measure the rotations of links in nonuniform fields. With the opposite-facing magnetometers, hard iron distortion can be estimated regardless of position.

5.1.3 Proposed Magnetometer Sensor Model

Rather than assuming constant hard iron distortion with prior calibration in a constant position, and using the initial measurement as the reference heading for every time step, the proposed method is to use the calibrated measurement from the last time step as the reference heading. These changes to conventional usage of dynamic measurement fusion are depicted in the flow chart seen in Fig. 5.6. The real-time calibration accomplished using coupled magnetometers is seen as a new form of measurement. The utilization of the most recently measured magnetic north vector is seen as a change to the sensor model accomplishing correction to the estimation. As the measured magnetic field vector changes by position, the proposed method has the

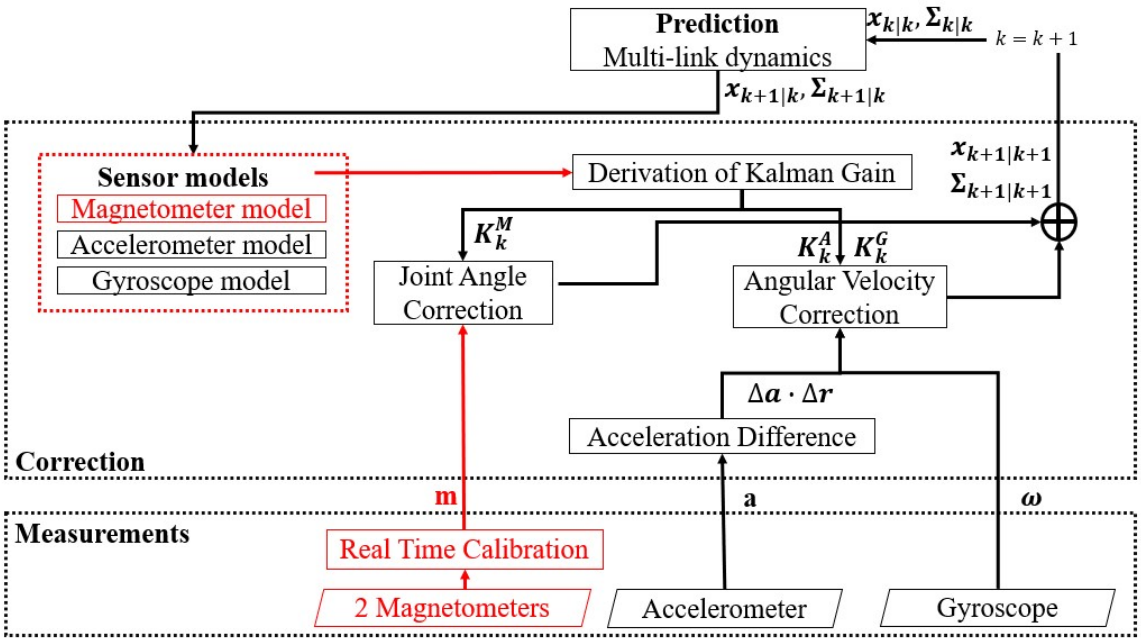

Figure 5.6: The proposed dynamic measurement fusion framework with real-time calibration.

advantage of using the last measured vector to observe the change in orientation to the current step. With positional change of the links, the initial measured magnetic north vector may not be useful as compared to the most recent measurement of local magnetic north as the duration of the estimation progresses. $\mathbf{Q}(x_{1,k-1})$ is used in the sensor model rather than $\mathbf{Q}(x_{1,0})$ as

$$\begin{aligned} \mathbf{z}_{m,k} = \mathbf{h}_m(\mathbf{x}_{1,k}) + \mathbf{v}'_{m,k} = \mathbf{Q}(\mathbf{x}_{1,k})\mathbf{Q}(\mathbf{x}_{1,k-1})^T \mathbf{z}_{m,k-1} \\ + (\mathbf{v}_{m,k} - \mathbf{Q}(\mathbf{x}_{1,k})\mathbf{Q}(\mathbf{x}_{1,k-1})^T \mathbf{v}_{m,k-1}). \end{aligned} \tag{5.3}$$

Since both models are nonlinear with respect to $\mathbf{x}_{1,k}$, the Jacobian of the sensor model $\mathbf{H}^M \in \mathbb{R}^{4\times 4}$ is derived by taking the derivative with respect to the state variable as

$$\mathbf{H}^M = \left[\left. \frac{\partial \mathbf{h}_m(\mathbf{x}_{1,k})}{\partial \mathbf{x}_1} \right|_{\mathbf{x}_{1,k}} \quad \mathbf{0}_{4\times 2} \right]. \tag{5.4}$$

5.2 Summary

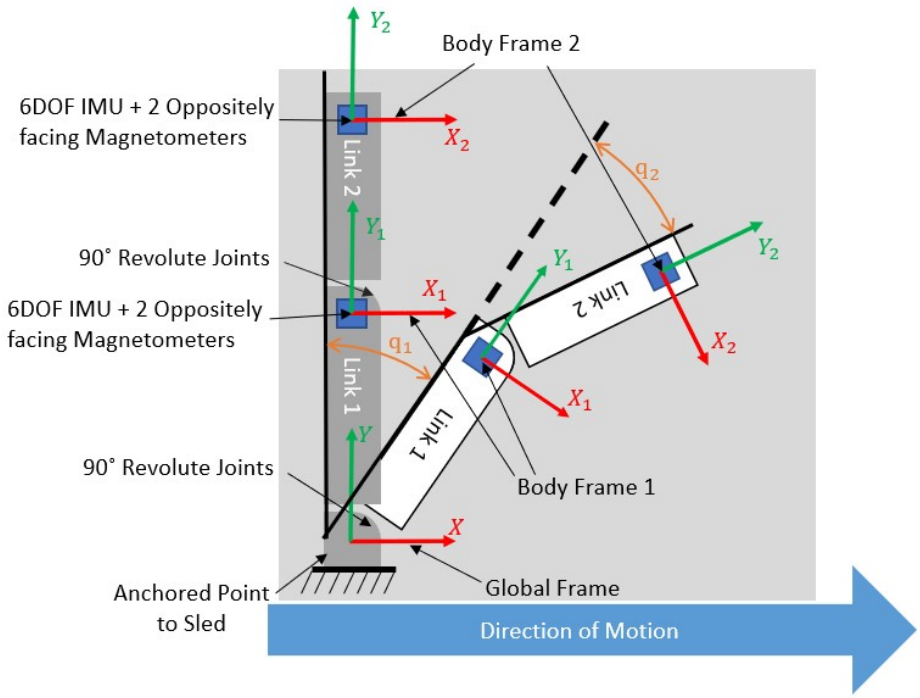

Figure 5.7: The global and body frames of the two-link system for state estimation.

The process of development for visualizing the inconsistency of magnetic north leading to the usage of coupled magnetometers is explained. Using oppositely facing, closely positioned magnetometers, local hard iron distortion, along with the direction of magnetic north, can be measured. Although magnetic north may not point the same direction throughout spaces in proximity to ferrites, the usage of sensors allows for better measurements with real-time calibration. Inconsistency of magnetic north is compensated for by using the most recent previously measure magnetic north vector as reference, rather than the initially measured magnetic north vector as with conventional magnetometer usage assuming uniform magnetic fields. Experimental validation using a proof of concept system is designed to prove the value of the proposed sensor usage as seen in Fig. 5.7. The system used is the same two-link system

with two degrees of freedom used for validation of dynamic measurement fusion in uniform fields. Iron blocks are mounted to the platform to cause distortion in the space the links pass through as later discussed. The sensor mount pictured in Fig. 5.8 shows the prototype sensor package developed mounted to the ends of the aluminum link.

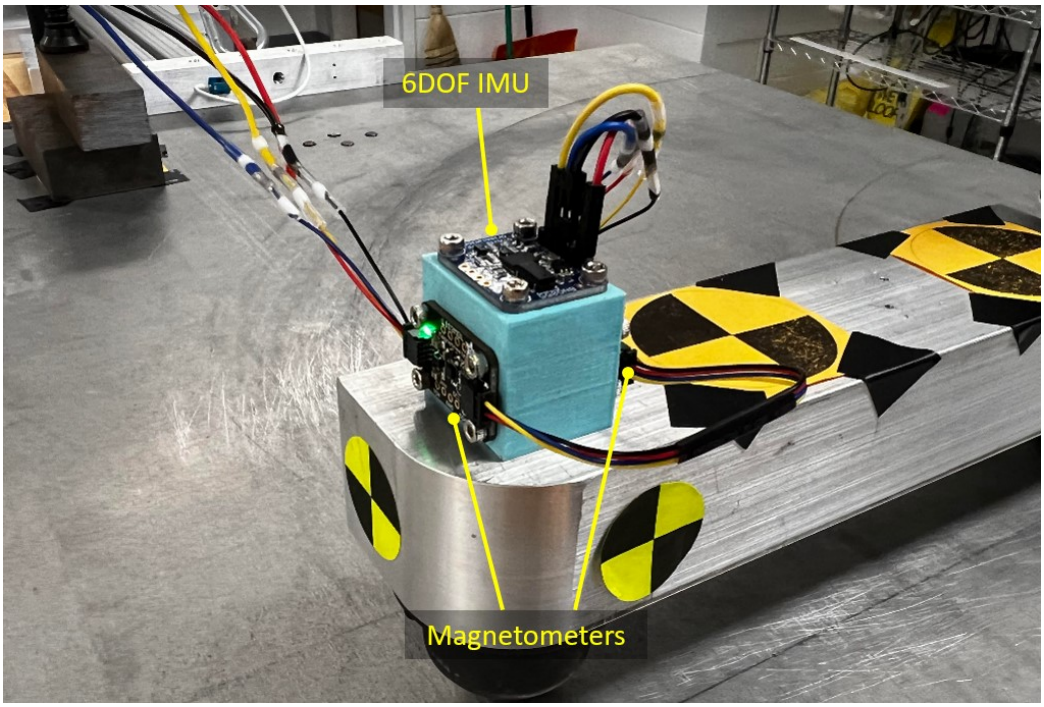

Figure 5.8: The prototype sensor mount used to measure a motion with an IMU along with coupled magnetometers.

Chapter 6

Experimental Validation with Two Degree of Freedom System

6.1 2DOF System Configuration

6.1.1 Highly Dynamic Motion Inducing System

Figure 6.1 shows the proof of concept system used for validation of the estimation methods proposed throughout this thesis, which consists of an aluminum two-link arm, a platform mounted on a slider on a rail, a quick release latch, an impulser, a stopper, and a data acquisition system [3]. The quick release is used to trigger the initiation of the motion, allowing the weight of the impulser to pull the platform by the cable attached between the platform and the impulser weight, with a pulley wheel re-directing the motion of the weight to the linear motion of the platform down the rail. The momentum of the sled is transferred to the angular rotation of the linkage arms to be measured once the platform collides with the stopper. The two-link arm system consists of two aluminum rectangular bars joined together by a revolute joint, along with another joint anchored to the platform. Each revolute joint is constrained to a quarter turn by design to constrain the motion similar to a humanoid. To prevent extraneous friction that could occur with contact between the two links and

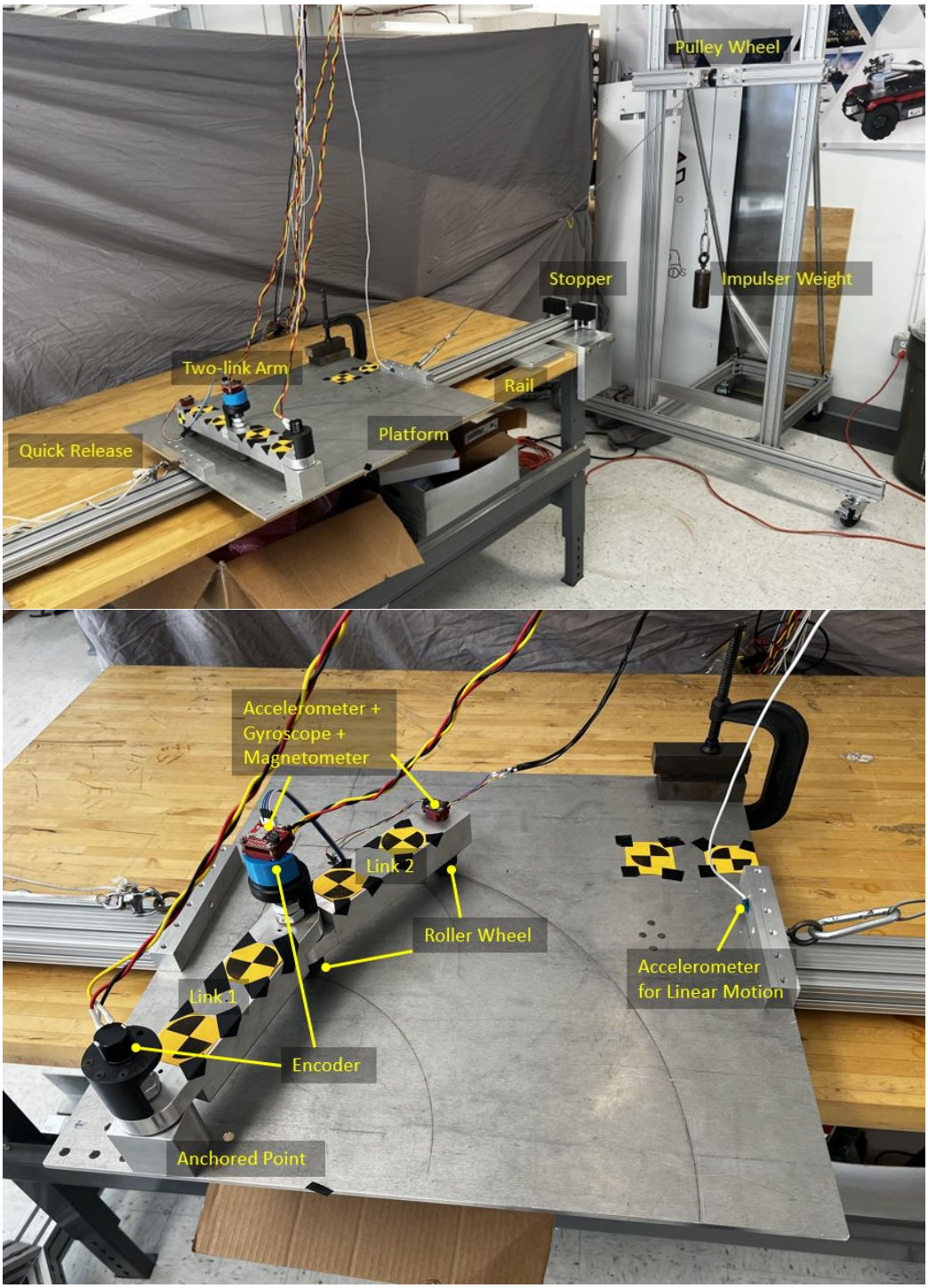

Figure 6.1: The experimental setup used to induce and measure a highly dynamic swinging motion.

the platform, spherical rollers are installed to the end of the links in contact with the sled platform.

Using gained momentum from the induced motion of the sled platform, the highly dynamic swinging motion of the linkage arms being measured occurs after contact with the stopper. To investigate the performance of estimation methods for a wide range of motion speed including high speed, the proposed technique is applied to motion tracking with different induced initial velocities of the platform prior to the moment of collision. Different impulser weights are used to change the intensity of the highly dynamic motion. The system links are initially pointed perpendicular to the direction of the motion. Because the experiment is only of planar motion, the IMUs only require a 2-axis magnetometer and accelerometer for measuring the axes on the plane of motion, and the axis of gyroscope perpendicular to the motion.

Crosstalk is when a signal transmitted from one circuit creates an undesired effect in another circuit or channel. Given that the use of measured magnetic fields is crucial to the work presented in this paper, diligence is required to reduce the effects that can be prevented. In addition to using aluminum hardware pieces to reduce magnetic effects in the tests, factors throughout the electronics must also be considered. Each channel and lead to sensors required for measurement is wired to the central data acquisition system. Minimization of materials was first considered, as the chances of induced effects increases with more materials. Wires to sensors not manufactured with shielding and coating were all braided to take advantage of twisted theorem. Usage of twisted pair reduces crosstalk and improves rejection of external interference [59].

6.1.2 Ground Truth Measurement of Motion

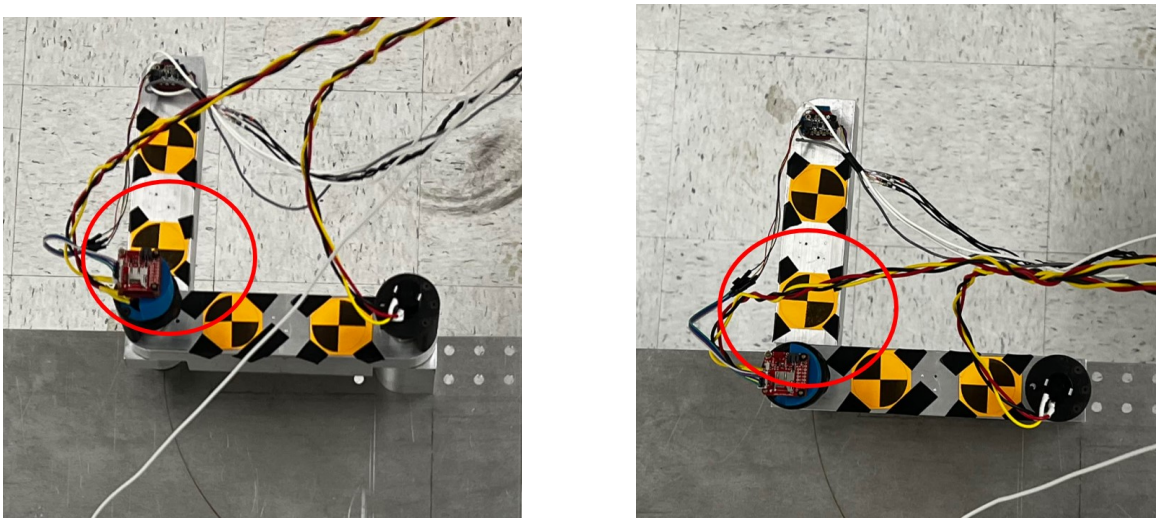

(a) Original camera positioning (b) Optimized camera positioning

Figure 6.2: Different positioning of the camera allows for change in performance of ground truth measurement.

The ground truth measurement used for comparison of estimations presented in this thesis are all produced with visual motion tracking techniques. In order to measure the true actual positions of the two links of the experimental test system, the system was modified to make possible proper observability of the links with a camera from above. Wires were tucked in positions making the sight of the links visible during recording. TEMA Motion Analysis is commonly used for tracking the motion of points of interest, and is capable of tracking 2D motion of the yellow and black quadrant symbols stuck to different points of interest. The technology has been extended to track motion in 2.5D with calibration for depth in between targets. Similarly, the tracking required during experimentation only of planar motion of the links was accomplished with image processing. The method used for tracking the links is heavily influenced by the work of TEMA Motion Tracking, using the distinct coloration of quadrant targets to measure the pose of the system. The camera used was a GoPro

Hero 7 capable of 240 fps, a faster frame rate than data acquisition using Arduino. Firstly, the camera was posed to best influence the observation of the entirety of the motion, targeting the visibility of the quadrant symbols throughout the motion. The camera is positioned so that the background in the images is minimized as originally considered as opposed to keeping better observability in mind, as seen in Fig. 6.2. Two black and orange quadrant symbols were attached to the links of the system and the platform for measuring final velocity of the platform prior to collision, also seen in Fig. 6.2. The redundancy is used to compensate for when a target may not be seen due to visual obstruction, making image processing for pose impossible. Distortion of the images recorded due to shape of the lens was compensated for with camera calibration. The image processing as required for the ground truth measurement first takes a color gradient of the image to filter for where distinct color changes are visible. With the quadrants of different distinct colors, the targets are fairly easily found by looking for lines within the color gradient with a minimum length. Crossed lines found indicate a found quadrant symbol within the image, pinpointing observation of the link in that system. This is illustrated in Fig. 6.3 where the targets spotted on the link to the right are marked with yellow dots while the other blurrier target was

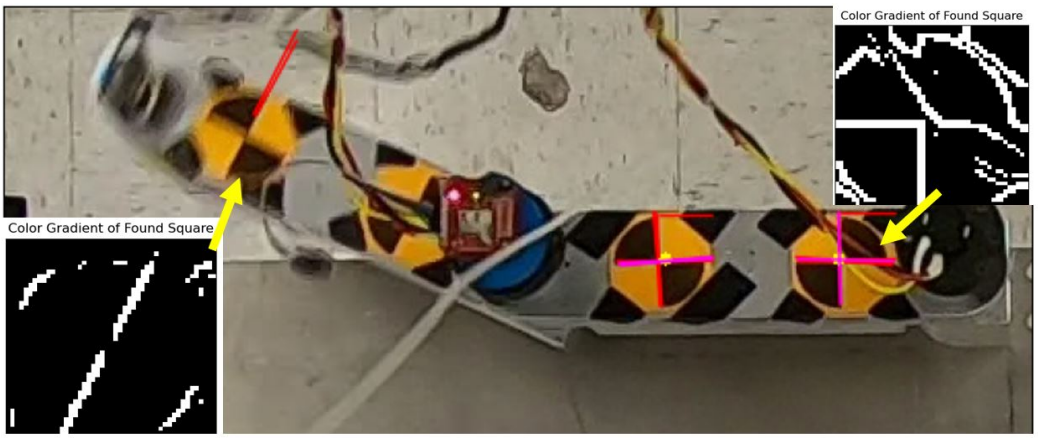

Figure 6.3: Images of the required processing to output a ground truth orientation of the links.

missed.

Figure 6.4 shows an example of images captured for measuring the ground truth positioning of the links as the motion occurs. Within the images are a few distinct swing poses well observed regardless of the intensity of the motion that may be useful for qualitatively analyzing the performance of the estimation methods.

At the moment of the collision with the stopper, link 2 rotates ahead of link 1, and then completely rotates once link 1 has stopped rotating, as seen in Fig. 6.4. Measurement of the change in q_2 prior to when the motion stops at q_1 is an indicative feature of the accuracy of the estimation methods.

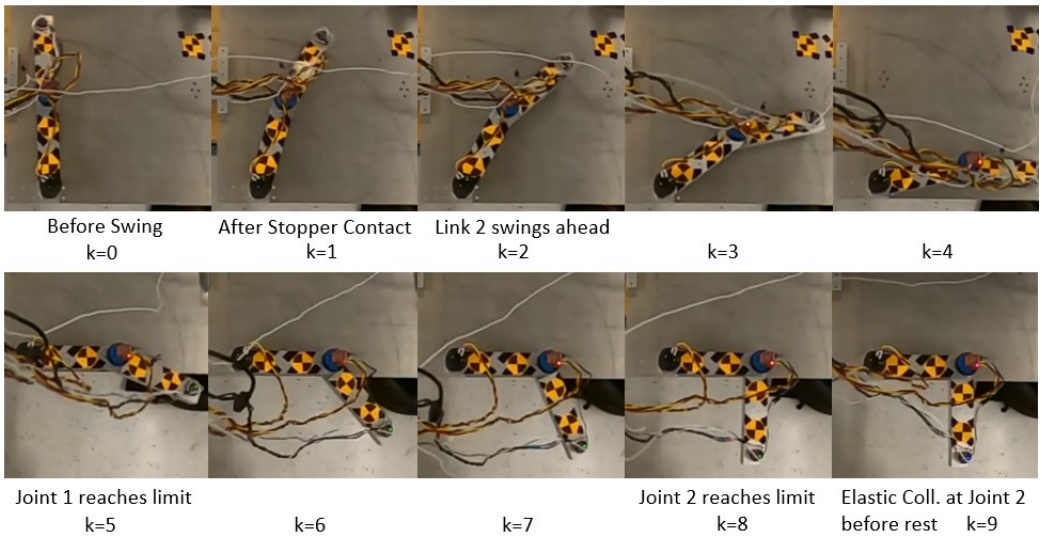

Figure 6.4: Images from above of the swinging motion of the 2DOF system after impacting the stopper.

6.2 Dynamic Measurement Fusion with 9DOF IMUs in Uniform Field

6.2.1 Experimental Configuration

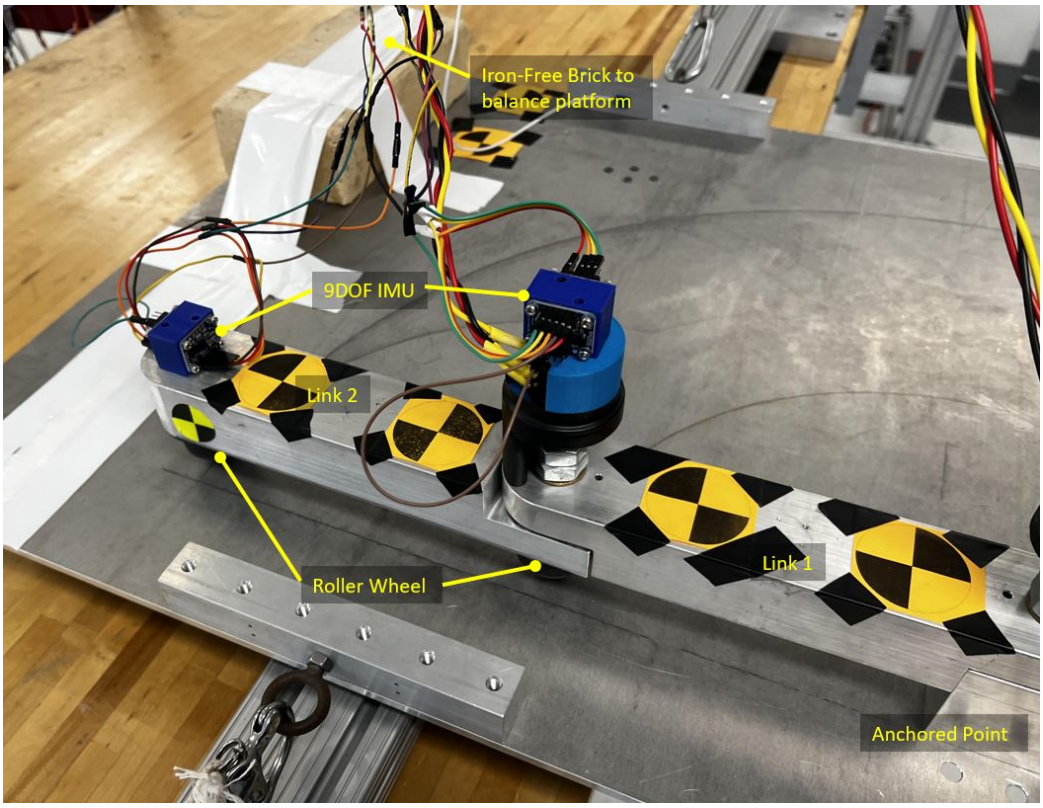

Figure 6.5: The distortion-free experimental setup used to induce and measure a highly dynamic swinging motion with dynamic measurement fusion.

To demonstrate the motion tracking of highly dynamic multi-link bodies, a model problem of a two-link body is considered. The system used to simulate a highly dynamic swing as described in Section 6.1 is used. As the objective is to track the rotations of links of a multi-link body using only externally mounted sensors, IMUs are installed on each link to measure the motion of the links. Dynamic Measurement

Fusion changes the role of accelerometers from linear translation estimation to another measurement of angular velocity with measurement of centrifugal forces. With redundancy of measurements to states being estimated, error of the estimated states is expected to be minimal compared to reliance on only gyroscopes for rotational rate measurement. To prevent nonuniformity of the magnetic field throughout the space the links travel through, ferrous pieces were removed from proximity of the motion. Iron pieces used on the sled were replaced to pieces of different materials so there are no contributors to nonuniformity of the magnetic field. One example of material switched is the iron blocks clamped to the top right of the platform as seen in Fig. 6.5 being replaced with a taped brick for balancing the platform so that there isn't a torsion along the tracks as the platform translates down to the stopper.

Usage of the camera for ground truth measurement is described in Section 6.1. Unlike a conventional technique assuming a uniform magnetic field that assumes a quasi-static motion where the acceleration is negligible, this approach considers the multi-link body at high-speed angular motion.

As the experimental setup is configurable to change intensity of the motion, three different intensities of motion were trialed. Table 6.9 lists the physical parameters of the experimental setup, as well as sensors used for experimentation. The system links are initially pointed perpendicular to the motion of the platform described in section 6.1. The initial poses used are so that plotted estimations do not overlap and are more visible for analysis.

Table 6.1: Parameters of the two-link system tests

Parameter	Value
Link lengths $l_1 = l_2 = l$ [m]	0.25
Link mass $m_1 = m_2 = m$ [kg]	0.5
Initial pose $\mathbf{q}_0$ [rad]	$[-\pi/2, 0]^\top$
Platform collision velocities [m/s]	1.43, 1.83, 2.1
IMU	BNO055 unit, Bosch Sensortec

6.2.2 Tracking of Time-varying Motion

Experimentation using a real linkage system is investigated to further determine capability and limitations of the proposed technique not observable in the simulated surrogate model. Since drift caused by net system translation is well studied and can be corrected by conventional techniques, only drift in angular motion is targeted. The initial velocity 2.1 m/s of the platform prior to collision, which is high speed for this class of system, is used to observe the effects of the intensity of the motion to the estimation.

Figure 6.6 shows the snapshot of the motion tracked by the proposed technique at every three intervals of motion recorded every 0.12 s. Links 1 and 2 are shown in black and red, respectively, whereas the true motion measured by the camera is shown with blue broken lines. The result shows that the proposed technique estimates the states of the links with consistently small error that match well with the ground truth. The largest error is found when the system is moving fast. While the magnetometer measurements globally correct the link orientation, the error tends to be larger during the high-speed motion.

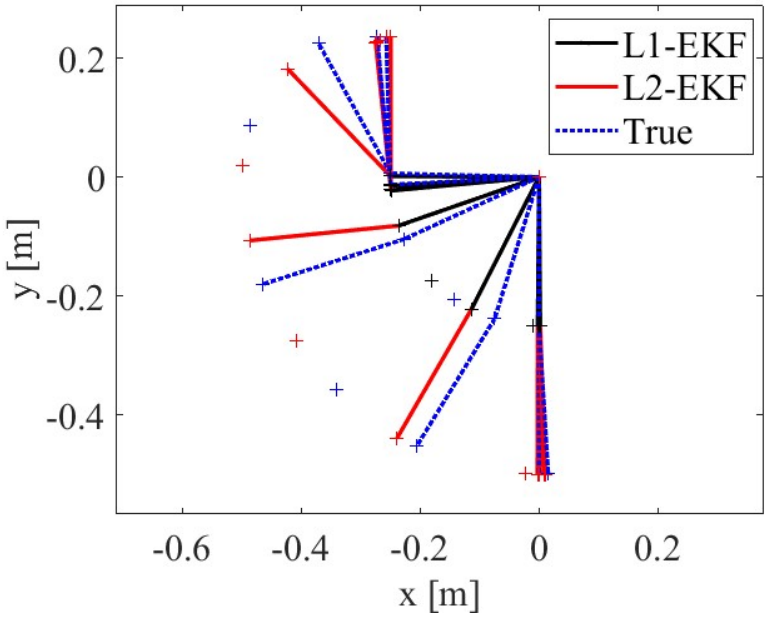

Figure 6.6: A simulated swinging motion of the links.

After the initial collision, link 2 rotates ahead of link 1, and then completely rotates once link 1 has stopped rotating, as seen in Fig. 6.6. These motions, visible in the images of the motion, are well observed in the estimations. The estimation results observe the change in q_2 prior to when the motion stops of q_1.

To quantify the time-varying motion in more detail, Fig. 6.7 plots the estimated states of link 1 and link 2 for the test with respect to time together with the true motion. For comparison, the orientation of the links based on raw magnetometer measurements and the states estimated by the conventional technique are also shown, which are given by markers and green lines, respectively. It is to be noted that gravity's effect on this experiment is neglected since the system's motion resides only through the ground plane. It is first seen that the proposed technique estimates the states close to the ground truth over the highly dynamic motion while the conventional technique exhibits significant drifts. The drifts begin to accumulate when the system starts

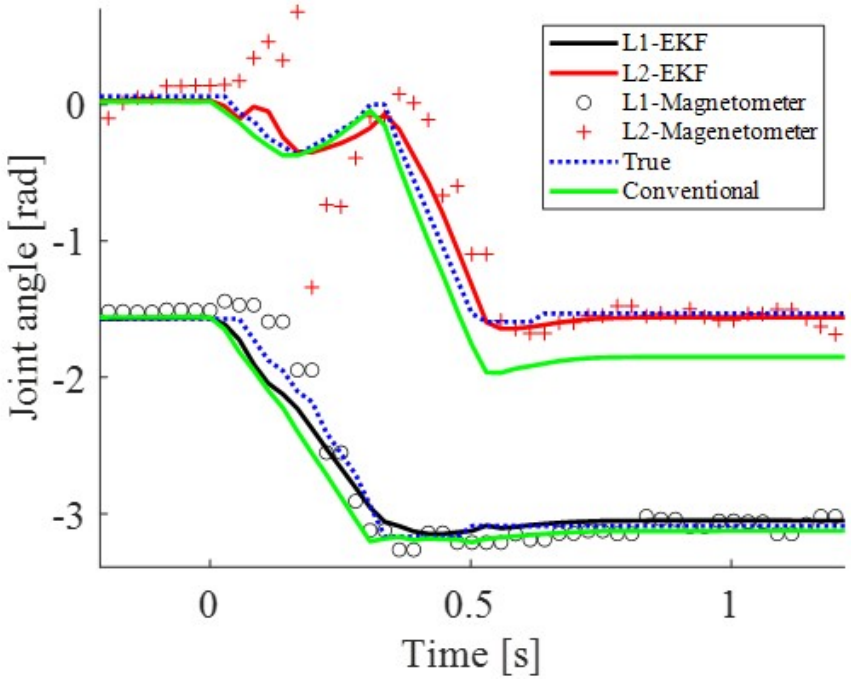

(a) The joint angle results of the proposed method, conventional reliance on gyroscopes to correct angular velocity, ground truth position, and orientation based magnetometer measurements.

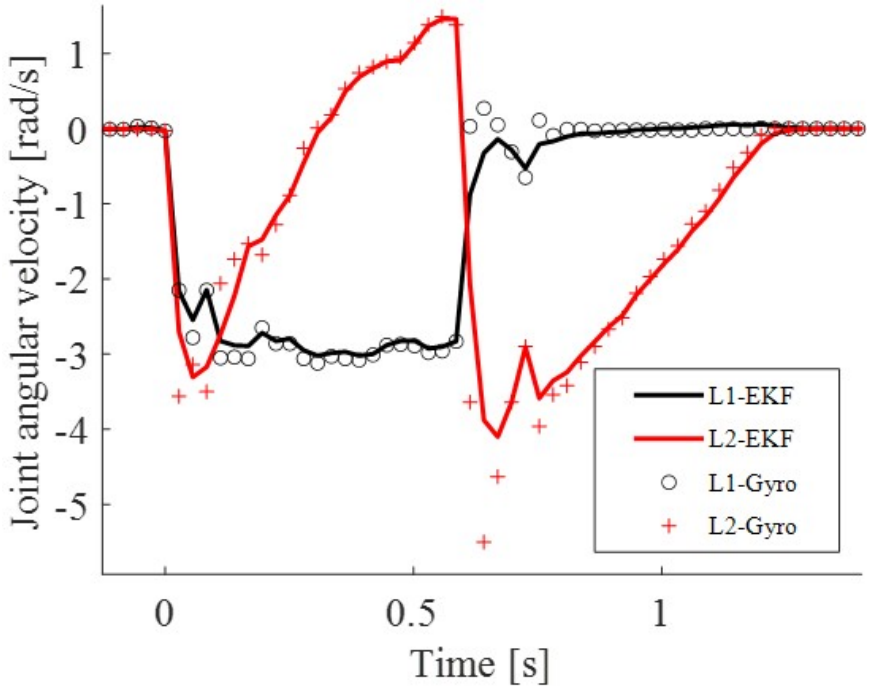

(b) The estimated angular velocities of the joints of the system, and the gyroscope measurements for comparison.

Figure 6.7: The joint angle and rotational rate results of the conventional method, the proposed estimation method, and the ground truth of both links.

to move highly dynamically. The noise of the global corrector is observable in the results from the magnetometer measurements. While the magnetometer corrects the angle estimation with the conventional technique, the estimation did not converge to the true state until more than two seconds after the motion was completed. Figure 6.7 shows the estimated angular rotation of the links along with the rotational rate used by the conventional method based on gyroscope measurements. The accumulated drift of the gyroscope is clear in the estimated joint angles by the conventional method.

6.2.3 Effect of Speed

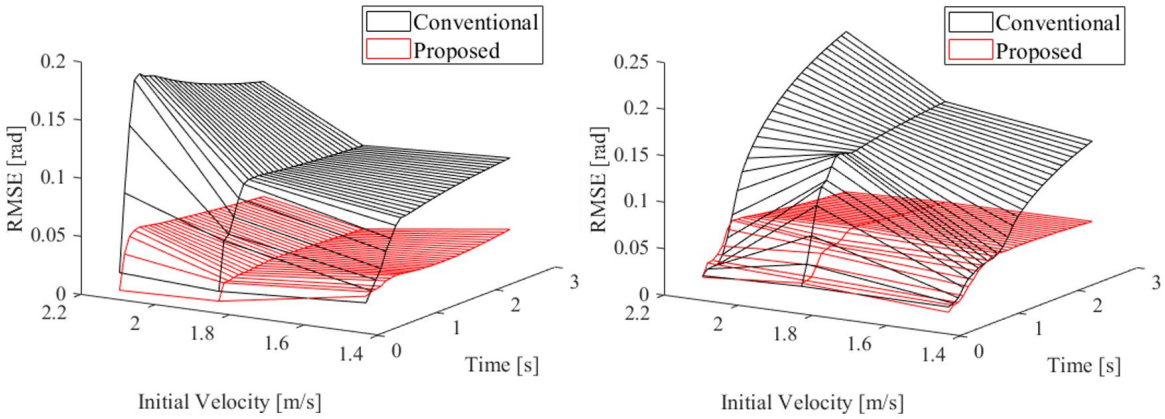

(a) Link 1 (b) Link 2

Figure 6.8: Root Mean Square Error of each link with various initial velocities

The Root Mean Square Error (RMSE) of the estimations over time, using different initial velocities, is plotted in Fig. 6.8. The red surface is the result of the proposed technique, whereas that of the conventional method is shown in black for comparison. The RMSE of the joint angles remains below 3.4°(0.06 radian) constantly for the proposed technique, regardless of the speed and time. This indicates that the proposed technique can accurately estimate the states not only at high speed, but also for a wide range of motion speed. The efficacy of the proposed technique is clear in its

comparison to the conventional technique. The RMSE of the conventional technique is several times more than that of the proposed technique and is more significant at high speed, which includes results with high initial velocities. Using the conventional technique with the highest initial velocity, the RMSE of link 2 is larger than that of link 1, as link 2 swings faster and more intensely. While the conventional methods work well with slower speeds, indicative by the decrease in error with slower initial velocity, the maximum RMSE is found to be eight times greater for the conventional method than the proposed method.

6.3 Coupled Magnetometers in Nonuniform Magnetic Field

6.3.1 Experimental Configuration

To demonstrate the motion tracking of a highly dynamic multi-link body in a nonuniform magnetic field, a model problem of a two-link body is considered. To simulate motion tracking in an environment with a nonuniform field, ferrous structures are added to the environment. Distortion to the magnetic measurements is assumed to be caused by materials in the environment, and not due to ferrous materials in the bodies being tracked. For this experimentation, it is assumed that the bodies being tracked are maneuvered with ferrous structures that motions are tracked with respect to. Similar to a dummy being tracked in a vehicle frame, a multi-link system being tracked on a chassis used to move it around, or humans being tracked around ferrous props, the reference ferrous structures are assumed to be the only source of magnetic distortion to the the locally uniform earth's magnetic field.

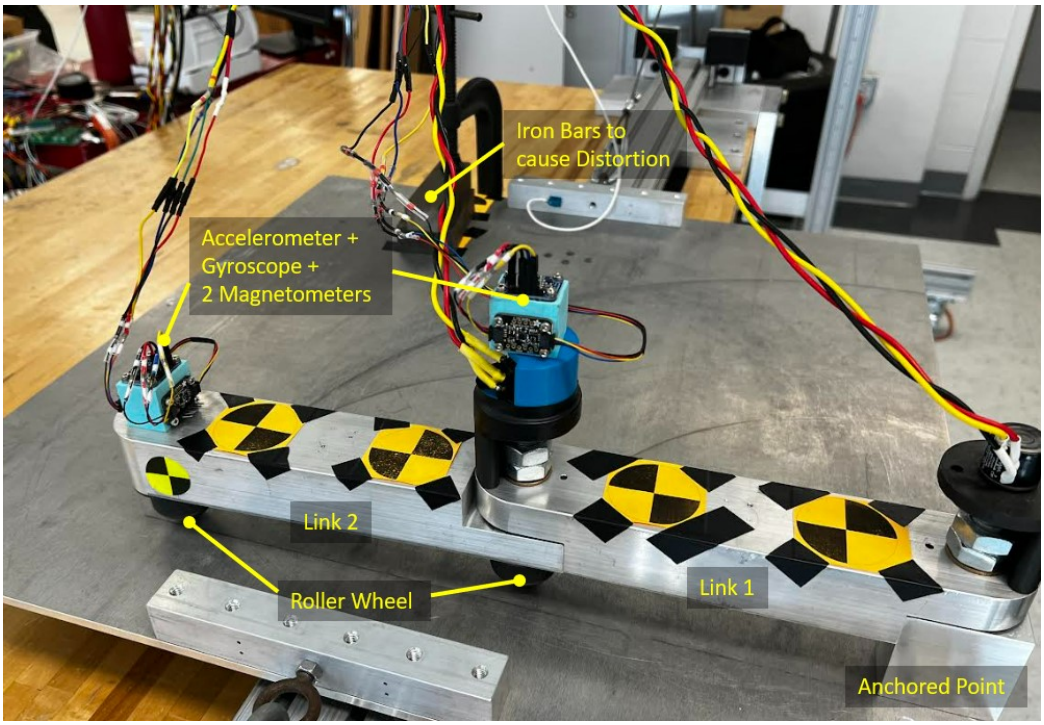

Figure 6.9: The experimental setup used to induce and measure a highly dynamic swinging motion in a distorted field with dynamic measurement fusion and coupled magnetometers.

Table 6.2: Parameters of the two-link system tests

Parameter	Value
Link lengths $l_1 = l_2 = l$ [m]	0.25
Link mass $m_1 = m_2 = m$ [kg]	0.5
Initial pose $\mathbf{q}_0$ [rad]	$[-\pi/2, 0]^\top$
Platform collision velocities [m/s]	1.43, 1.83, 2.1
IMU	BNO055 unit, Bosch Sensortec
Coupled Magnetometers	LIS3MDL unit, STMicroelectronics

A camera is placed above the planar motion for measuring the motion to compare to the estimation results as described in Section 6.1. To produce nonuniformity of the magnetic field through the space traveled by the multi-link system, ferrous blocks are mounted to the platform in proximity to the motion. The nonuniformity of magnetic north within the space is observed with a compass, as seen in Fig. 6.10. As the experimental setup is configurable to change the intensity of the motion, three

different intensities of motion were trialed. Table 6.9 lists the physical parameters of the experimental setup, as well as sensors used for experimentation. The system links are initially pointed perpendicular to the motion of the platform described in section 6.1. The initial poses used are so that plotted estimations do not overlap and are more visible for analysis.

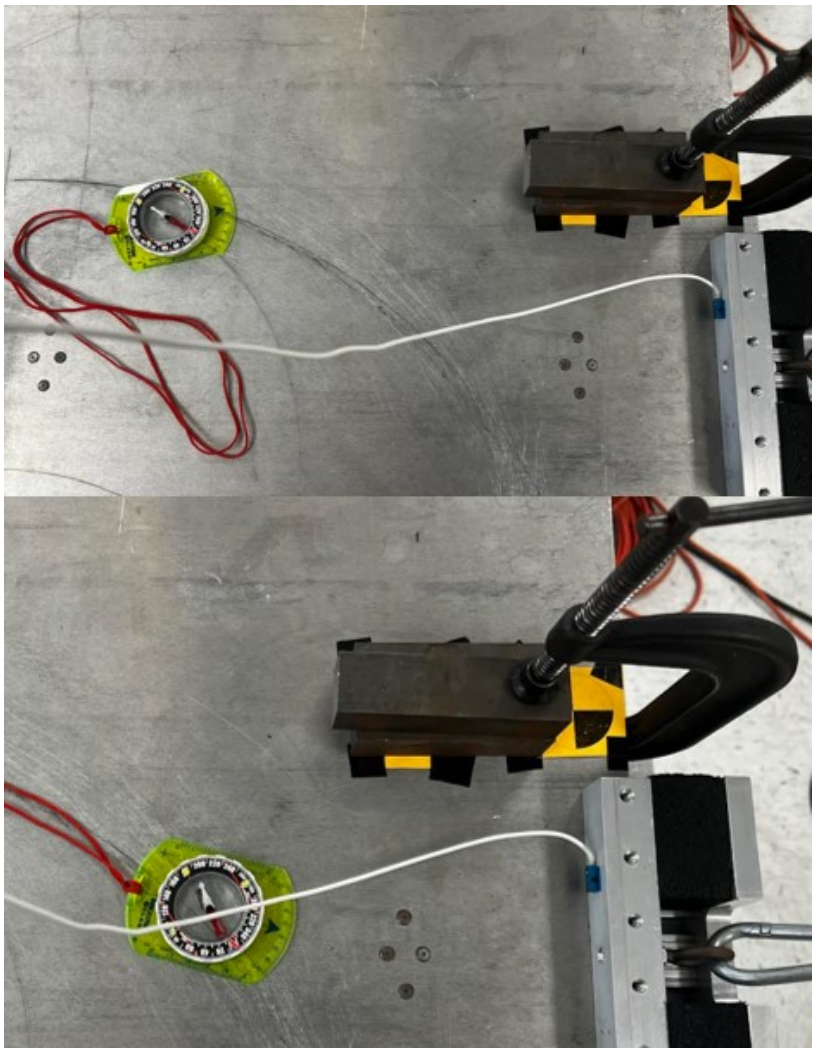

Figure 6.10: Observed nonuniformity of the magnetic field throughout the space traveled through by the multi-link system.

6.3.2 Tracking of Time-varying Motion

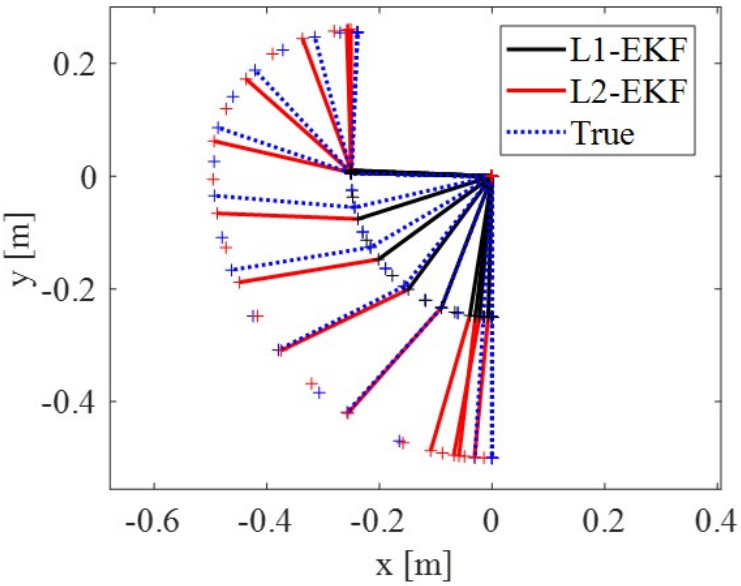

Figure 6.11: A simulated swinging motion of the links.

Experimentation using a real linkage system in a manufactured nonuniform magnetic field is investigated to further determine capability and limitations of the proposed technique not observable in the simulated surrogate model. Because the system's motion resides only through the ground plane, gravity's effects on the motion can again be neglected. This experimentation is used determine the effectiveness of global correction in nonuniform magnetic fields. As the motion tracking method used accurately measures rotational rate of links compared to the integration of gyroscope measurements, only the effects of magnetic distortion to the correction of the estimation are considered. The initial velocity 1.43 m/s of the platform prior to collision, which is the lowest speed for this series of tests, is used to better observe the effects of the nonuniform magnetic field to the estimation. Figure 6.11 shows a snapshot of the estimated motion at every three intervals recorded every 0.12 s, indicating that the constrained swing of the links is well observed by the IMUs.

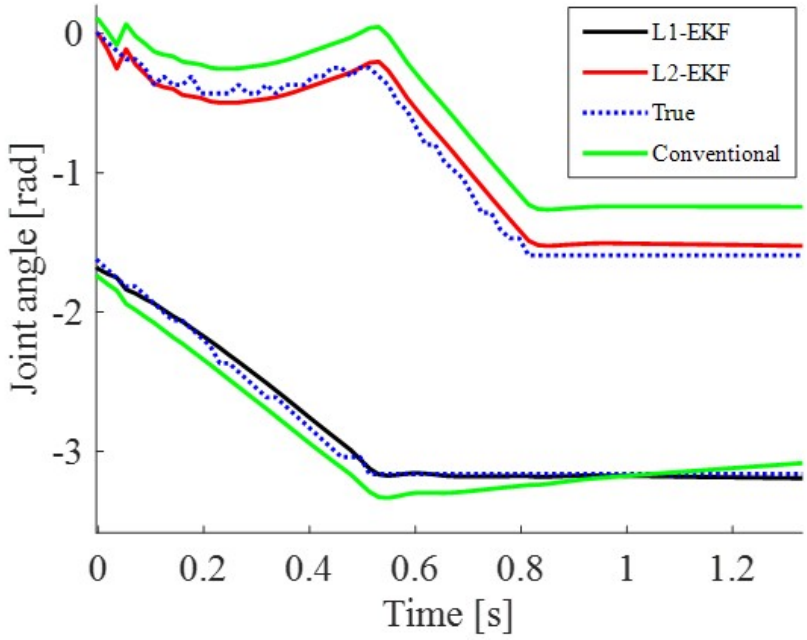

(a) The joint angle results of proposed magnetometer usage, the conventional usage referencing the initially measured magnetic north, and ground truth position.

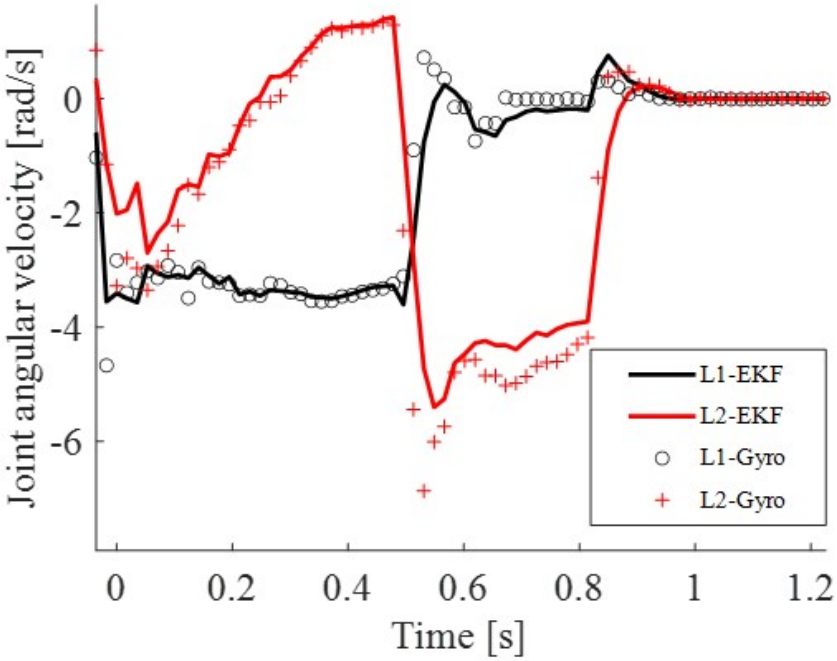

(b) The estimated angular velocities of the joints of the system, and the gyroscope measurements for comparison.

Figure 6.12: The state results including the joint angles and angular velocities of the links of the system.

The states of link 1 and 2 estimated with the proposed sensor model and real time calibration during the duration of the motion, along with the true motion, with respect to time, are plotted in Fig 6.12. For comparison, the orientation of the links based on raw magnetometer measurements and the states estimated using the conventional magnetometer sensor model and calibration prior to the motion, both with respect to the initially measured magnetic north, are shown by markers and green lines, respectively. Figure 6.13 plots the estimated orientations with time prior to and after the motion to better observe the variation of magnetic north throughout the space. Although the inconsistency of magnetic north causes an offset of the state prior to the motion using the proposed method, the change of orientation is well observed during the duration of the motion as seen in Fig 6.12. The state estimated by the conventional method prior to the motion only varies slightly from the true position, but ends away from the true position at the end of the motion. The expected correction of the state at the end of the motion diverges from the true state using the conventional method

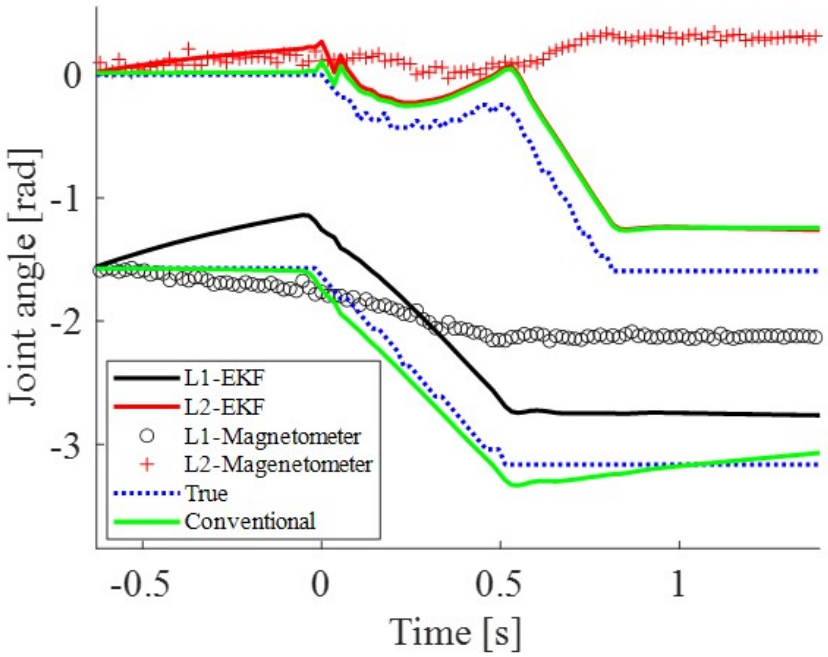

Figure 6.13: The joint angle estimation results of both links, as well as the pose based on initial magnetometer measurement in nonuniform magnetic field.

with inconsistent magnetic north. The estimated state after the motion using the proposed method does not diverge from the true position, as no change in magnetic north is measured.

6.3.3 Effects of speed

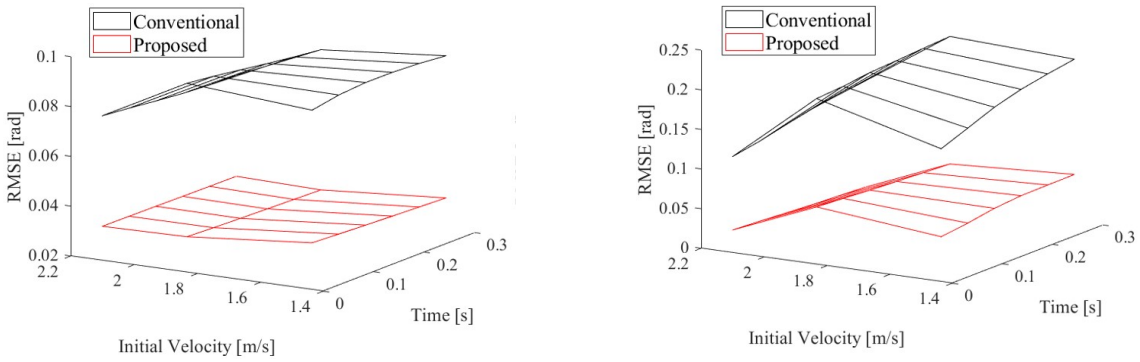

(a) Link 1 (b) Link 2

Figure 6.14: Root Mean Square Error of each link with various initial velocities

The Root Mean Square Error (RMSE) of the estimations over time, using different initial velocities, is plotted in Fig. 9. The red surface is the result of the proposed technique, whereas that of the conventional method is shown in black for comparison. The RMSE of the joint angles remains below 2.86°(0.05 radian) during the duration of the motion for the proposed technique for all speeds tested. This is indicative of the efficacy of the proposed sensor suite and model for the magnetometers, for a wide range of motion intensities. The RMSE of the conventional technique is consistently several times more than that of the proposed technique, reaching a maximum of five times more than that of the proposed method.

Chapter 7

Proof of Concept Humanoid Tracking

7.1 Application of Dynamic Measurement Fusion

7.1.1 Kinematic of Multi-link System

One application of motion tracking of a highly dynamic, multi-link system is tracking of humanoids. Humanoids can be generalized as multi-link systems for the kinematic models used for the estimation of motion. The method of dynamic measurement fusion is used to estimate the rotations of links with respect to other links. With no point of the multi-link system anchored to a reference point, the positional and rotational motion of at least one link must be tracked, allowing dynamic measurement fusion to estimate the rotations of the other links with respect to the pose of the tracked link. Any part still observable for visual motion tracking of the multi-link system of interest can be used as a reference link for estimating the absolute position of the system.

Consideration of the motion constraints of joints is conducted to produce a kinematic model of a humanoid. In order to properly estimate the motion of a humanoid, a kinematic model for the links of the humanoid must be constructed. Required for

a motion model are the constraints of each of the joints connecting the linkages of the test dummy. There are two types of matrices used to model the kinematics of a system: (1) a joint matrix used to map the transformation between the coordinate frames of links in a system that may change over time and (2) a shape matrix used to map the transformations between coordinate frames on a linkage that remains static, assuming no deformation to bodies tracked. For the intended implementation, shape matrices map both joint positions and sensor positions per link of the system. The transformations between points on a linkage of the multi-link system of interest can be measured with a coordinate measuring machine (CMM) or using CAD.

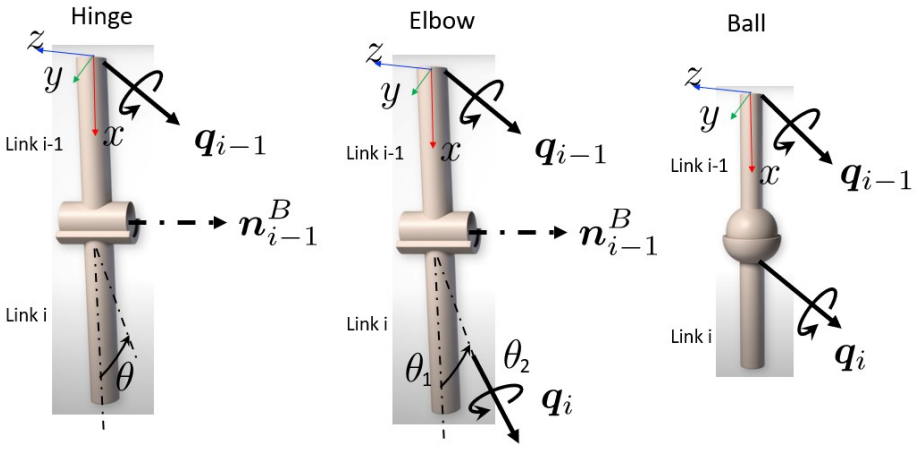

Figure 7.1: Joint types found in multi-link systems such as humanoids.

The different joint types considered for construction of a kinematic model of the humanoid systems are hinge joints, elbow joints, and ball joints. The degrees of freedom of each of the listed joint are diagrammed in Fig. 7.1. These joints are modeled as the coordinate frame transformations that occur at each joint between links as joint matrices. The transformations at these types of joints only occur as rotations, as positional motion is constrained by these joints. The transformations are modeled with Euler angles or quaternion depending on the degrees of freedom of the joint.

One degree of freedom rotation joints, better known as revolute or hinge joints, constrain two links with a rotation around one axis between the joints, as seen in Fig. 7.1. Some examples of one degree of freedom joints on humans are knees or knuckles. To construct the joint transformation matrix, the hinge joint rotation around one axis with angle θ can be found with Equation 7.1.

$$\mathbf{\Phi}_j(\theta) = \begin{bmatrix} \cos(\theta) & -\sin(\theta) & 0 \\ \sin(\theta) & \cos(\theta) & 0 \\ 0 & 0 & 1 \end{bmatrix} \tag{7.1}$$

The next type of joint modeled for humanoids are joints that are constrained like a hinge joint experiencing flexion and extension, and rotation around the direction that the link faces due to the hinge joint experiencing pronation and supination. One example of this type of joint on humans is the elbow. As an extension to the hinge joint, the rotation around the rotated axis is represented with a second angle θ_2 to the calculation of the joint matrix as seen in Equation 7.2.

$$\mathbf{\Phi}_j(\theta_1, \theta_2) = \begin{bmatrix} \cos(\theta_1) & -\sin(\theta_1) & 0 \\ \sin(\theta_1) & \cos(\theta_1) & 0 \\ 0 & 0 & 1 \end{bmatrix} \begin{bmatrix} 1 & 0 & 0 \\ 0 & \cos(\theta_2) & -\sin(\theta_2) \\ 0 & \sin(\theta_2) & \cos(\theta_2) \end{bmatrix} \tag{7.2}$$

For joints allowing rotations in three degrees of freedom, or ball joints, no physical constraint is modeled to constrain the possible rotation of the joint. Shoulder, ankle, and pelvic joints are all examples of ball joints found in humans. Although the rotation of the physical joints is limited due to linkages not being able to pass through each other or due to limited extention or mobility of limbs, no feature of the joint constrains the rotation. Equation 7.3 shows the joint matrix of the ball joint using

quaternion to avoid gimbal lock in representing the rotation in the three degrees of freedom.

$$\mathbf{\Phi}_j\left(q_1, q_2, q_3, q_4\right) = \begin{bmatrix} q_4 + q_1 - q_2 - q_3 & 2(q_1 q_2 - q_4 q_3) & 2(q_4 q_2 + q_1 q_3) \\ 2(q_1 q_2 + q_4 q_3) & q_4 - q_1 + q_2 - q_3 & 2(q_2 q_3 - q_1 q_4) \\ 2(q_1 q_3 - q_2 q_4) & 2(q_4 q_1 + q_2 q_3) & q_4 - q_1 - q_2 + q_3 \end{bmatrix} \quad (7.3)$$

These matrices mapping transformations at joints of connected linkages, along with the shape matrices used to map sensor locations and centers of mass for linkages in each degree of freedom are used to estimate motion of these complex systems.

7.2 Motion Tracking of Arm in Nonuniform Magnetic Field

7.2.1 Experimental Configuration

Sensor Mounts

In order to track a motion with more complexity than the two degree of freedom system, sensor mounts need to be designed to make sensors wearable to the humanoid subject. The mounts used must provide a surface for two things: sensors used for estimation of motion and visual motion tracking markers for ground truth measurement. Ground truth measurement is recorded for comparison of estimated states.

Sensor mounts designed with mounting points for both visual markers and sensor

mounts in mind were prototyped for mating to surfaces on dummies. The mounts were modified to be wearable with adjustable elastic Velcro straps to maximize stability to linkages as seen in Fig. 7.2. The wearable mounts were fitted with threaded inserts

(a) OptiTrack motion capture results

(b) Trajectory with interpolated points

Figure 7.2: OptiTrack motion capture with positions and local orientations, and interpolated points to fill in missed time steps for ground truth comparison.

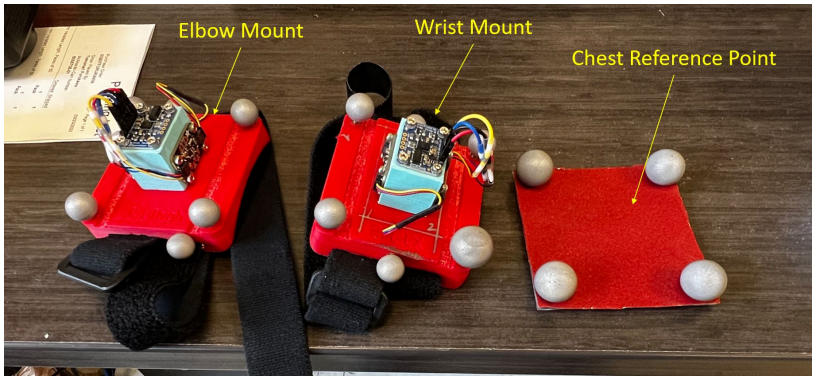

Figure 7.3: The sled buck used for better observing the motion of the test dummy with visual systems during a crash test.

to install the motion and magnetic sensors used for experimentation. The same prototype sensor package used for the two degree of freedom testing in a nonuniform magnetic field is used on the wearable mount with visual markers. The first motion of concern for this experimentation being measured is the rotations of the upper and lower arm with respect to the chest. As the pose of the chest link is only being used

as a reference, no usage of mounted motion or magnetic sensors is required for it. The third wearable mount fitted with just OptiTrack markers can be seen in Fig. 7.3

7.2.2 Dynamic Measurement Fusion with Coupled Magnetometers

To prove the efficacy of the usage of dynamic measurement fusion and the usage of coupled magnetometers, complexity of the two link motion is increased. For the application of dynamic measurement fusion to the targeted system, the kinematics of the system must be modeled, accounting for the positioning of sensors and joints per link.

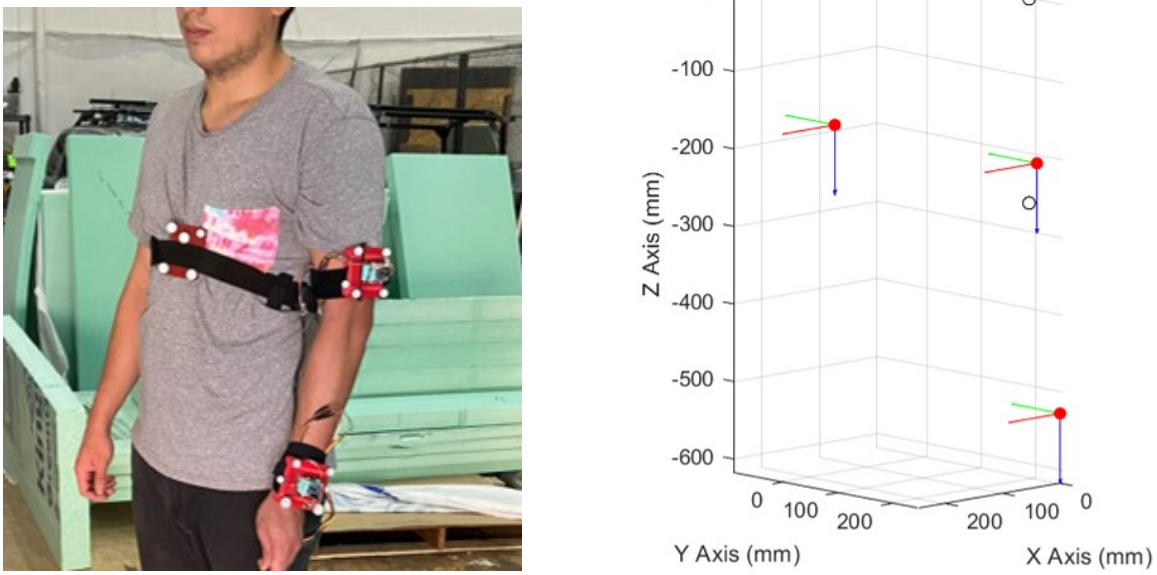

(a) OptiTrack motion capture results (b) Trajectory with interpolated points

Figure 7.4: OptiTrack motion capture with positions and local orientations, and interpolated points to fill in missed time steps for ground truth comparison.

Positions of Joints and Sensors

Dynamic measurement fusion uses an EKF framework to estimate the angular rotations and rates of links with respect to other links in the system. In order to predict the motion of the links, a motion model must be constructed. By utilizing joints as motion constraints, rotations of links can be modeled. The transformations between sensor and joint positions are important to the construction of the kinematic model for the system of interest. While wearing the sensors in the initial positioning used in experimental testing, the pose of sensor mounts and joints were measured using rulers. The positions of the sensors along with the positions of joints is modeled as seen in Fig. 7.4. Orientations of the links are visualized using SAE coordinate frame directions.

7.3 Application to Test Dummy

7.3.1 Experimental Configuration

Sensor Mounts

Sensor mounts stable to the links are required for motion tracking of the system to prevent misreads in measurements. If, throughout the measurement, the sensors move from the positions they were installed to on the links, the motion of the sensors becomes different than the motion of the links, causing misreads. For that reason, careful consideration of mounts acceptable for tracking the highly dynamic motion of a test dummy is required. Sensors, as well as OptiTrack motion capture markers, must be attached to each link of interest on the dummy. Motion capture markers

were required to be installed externally on the head, torso, pelvis, left thigh, left lower leg, and left foot. In the torso, head, and pelvis of the dummy, the accelerometers and gyroscopes were mounted to the internal structure of the dummy, providing its rigidity. As some of the pieces providing rigidity to the structure of the dummy are made of ferrous material, they cause distortion to the measured magnetic field in proximity. To prevent distortion of signals due to factors of the dummy, the magnetometers and markers were prepared to be mounted externally to each link. For links without internal locations, including the thigh, lower leg, and foot, accelerometers, gyroscopes, magnetometers, and markers are required to be mounted externally.

The Center of Applied Biomechanics (CAB) at the University of Virginia had previously experimented with externally mounted sensors on dummies. Mounts were taped to surfaces with double sided 30 lb test adhesive. When mounting a sensor to a skin contact point, gaffers tape was applied to the surface to protect the material of the dummy skin. In locations where there was concern of falling off with movement, the mounts can be secured with zip-ties using guides on the mounts to prevent movement. With some guidance, the following targeted components are used to ensure that the sensor mounts remain in contact with and stable to the links:

- Maximize surface area of sensor mount by initially relying on 30 lb tested double-sided adhesives and using zipties/straps for additional insurance, and
- Mating of surfaces to make perfect contact with the surface being taped to, as gaps and air pockets can lead to failure of local adhesive tape.

Using CAD as seen in Fig. 7.5, mounts are crafted by mating the surfaces of the parts on the dummy and the mounts developed with desired surface posing. The prototyped and fitted wearable mounts used to install sensors and visual motion tracking markers

to the skin of the parts of the dummy of interest can be seen in Fig. 7.6. Not all wearable mounts of the dummy needed to be mounted to the skin surface, as some parts of the dummy had exposed framework that can be used as rigid structures to mount to. One example of this is the mounting point used to secure the visual tracking markers to the torso of the dummy to measure the ground truth pose.

Luckily, an anchor point for an exposed sensor mounting location not covered by the skin is found at the top of the spine of the dummy for mounting motion-tracking markers, as seen in Fig. 7.7. Optical markers were taped and glued in an asymmetrical pattern on the face of the dummy for ground truth measurement. With the mounting location for optical markers and sensors exterior to the all links of interest accounted for, any extra sensors to be mounted to the exterior of the dummy can be considered.

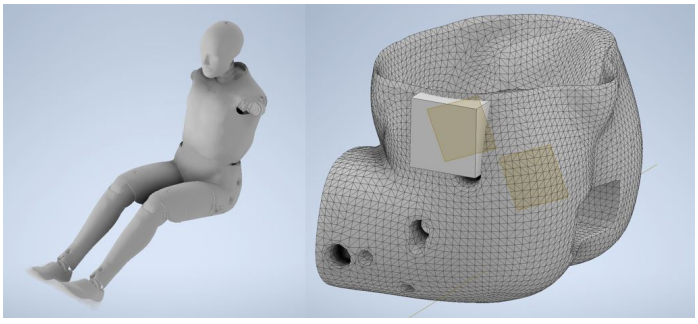

Figure 7.5: The joint angle and rotational rate results of the conventional method, the proposed estimation method, and the ground truth of both links.

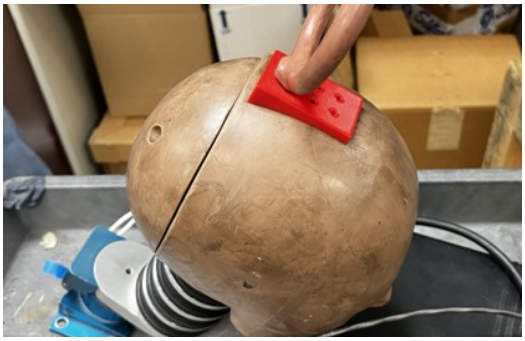

(a) Head mount with placement of magnetometer top rear.

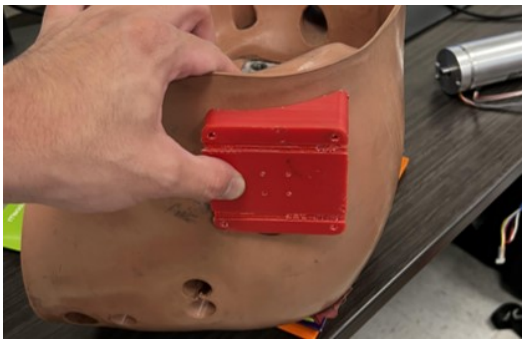

(b) Sensor and marker mount for the pelvis.

(c) Sensor and marker mount for the thigh.

(d) Sensor and marker mount for the lower leg.

(e) Sensor and marker mount for the thigh for the shoe.

Figure 7.6: Prototype sensor mounts 3D printed for fitment adjustments prior to the real crash test.

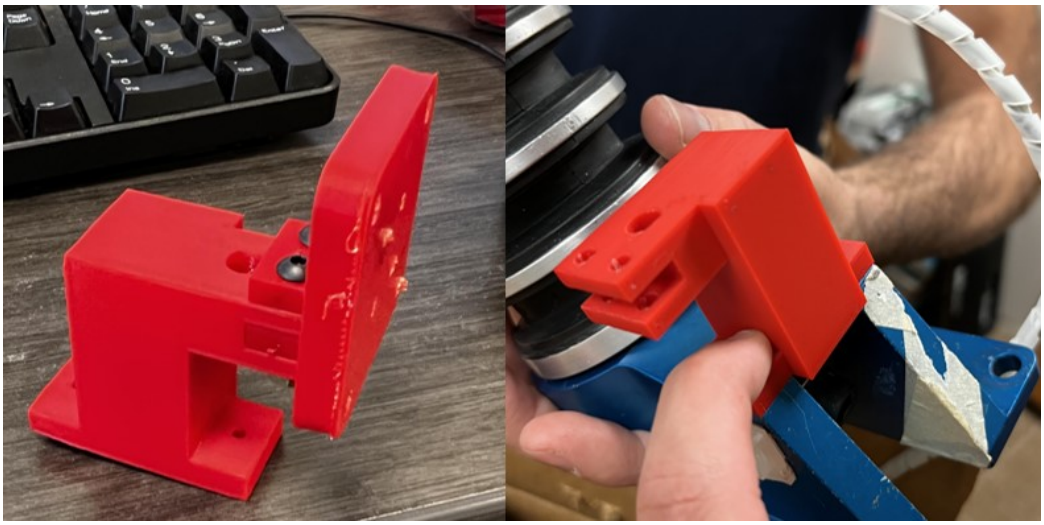

Figure 7.7: Data collected while walking through electrical room with constant heading

Extra Accelerometer Installation

The utilization of dynamic measurement fusion changes the number of sensors within an IMU used to measure the rotational rate of an object. The approach takes advantage of measurement redundancy to better observe a state of interest, adding a dimension to measurement, similar to how two cameras compare to a monocular camera. Keeping in mind the motivation behind the new sensor method, what might utilizing a third sensor on a link do to improve the measurement of a motion? Given that space and cost requirements, aside from the positions on the dummy that may be obstructed in motion, were not of concern, an extra accelerometer pointed to measure centrifugal acceleration was placed on the upper leg, lower leg, and foot, and an extra

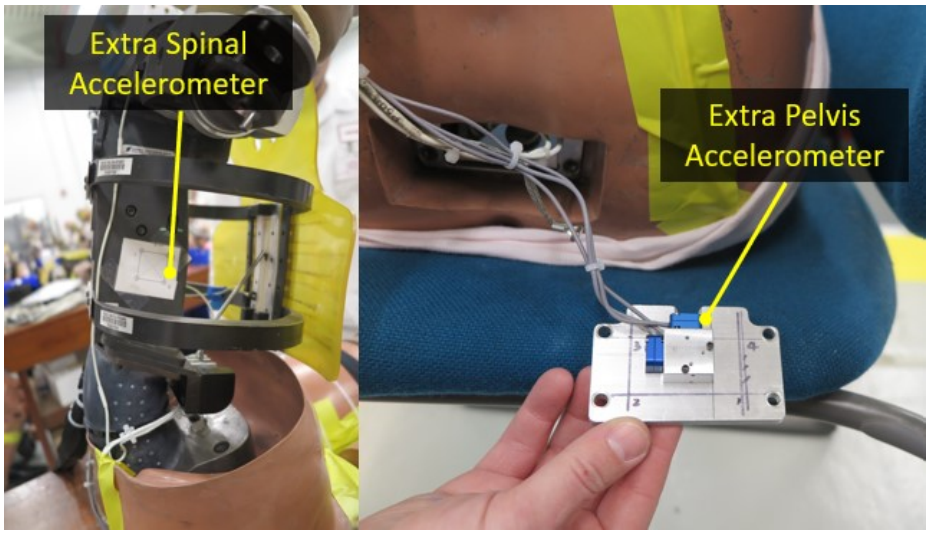

Figure 7.8: The sled buck used for better observing the motion of the test dummy with visual systems during a crash test.

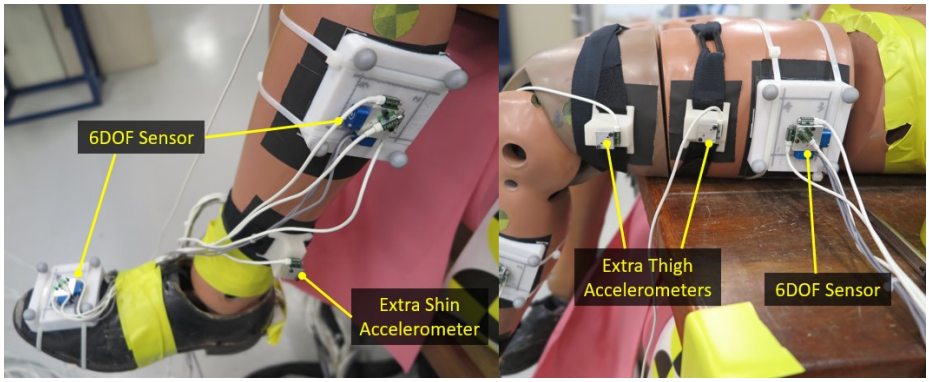

Figure 7.9: The sled buck used for better observing the motion of the test dummy with visual systems during a crash test.

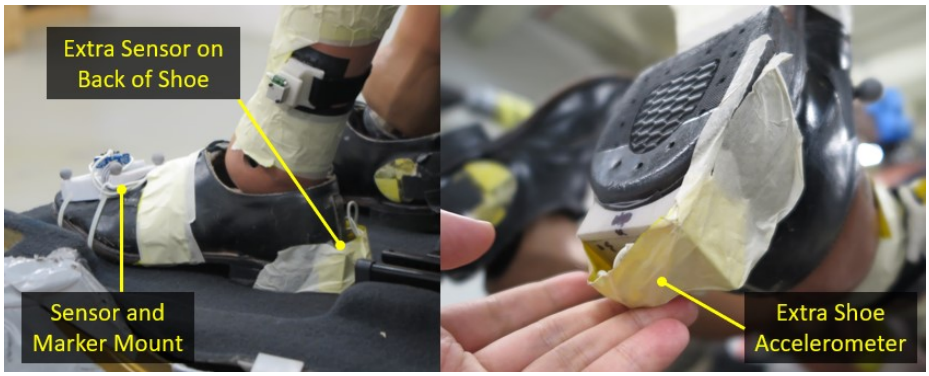

Figure 7.10: The sled buck used for better observing the motion of the test dummy with visual systems during a crash test.

single axis accelerometer was placed in the chest cavity of the dummy. The extra accelerometer for the pelvis and spine were mounted internally to the dummy given extra space and mounting points of sensors as seen in Fig. 7.8. Extra accelerometers mounted to the leg were mounted externally with an extra wearable mount made to be flush with the surface of the primary sensor mount location illustrated in Fig. 7.9

7.3.2 Application of Dynamic Measurement Fusion

Complexity of the motion is increased to validate the usage of dynamic measurement fusion to measure motions as complex as car crashes. Compared to the experimentation with the two degree of freedom system and the measurement of the three dimensional arm motion, measurement of the links of a dummy in a simulated crash test increases the degrees of freedom of the system. Compared to the degrees of freedom used in the arm test, the degrees of freedom increases from five to twelve. The joints modeled are that of the neck, pelvis to the spine, the hip, the knee, and the ankle. The joint matrices used to model the constraints of each joint are defined as discussed in Section 7.1.

As magnetometers that work at the desired sampling rate were unavailable during the time of this testing, psuedo-magnetometer data using orientation of links measured with the OptiTrack system were used for orientation correction of the links.

Positions of Joints and Sensors

Dynamic measurement fusion uses an EKF framework to estimate the angular rotations and rates of links in a system, predicting their motions using kinematic motion models, and correcting estimated states with measurements from sensors. In order

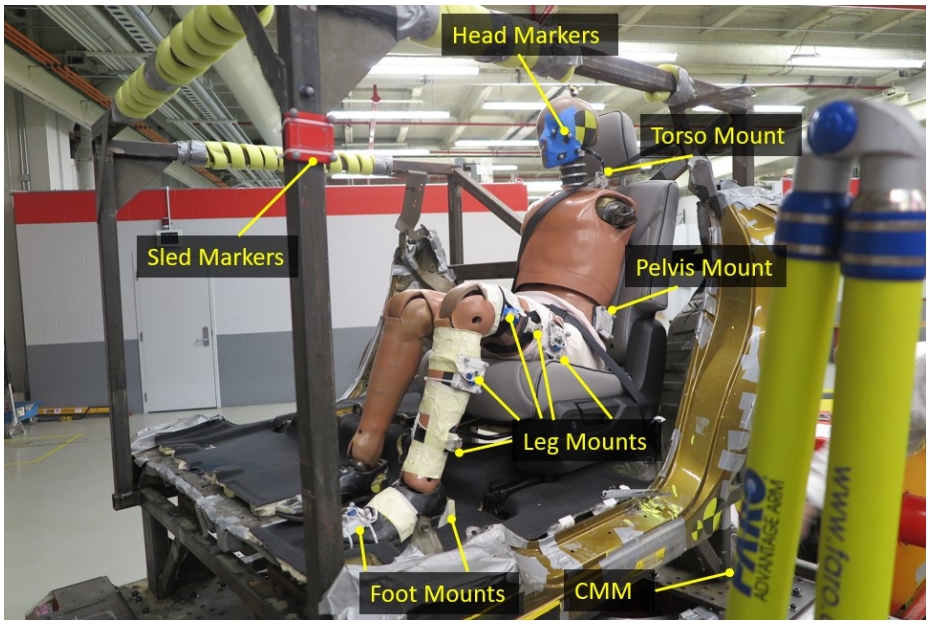

Figure 7.11: The sled buck used for better observing the motion of the test dummy with visual systems during a crash test.

to use dynamic measurement fusion to measure the motion of the dummy within the test buck, the transformations between the joints and the positions of sensors must be measured in order to properly produce a motion model of the dummy and its links. After outfitting the test dummy with all of the sensors to be used for motion measurement, as well as OptiTrack markers installed for ground truth measurement, the positions of the joints and markers, as well as the sensors' positions and orientations with respect to all joints, were measured using a high precision coordinate measurement machine (CMM), as seen in Fig. 7.11.

Figure 7.12 shows the sensor positions and local frames along with the positioning of joints of the dummy used for the crash tests. With this information, the transformation of measured links with consideration of motion constraints of joints and their positions can be used to estimate the rotations of each link with respect to one selected, better-observed link that can be tracked with a global frame ground truth. This is because while Dynamic Measurement Fusion is great for determining the ori-

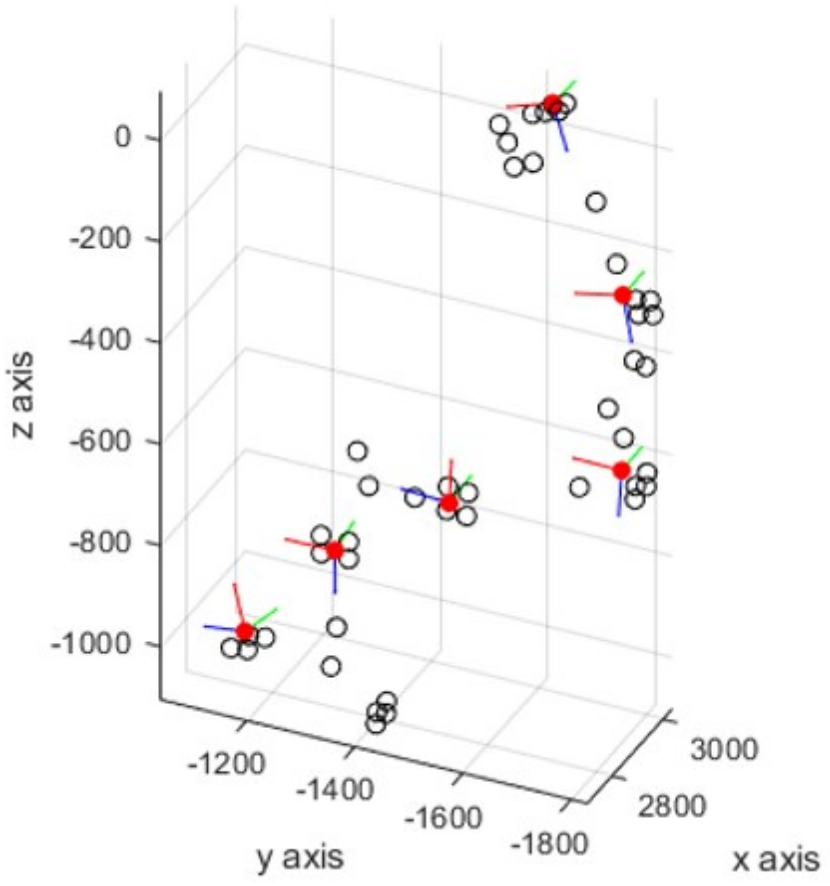

Figure 7.12: The sled buck used for better observing the motion of the test dummy with visual systems during a crash test.

entation change of links of a system with respect to themselves with correction only from magnetic north, it cannot track for transformation in the global frame nearly as well. The combination of externally mounted IMUs and one highly observable link used for visual motion tracking to better account for the motion of the dummy in the global or vehicle frame is aimed to prove a powerful tool for motion tracking in crash testing scenarios.

7.4 Experimental Validation

7.4.1 Tracking Arm with Coupled Magnetometers in Nonuniform Magnetic Field

Objective and Experimental Configuration

To prove the scalability of coupled magnetometers for orientation correction in nonuniform magnetic fields, experimentation is designed to increase the complexity of motion of a two-link system. Tracking the motion of a human arm, two links are still tracked while increasing the complexity of the motion from two degrees of freedom to five degrees of freedom. This extends the motion of the links to three dimensions rather than remaining planar. To test the proposed sensor methodology, the paired magnetometers are used for real-time distortion compensation with measurement. While all conditions are within the ferrite structure of a building, proximity to ferrites to cause distortion to local magnetic fields compared to usage in an open environment are tested for as seen in Fig. 7.13. The environments are used to compare the error of estimations in different conditions.

Ground Truth Measurement and Desired Performance

As discussed in Chapter 1, the OptiTrack motion capture system has been able to reduce error of a measured ball position to tenths of millimeters. For this reason the system is used for ground truth measurement of the three dimensional motion used to validate the usage of dynamic measurement fusion and coupled magnetometers. The cameras track the optical markers mounted to sensor mounts, indicating which

(a) OptiTrack motion capture results

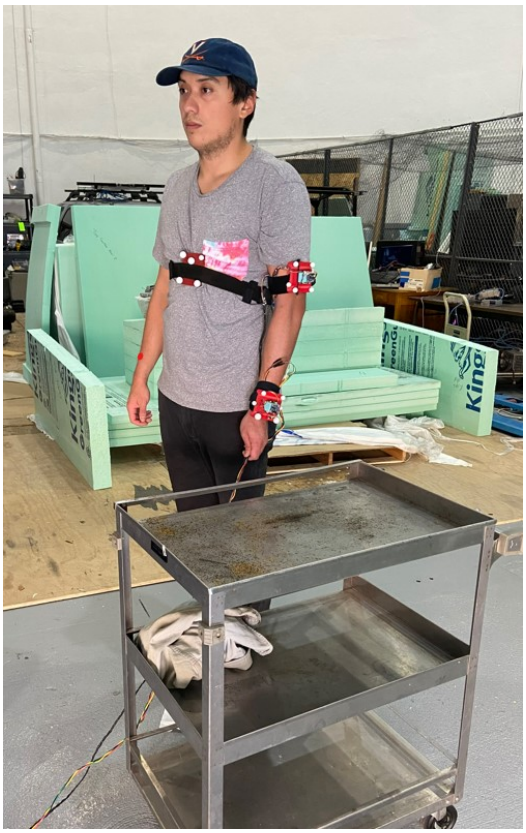

(b) Trajectory with interpolated points

Figure 7.13: OptiTrack motion capture with positions and local orientations, and interpolated points to fill in missed time steps for ground truth comparison.

sensor mounts are which. Using the OptiTrack Motion Capture system, groupings of markers can be confused between each other if the placement of markers on different links are similar. For this reason, there are two targeted goals in the placement of markers to each mount:

- Making differentiation of sensor mounts simple with unique configurations of markers per mount, and
- Using asymmetrical shapes with markers so that orientation is not confused during measurement.

The next consideration for usage with visual motion tracking is the usage of cameras.

The factors can be split between decisions for the amounts of cameras used and placements of cameras to best observe the motion. With more cameras, observation of the motion can be easier, however can be quite costly with the quality of devices required for good results. Cameras were placed surrounding the motion as seen in Fig. 7.14.

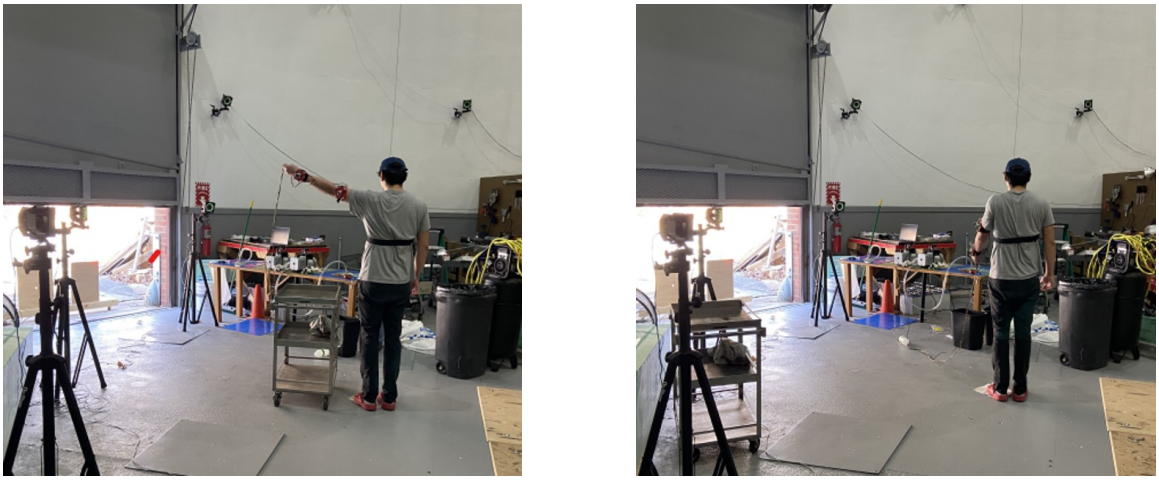

(a) OptiTrack motion capture results (b) Trajectory with interpolated points

Figure 7.14: OptiTrack motion capture with positions and local orientations, and interpolated points to fill in missed time steps for ground truth comparison.

Analysis of Results

With increasing the complexity of the motion from two dimensional to three dimensional motion, the ground truth measurement is collected with an upgrade to the monocular camera with image processing, the OptiTrack Motion Capture system. The visual motion capture system is used to measure the rotation of the parts of a human arm with respect to the chest. The chest motion is reduced as much as possible, trying to create a stable reference point for the measured links of the arm. Figure 7.15 shows the rotation of arm movement with respect to the global frame recorded with the OptiTrack system. Black lines are shown as the arm links at certain points during the motion.

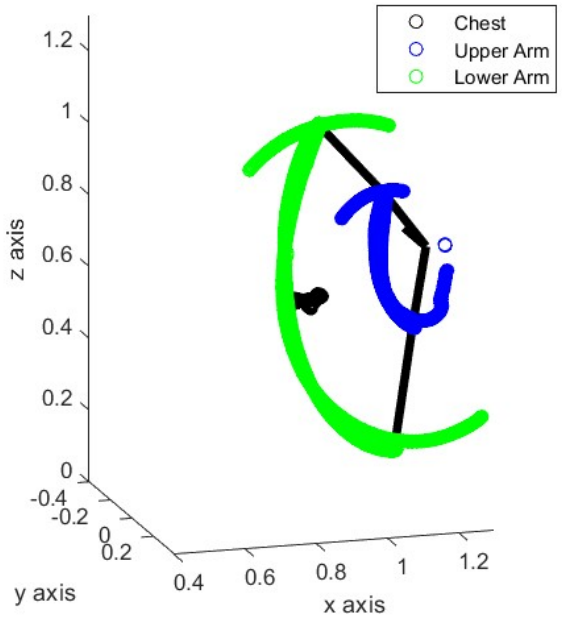

Figure 7.15: The path of the lower and upper arm throughout the duration of the motion, as seen with the OptiTrack motion capture system.

The estimated motions are animated as the plot seen in the left in Fig. 7.16, where the red lines are representative of the arm links as illustrated. The coordinate frame with the blue arrow pointed upward is representative of the global frame at the origin, while the frame with the arrow pointed downward is the local SAE coordinate frame

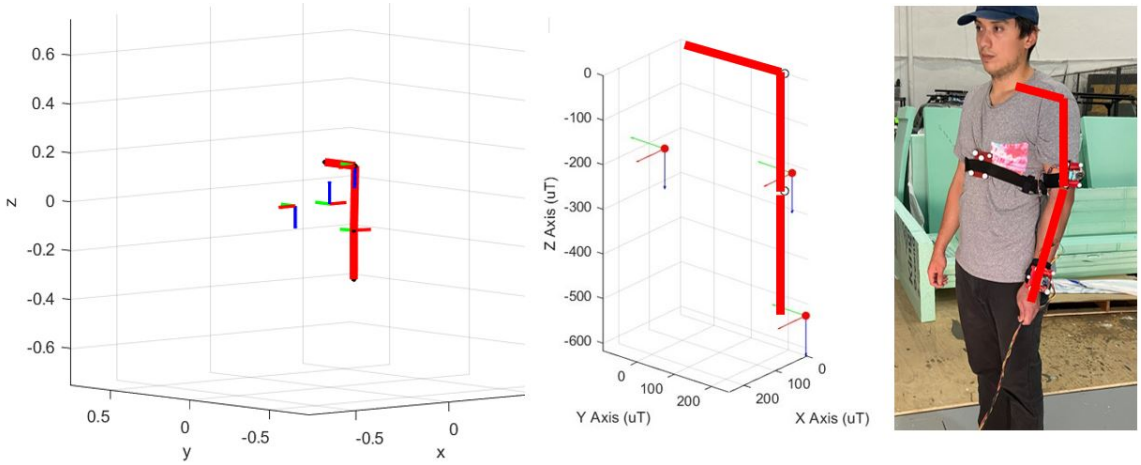

Figure 7.16: The sled buck used for better observing the motion of the test dummy with visual systems during a crash test.

for the chest markers. The red lines are used to visualize the motion of the arm links through space as drawn on the picture. A line is drawn from the shoulder joint to the center of the chest, indicating the static position of the chest

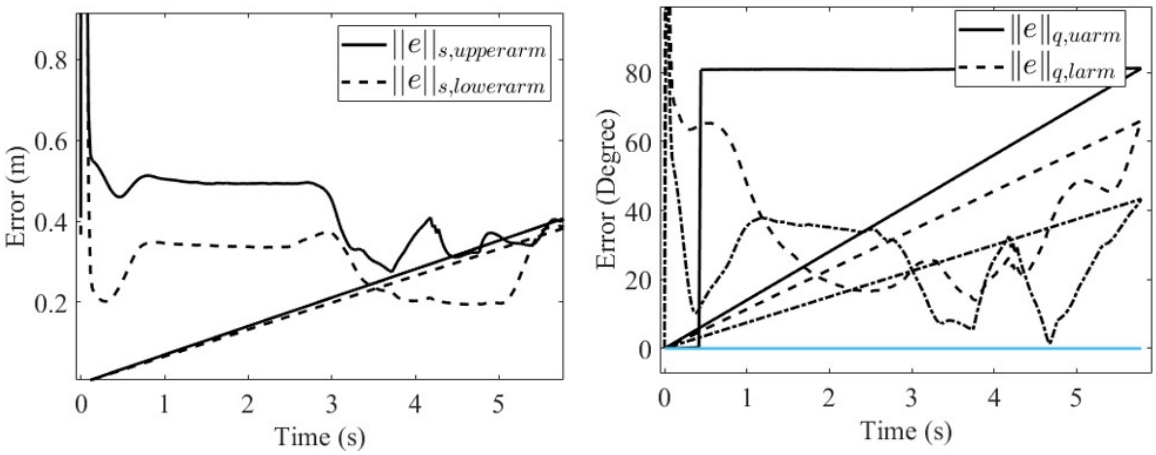

(a) Position error of the estimation of the arm movement.

(b) Orientation error of the estimated swinging.

Figure 7.17: Plots of the positional and orientation error between the estimated motion and the ground truth measurement throughout the duration of the arm swinging motion

As seen in Fig. 7.17, the estimation was not as accurate as when applied to a less complex, 2DOF motion. Using Bayesian estimation, the estimation also takes time to converge to the true poses, as indicated by peaks in error at the moment the motion begins.

Looking at the IMU signals recorded through the duration of the motion, the acceleration experienced by each link does not exceed 13 $\frac{m}{s^2}$, indicating that the system isn't reaching highly dynamic motion. For this reason, the gravity vector is more apparent in accelerometer signals than acceleration due to the motion. Rather than relying on dynamic measurement fusion for the estimation, a hybrid between dynamic measurement fusion for highly dynamic instances and zero-velocity inclination correction may best serve tracking slower humanoid motions.

7.4.2 Motion Tracking of Dummy on Sled Buck

Objective and Experimental Configuration

Figure 7.18: The sled buck used for better observing the motion of the test dummy with visual systems during a crash test.

The goal application of dynamic measurement fusion is to measure and estimate the rotation of links of a multi-link system. Part of the motivation for the development of methods to handle highly dynamic systems, and the required testing of a complexity-reduced system, is to prove the efficacy of the proposed methods for crash-testing applications. With a proof of concept completed for the implementation of dynamic measurement fusion on a two degree of freedom system that intensely swings, the time came for the method to be applied in a simulated crash test, prior to application in a real crash test.

The objective of this experimentation was to prove the efficacy of dynamic measurement fusion with externally mounted IMUs to track a motion with more complex-

ity than previously tested. Rather than using a complete vehicle frame that would obstruct the view of most parts of the dummy, a crash buck, as seen in Fig.7.18, was used. This vehicle frame was modified to keep rigidity but minimize the visual obstruction of motion inside the frame so that the motion of the dummy was still observable by visual tracking systems for ground truth measurement. To make the core of the test dummy more observable from cameras mounted statically outside of the test buck, the arms of the dummy were removed, only targeting measurement of the head, torso, pelvis, thigh, lower leg, and foot of the dummy. For this experimentation, only accelerometers and gyroscopes were used due to the unavailability of magnetometers that could perform at the desired sampling rates.

Ground Truth Measurement and Desired Performance

Using the described sled buck enables ground truth measurement of motions within a test buck to validate the proposed estimation method using the externally mounted IMUs. As discussed in chapter 1, the OptiTrack motion capture system has been able to reduce error of a measured ball position to tenths of millimeters. Positions of markers measured by the cameras compared to estimated marker locations using the proposed method make the error between the estimation and the measured ground truth. The range of positional error targeted was 10 to 15 centimeters to be considered reasonable.

Important for proper ground truth measurement is positioning cameras to minimize obstruction of the motion of interest. To ensure coverage of the motion, alternating cameras are pointed and placed to maximize coverage between the placement of the sled at the beginning of the motion, and at the end of the duration of interest along the path the sled is shot, simulating the crash motion. Optical markers are also placed on

the sled buck to use as a reference throughout the duration of the motion. With unique marker placements between sensor mounts, and asymmetry to prevent confusion of the orientation of the tracked links, ground truth measurement preparations is completed for the testing.

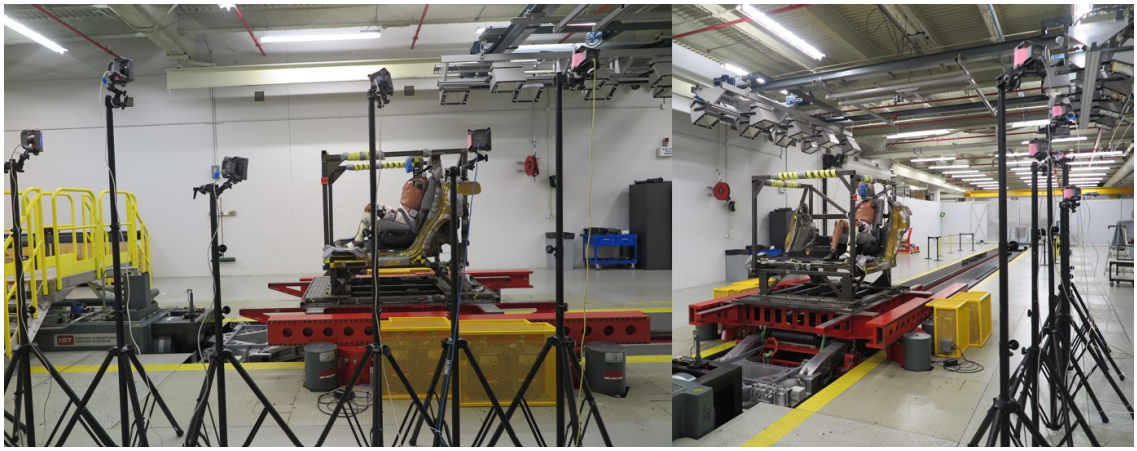

Figure 7.19: The sled buck used for better observing the motion of the test dummy with visual systems during a crash test.

Analysis of Results

The conventional method for motion tracking in automotive applications is the TEMA Advanced Motion Tracking system mentioned in Section 6.1 used to track quadrant targets placed on dummies. The result is the motion projected to 2D, reducing the 3D motion to a planar profile as seen in Fig. 7.20. Reference positions on linkages and extra bodies of interest are tracked with a high speed camera. Referenced bodies can be used estimate motion with respect to the sled buck accelerated during the simulated crash. TEMA is useful for measuring the path of travel of links within the buck. What is not produced with TEMA is a complete pose estimation for the duration of the experiment.

A complete pose estimation is produced with externally mounted IMUs including ori-

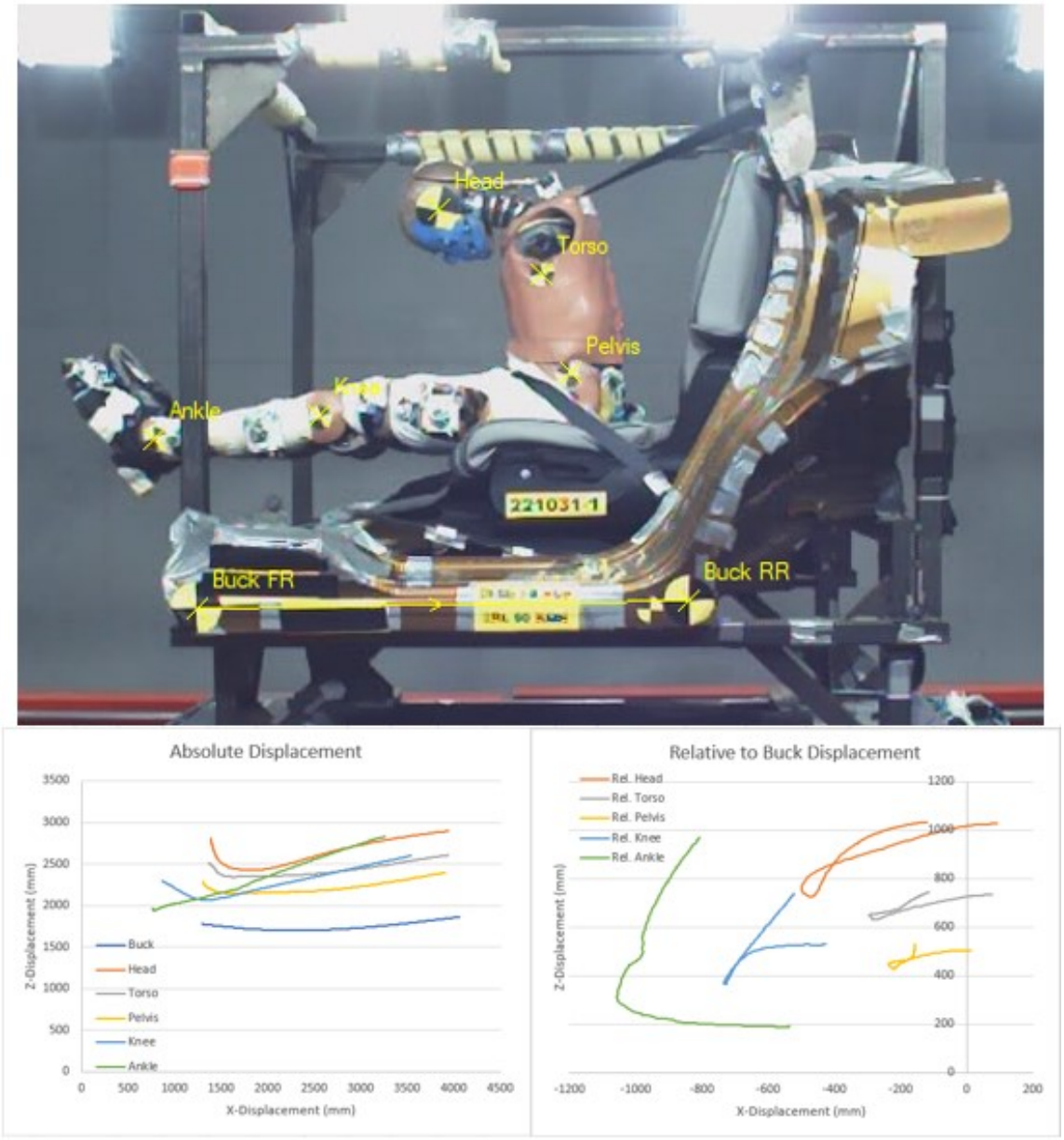

Figure 7.20: Results of planar displacement using TEMA motion capture provided by Honda.

entation and position in the three degrees of freedom. As a ground truth measurement of the motion is taken for comparison of the estimation methods, ensuring the OptiTrack system has properly captured the motion is crucial. Due to visual obstruction at stages during the duration of the measurement, the OptiTrack system is unable to capture every instant. For minimal gaps left, pose of the object at those instants

is interpolated. The difference between the motion data with missing measurement and interpolated measurements can be seen in Fig. 7.21, where gaps are connected in the interpolated data.

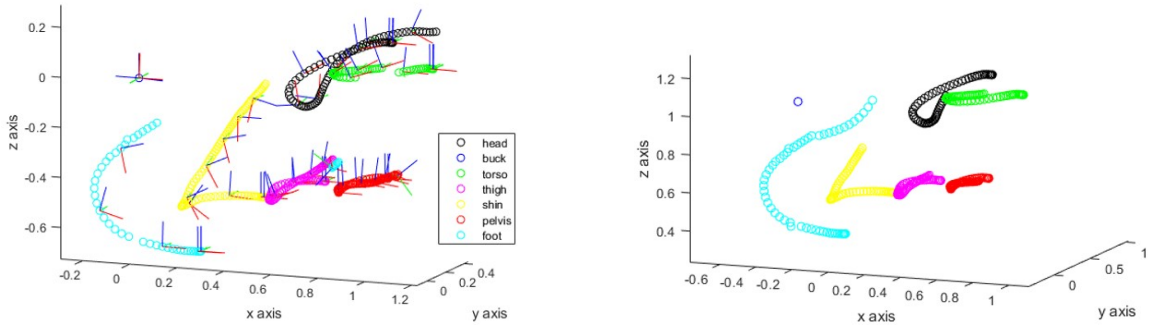

(a) OptiTrack motion capture results (b) Trajectory with interpolated points

Figure 7.21: OptiTrack motion capture with positions and local orientations, and interpolated points to fill in missed time steps for ground truth comparison.

The estimated motion appears visibly similar to the motion captured with the high speed motion camera, and the animation produced from the OptiTrack data. The estimation results seen in Fig. 7.22 are produced with respect to the head motion captured by the OptiTrack Motion Capture system. Although the motion is visually comparable to that of the videos and animations recorded of the motion, the estimation did not meet targeted performance for one of the links. Positional error in three degrees of freedom did not exceed 25 cm as seen in Fig. 7.23; however, this is past the range of the targeted error. Future work must be done to better estimate complex motions with dynamic IMU measurement fusion.

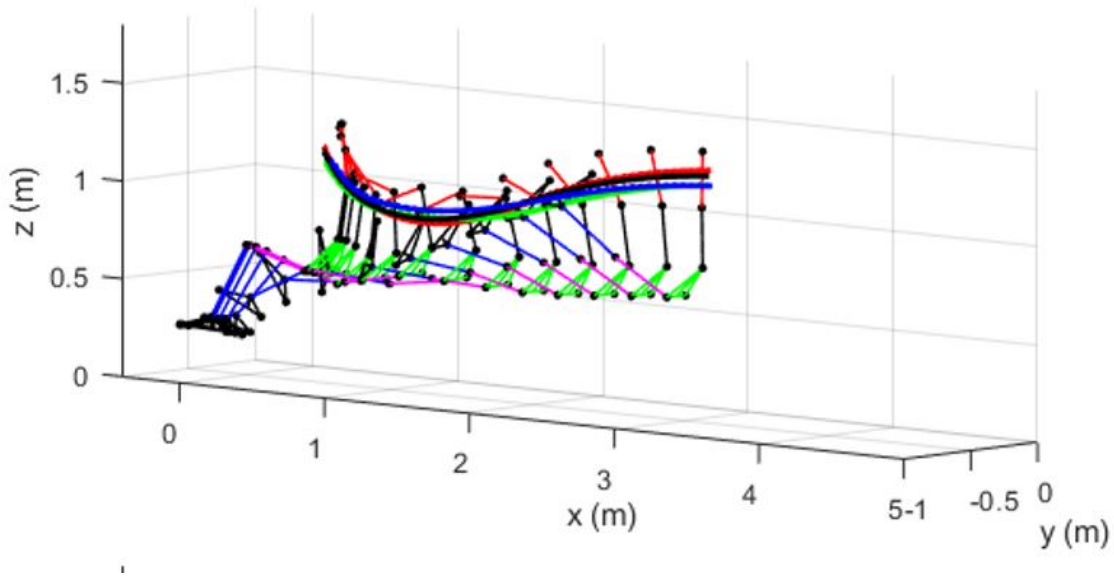

Figure 7.22: The estimated motion of the links of the system after the sled motion begins.

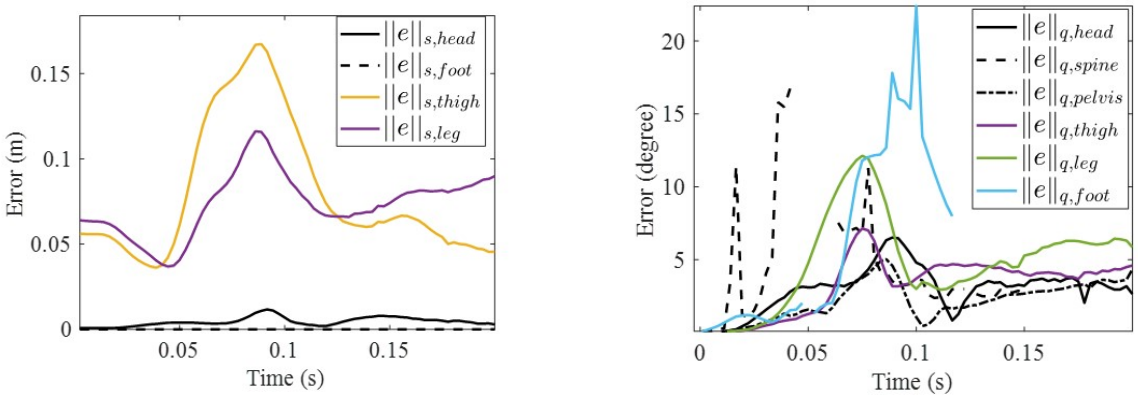

(a) Position error of the estimation. (b) Orientation error of the estimation.

Figure 7.23: Plots of the positional and orientation error between the estimated motion and the ground truth measurement throughout the duration of the motion

7.5 Summary

After the proof of concept experimentation conducted with the two-link system was used to validate the use of dynamic measurement fusion, the next goal was to prove

the efficacy of the method as the complexity of motion increased. Using visual motion capture and a sled buck modified to increase the visibility of the dummy for ground truth measurement, the dummy was prepared for analysis of performance. With a lack of magnetometers that could perform at the required sampling rates for the simulated crash tests, only accelerometers and gyroscopes, along with additional single-axis accelerometers configured to measure centrifugal forces, were used in a simulated crash. The application of dynamic measurement fusion for the intended use on test dummies required the development of mounts to externally place sensors on links of the dummy, measurements of the transformations between sensor and joint locations, and specifications to the degrees of freedom of joints on the dummy. With this preparation, the estimation results produced with dynamic measurement fusion were evaluated for accuracy below 17 cm prior to usage in a real crash test.

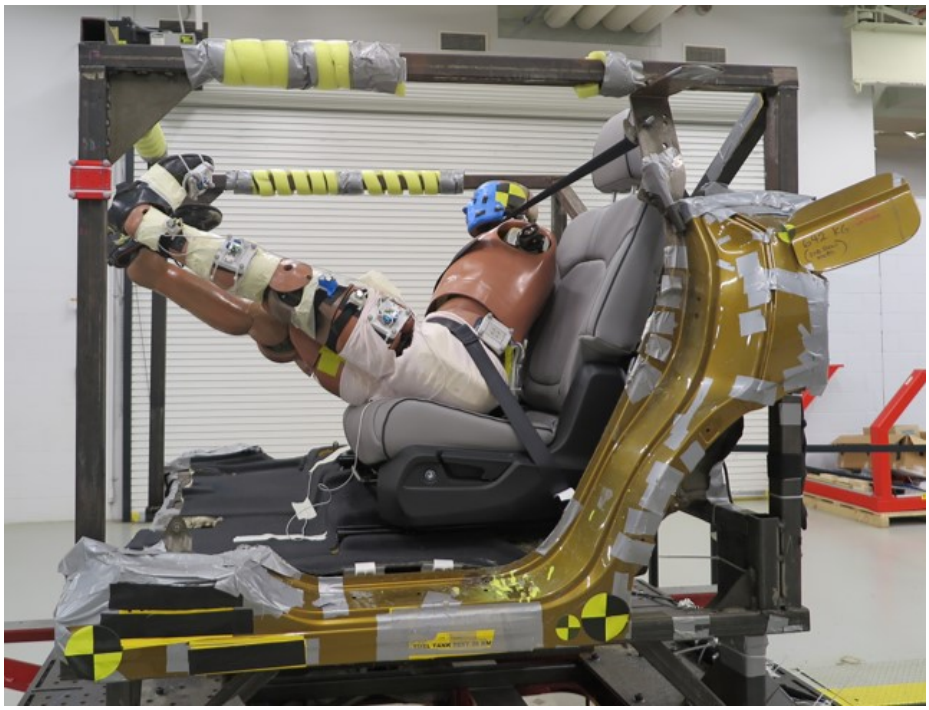

Figure 7.24: The sled buck used for better observing the motion of the test dummy with visual systems during a crash test.

Chapter 8

Conclusions

8.1 Summary

This thesis has first presented a motion tracker with dynamic IMU measurement fusion for highly dynamic multi-link systems in uniform magnetic fields. The hardware unit of the proposed tracker with an accelerometer, a gyroscope, and a magnetometer is attached to the end of each link, instead of its center. The proposed tracking method enables the measurement of both linear acceleration and angular rate without global correction relying on remaining in quasi-static motion. The role of the accelerometer is altered to provide correction for angular velocity given the relationship between rotational rate and centrifugal acceleration. The probabilistic extension of the sensor and motion models allows enhanced motion tracking by the EKF.

The time-varying performance of a two-link system first shows that the proposed motion tracker measures a dynamic motion significantly more accurately than the conventional technique reliant on gyroscope measurements for angular velocity correction. As the intensity of the highly dynamic motion increased, the performance of the proposed method increased, unlike the conventional method. The proposed method performed almost a whole order of magnitude better than the conventional method.

The satisfactory performance of dynamic measurement fusion for tracking a motion less complex than a test dummy led to it being used for the original end goal use, tracking a dummy's highly dynamic motion. With a modified sled buck for easier visual observability of the dummy from the outside for ground truth measurement with visual motion tracking, the performance of dynamic measurement fusion was analyzed. Due to the lack of magnetometers during testing, only the performance analysis of dynamic measurement fusion with gyroscopes and accelerometers was considered. The estimation of the motion of links of interest was compared to that of the ground truth measurement, leaving a maximum positional error of 16.5 cm.

This work has also introduced a real-time magnetometer calibration method and sensor model for motion tracking of a multi-link system within a nonuniform magnetic field. To compensate for dead-reckoning drift, magnetometers are used for orientation estimation correction using reference magnetic north. The conventional use of magnetometers involves compensation for local distortion with calibration prior to the measurement of a motion. In spaces of nonuniform magnetic field, conventional calibration only compensates for distortion in one position. To alleviate the computation required for the estimation of calibration parameters from position to position, two oppositely-faced sensors are used for real-time calibration.

While the coupled magnetometer method accounts for local hard iron distortion, the array fails to correct orientation where the magnetic field direction in a space is inconsistent. To account for the inconsistent direction of magnetic north throughout the space, rather than using the initial orientation of the tracker as reference, the latest orientation measured prior to the current time step is used as reference. Using this change to the magnetometer sensor model allows for more adaptive orientation correction.

The time-varying performance of a two-link system first shows that the proposed technique converges closer to the true states than the conventional magnetometer usage. The estimations produced results comparable to noticeable events in images of the motion. The proposed method performed half of an order of magnitude better than the conventional method.

To further validate usage of the developed methodology to track motion while compensating for magnetic field distortion, testing with increased motion complexity is targeted. Increasing complexity of the motion can be achieved by using more degrees of freedom, adding more links to the system, or intensifying the motion measured. With increasingly complex motions, the margins of error grow. As the number of links away from the parent link increases, the margin of error of measuring that motion with respect to the parent link grows.

8.2 Future Work

Currently, the usage of coupled magnetometers in the targeted scenario of a crash test is postponed until the production of the required sensors. While work has been done to validate the use of coupled magnetometers to track highly dynamic motion, the magnetometers' use peaked at a sampling frequency rate of 300 Hz. In order to measure a motion as intense as a crash test, magnetometers that work at the frequency range of 5,000-20,000 Hz, matching the performance of the accelerometers and gyroscopes, are required. Instrumentation of desired specifications is currently difficult to acquire since there are only a few manufacturers with limited materials. While already purchased, construction and repair of the sensors have been quoted with an extensive lead time. Work to validate the proposed sensor usage of coupled

magnetometers in a motion as complex as the targeted end goal of inside a vehicle will require repeating the previous experimentation with the magnetometers as soon as acquired.

Future work to improve and better understand the limitations of dynamic measurement fusion includes the comparison of results produced with different sensor suites of different noise levels and frequencies, higher intensity motions, and the extension of a higher-DOF system. We aim to determine the motion intensity at which the performance of the proposed estimation method begins to significantly drop.

Future work to better correct estimations in nonuniform magnetic fields includes estimation of the referenced magnetic north with respect to the global frame, experimentation with different levels of distortion, studies to identify key usages of shielding to prevent nonuniformity of magnetic field in spaces, and the production of methods to create an artificial homogeneous magnetic field within the space.

Bibliography

[1] A. Klimchik and A. Pashkevich. "Robotic manipulators with double encoders: accuracy improvement based on advanced stiffness modeling and intelligent control". In: *IFAC-PapersOnLine* 51.11 (2018). 16th IFAC Symposium on Information Control Problems in Manufacturing INCOM 2018, pp. 740–745. ISSN: 2405-8963. DOI: https://doi.org/10.1016/j.ifacol.2018.08.407. URL: https://www.sciencedirect.com/science/article/pii/S2405896318315337.

[2] London Rhodes. *What is the most common cause of encoder failure?* Mar. 2021. URL: https://www.dynapar.com/faq/what-is-the-most-common-cause-of-encoder-failure.

[3] Tomonari Furukawa, J. Josiah Steckenrider, and Gamini Dissanayake. "State Estimation of a Partially Observable Multi-Link System with No Joint Encoders Incorporating External Dead-Reckoning". In: *2021 IEEE/RSJ International Conference on Intelligent Robots and Systems (IROS)*. 2021, pp. 7342–7348.

[4] Robert Pfaff, Joseph Borovsky, and D. Young. "Measurement Techniques in Space Plasmas – Fields". In: *Washington DC American Geophysical Union Geophysical Monograph Series* (Jan. 1998).

[5] H. Choset et al. *Principles of Robot Motion: Theory, Algorithms, and Implementation*. Intelligent robots and autonomous agents. MIT Press, 2005. ISBN: 9786612096204. URL: https://books.google.com/books?id=e-oqvQEACAAJ.

[6] Wei Liu et al. "Comparative Analysis between Error-State and Full-State Error Estimation for KF-Based IMU/GNSS Integration against IMU Faults".

en. In: *Sensors* 19.22 (Nov. 2019), p. 4912. ISSN: 1424-8220. DOI: 10.3390/s19224912. URL: https://www.mdpi.com/1424-8220/19/22/4912 (visited on 03/06/2023).

[7] Ha-Hyoung Jung, Min-Kyoung Kim, and Joon Lyou. "Realization of a hybrid human motion capture system". en. In: *2017 17th International Conference on Control, Automation and Systems (ICCAS)*. Jeju: IEEE, Oct. 2017, pp. 1581–1585. ISBN: 978-89-93215-14-4. DOI: 10.23919/ICCAS.2017.8204238. URL: http://ieeexplore.ieee.org/document/8204238/ (visited on 01/18/2023).

[8] Malcolm David Shuster and S D_ Oh. "Three-axis attitude determination from vector observations". In: *Journal of Guidance and Control* 4.1 (1981), pp. 70–77.

[9] National Geomagnetism Program. *Geomagnetism, [Online]*. URL: https://usgs.gov/programs/geomagnetism.

[10] Bertram Taetz, Gabriele Bleser, and Markus Miezal. "Towards Self-Calibrating Inertial Body Motion Capture". In: *CoRR* abs/1606.03754 (2016). arXiv: 1606.03754.

[11] Manon Kok, Jeroen D. Hol, and Thomas B. Schön. "An optimization-based approach to human body motion capture using inertial sensors". In: *IFAC Proceedings Volumes* 47.3 (2014), pp. 79–85. ISSN: 1474-6670.

[12] Amin Ahmadi et al. "3D Human Gait Reconstruction and Monitoring Using Body-Worn Inertial Sensors and Kinematic Modeling". In: *IEEE Sensors Journal* 16 (2016), pp. 8823–8831.

[13] Stefan Lambrecht et al. "Inertial Sensor Error Reduction through Calibration and Sensor Fusion". en. In: *Sensors* 16.2 (Feb. 2016), p. 235. ISSN: 1424-8220.

DOI: 10.3390/s16020235. URL: http://www.mdpi.com/1424-8220/16/2/235 (visited on 03/06/2023).

[14] Luciano Cantelli et al. "A Joint-Angle Estimation Method for Industrial Manipulators Using Inertial Sensors". In: *IEEE/ASME Transactions on Mechatronics* 20.5 (2015), pp. 2486–2495.

[15] M. Euston et al. "A complementary filter for attitude estimation of a fixed-wing UAV". en. In: *2008 IEEE/RSJ International Conference on Intelligent Robots and Systems*. Nice: IEEE, Sept. 2008, pp. 340–345. ISBN: 978-1-4244-2057-5 978-1-4244-2058-2. DOI: 10.1109/IROS.2008.4650766. URL: http://ieeexplore.ieee.org/document/4650766/ (visited on 01/21/2023).

[16] Zhelong Wang et al. "Stance-Phase Detection for ZUPT-Aided Foot-Mounted Pedestrian Navigation System". In: *IEEE/ASME Transactions on Mechatronics* 20.6 (2015), pp. 3170–3181.

[17] M. Angermann and P. Robertson. "FootSLAM: Pedestrian Simultaneous Localization and Mapping Without Exteroceptive Sensors—Hitchhiking on Human Perception and Cognition". en. In: *Proceedings of the IEEE* 100.Special Centennial Issue (May 2012), pp. 1840–1848. ISSN: 0018-9219, 1558-2256. DOI: 10.1109/JPROC.2012.2189785. URL: http://ieeexplore.ieee.org/document/6178000/ (visited on 12/20/2022).

[18] Maria Garcia Puyol, Patrick Robertson, and Oliver Heirich. "Complexity-reduced FootSLAM for indoor pedestrian navigation". en. In: *2012 International Conference on Indoor Positioning and Indoor Navigation (IPIN)*. Sydney, Australia: IEEE, Nov. 2012, pp. 1–10. ISBN: 978-1-4673-1954-6 978-1-4673-1955-3. DOI: 10.1109/IPIN.2012.6418898. URL: http://ieeexplore.ieee.org/document/6418898/ (visited on 12/20/2022).

[19] Nagesh Yadav and Chris Bleakley. "Accurate Orientation Estimation Using AHRS under Conditions of Magnetic Distortion". In: *Sensors (Basel, Switzerland)* 14 (Nov. 2014), pp. 20008–24.

[20] Xiaoping Yun and Eric R. Bachmann. "Design, Implementation, and Experimental Results of a Quaternion-Based Kalman Filter for Human Body Motion Tracking". en. In: *IEEE Transactions on Robotics* 22.6 (Dec. 2006), pp. 1216–1227. ISSN: 1552-3098. DOI: 10.1109/TRO.2006.886270. URL: http://ieeexplore.ieee.org/document/4020379/ (visited on 03/07/2023).

[21] Robert Mahony, Tarek Hamel, and Jean-Michel Pflimlin. "Nonlinear Complementary Filters on the Special Orthogonal Group". In: *IEEE Transactions on Automatic Control* 53.5 (2008), pp. 1203–1218.

[22] Roberto G. Valenti, Ivan Dryanovski, and Jizhong Xiao. "Keeping a Good Attitude: A Quaternion-Based Orientation Filter for IMUs and MARGs". In: *Sensors* 15.8 (2015), pp. 19302–19330. ISSN: 1424-8220.

[23] Daniel Laidig et al. "VQF: A Milestone in Accuracy and Versatility of 6D and 9D Inertial Orientation Estimation". In: *2022 25th International Conference on Information Fusion (FUSION)*. 2022, pp. 1–6.

[24] Sebastian O. H. Madgwick, Andrew J. L. Harrison, and Ravi Vaidyanathan. "Estimation of IMU and MARG orientation using a gradient descent algorithm". In: *IEEE International Conference on Rehabilitation Robotics*. 2011, pp. 1–7.

[25] Jie Li et al. "Real-Time Human Motion Capture Based on Wearable Inertial Sensor Networks". In: *IEEE Internet of Things Journal* 9.11 (2022), pp. 8953–8966.

[26] D. Roetenberg et al. “Compensation of magnetic disturbances improves inertial and magnetic sensing of human body segment orientation”. In: *IEEE Transactions on Neural Systems and Rehabilitation Engineering* 13.3 (2005), pp. 395–405.

[27] W.E. Tolles and J.D. Lawson. “Magnetic compensation of MAD equipped aircraft”. In: Mineola, N.Y.: Airborne Instruments Lab. Inc., June 1950.

[28] S.H. Bickel. “Small Signal Compensation of Magnetic Fields Resulting from Aircraft Maneuvers”. en. In: *IEEE Transactions on Aerospace and Electronic Systems* AES-15.4 (July 1979), pp. 518–525. ISSN: 0018-9251. (Visited on 01/25/2023).

[29] Demoz Gebre-Egziabher et al. “Calibration of Strapdown Magnetometers in Magnetic Field Domain”. en. In: *Journal of Aerospace Engineering* 19.2 (Apr. 2006), pp. 87–102. ISSN: 0893-1321, 1943-5525. (Visited on 01/16/2023).

[30] Michael Caruso. “Applications of Magnetoresistive Sensors in Navigation Systems”. In: *PROGRESS in TECHNOLOGY* 72 (Feb. 1997).

[31] M.J. Caruso. “Applications of magnetic sensors for low cost compass systems”. In: *IEEE 2000. Position Location and Navigation Symposium (Cat. No.00CH37062).* 2000, pp. 177–184.

[32] Manon Kok et al. “Calibration of a magnetometer in combination with inertial sensors”. en. In: ().

[33] Bagus Adiwiluhung Riwanto et al. “Particle Swarm Optimization With Rotation Axis Fitting for Magnetometer Calibration”. en. In: *IEEE Transactions on Aerospace and Electronic Systems* 53.2 (Apr. 2017), pp. 1009–1022. ISSN: 0018-9251, 1557-9603, 2371-9877. DOI: 10.1109/TAES.2017.2667458. URL: https://ieeexplore.ieee.org/document/7849225/ (visited on 01/12/2023).

[34] Muhammad Tahir, Abdullah Moazzam, and Khurram Ali. "A Stochastic Optimization Approach to Magnetometer Calibration With Gradient Estimates Using Simultaneous Perturbations". In: *IEEE Transactions on Instrumentation and Measurement* 68.10 (2019), pp. 4152–4161. DOI: 10.1109/TIM.2018.2885624.

[35] Roberto Alonso and Malcolm D. Shuster. "TWOSTEP: A fast robust algorithm for attitude-independent magnetometer-bias determination". In: *The Journal of the Astronautical Sciences* 50.4 (2002), pp. 433–451.

[36] John L. Crassidis, Kok-Lam Lai, and Richard R. Harman. "Real-Time Attitude-Independent Three-Axis Magnetometer Calibration". en. In: *Journal of Guidance, Control, and Dynamics* 28.1 (Jan. 2005), pp. 115–120. ISSN: 0731-5090, 1533-3884. (Visited on 12/26/2022).

[37] S. Suksakulchai et al. "Mobile robot localization using an electronic compass for corridor environment". en. In: *SMC 2000 Conference Proceedings. 2000 IEEE International Conference on Systems, Man and Cybernetics. 'Cybernetics Evolving to Systems, Humans, Organizations, and their Complex Interactions' (Cat. No.00CH37166)*. Vol. 5. Nashville, TN, USA: IEEE, 2000, pp. 3354–3359. ISBN: 978-0-7803-6583-4. DOI: 10.1109/ICSMC.2000.886523. URL: http://ieeexplore.ieee.org/document/886523/ (visited on 12/20/2022).

[38] Brandon Gozick et al. "Magnetic Maps for Indoor Navigation". en. In: *IEEE Transactions on Instrumentation and Measurement* 60.12 (Dec. 2011), pp. 3883–3891. ISSN: 0018-9456, 1557-9662. DOI: 10.1109/TIM.2011.2147690. URL: http://ieeexplore.ieee.org/document/5773083/ (visited on 12/20/2022).

[39] Danilo Navarro and Gines Benet. "Magnetic map building for mobile robot localization purpose". en. In: *2009 IEEE Conference on Emerging Technologies*

& Factory Automation. Palma de Mallorca, Spain: IEEE, Sept. 2009, pp. 1–4. ISBN: 978-1-4244-2727-7. DOI: 10.1109/ETFA.2009.5347181. URL: http://ieeexplore.ieee.org/document/5347181/ (visited on 12/22/2022).

[40] Etienne Le Grand and Sebastian Thrun. "3-Axis magnetic field mapping and fusion for indoor localization". en. In: *2012 IEEE International Conference on Multisensor Fusion and Integration for Intelligent Systems (MFI)*. Hamburg, Germany: IEEE, Sept. 2012, pp. 358–364. ISBN: 978-1-4673-2512-7 978-1-4673-2510-3 978-1-4673-2511-0. DOI: 10.1109/MFI.2012.6343024. URL: http://ieeexplore.ieee.org/document/6343024/ (visited on 12/20/2022).

[41] Naoki Akai and Koichi Ozaki. "3D magnetic field mapping in large-scale indoor environment using measurement robot and Gaussian processes". en. In: *2017 International Conference on Indoor Positioning and Indoor Navigation (IPIN)*. Sapporo: IEEE, Sept. 2017, pp. 1–7. ISBN: 978-1-5090-6299-7. DOI: 10.1109/IPIN.2017.8115960. (Visited on 12/20/2022).

[42] Arno Solin et al. *Modeling and interpolation of the ambient magnetic field by Gaussian processes*. en. arXiv:1509.04634 [cs, stat]. Mar. 2018. URL: http://arxiv.org/abs/1509.04634 (visited on 12/20/2022).

[43] Prince E. Kuevor, James W. Cutler, and Ella M. Atkins. "Improving Attitude Estimation Using Gaussian-Process-Regression-Based Magnetic Field Maps". en. In: *Sensors* 21.19 (Sept. 2021), p. 6351. ISSN: 1424-8220. DOI: 10.3390/s21196351. URL: https://www.mdpi.com/1424-8220/21/19/6351 (visited on 12/20/2022).

[44] Naoki Akai et al. "Development of magnetic navigation method based on distributed control system using magnetic and geometric landmarks". en. In: *ROBOMECH Journal* 1.1 (Dec. 2014), p. 21. ISSN: 2197-4225. DOI: 10.1186/s40648-014-

0021-8. URL: https://robomechjournal.springeropen.com/articles/10.1186/s40648-014-0021-8 (visited on 12/22/2022).

[45] Patrick Robertson et al. "Simultaneous Localization and Mapping for pedestrians using distortions of the local magnetic field intensity in large indoor environments". en. In: *International Conference on Indoor Positioning and Indoor Navigation*. Montbeliard, France: IEEE, Oct. 2013, pp. 1–10. ISBN: 978-1-4799-4043-1. DOI: 10.1109/IPIN.2013.6817910. URL: http://ieeexplore.ieee.org/document/6817910/ (visited on 12/20/2022).

[46] Nabih M. Alem. "Simulation of head injury due to combined rotation and translation of the brain". In: *SAE Technical Paper Series* (1974). DOI: 10.4271/741192.

[47] A. J. Padgaonkar, K. W. Krieger, and A. I. King. "Measurement of Angular Acceleration of a Rigid Body Using Linear Accelerometers". en. In: *Journal of Applied Mechanics* 42.3 (Sept. 1975), pp. 552–556. ISSN: 0021-8936, 1528-9036. DOI: 10.1115/1.3423640. URL: https://asmedigitalcollection.asme.org/appliedmechanics/article/42/3/552/388209/Measurement-of-Angular-Acceleration-of-a-Rigid (visited on 03/16/2023).

[48] Frank P DiMasi et al. *Transformation of nine-accelerometer-package (NAP) data for replicating headpart kinematics and dynamic loading*. Tech. rep. United States. National Highway Traffic Safety Administration, 1995.

[49] Erik G Takhounts, Vikas Hasija, and Rolf H Eppinger. "Analysis of 3D rigid body motion using the nine accelerometer array and the randomly distributed in-plane accelerometer systems". In: *Proceedings of International Technical Conference on the Enhanced Safety of Vehicle, Stuttgart, Germany*. 2009.

[50] Fredrik Br Gustafsson and Niklas T Wahlstroem. *Method and device for pose tracking using vector magnetometers*. Jan. 2015.

[51] Chen Wang et al. "A Fast Calibration Method for Magnetometer Array and the Application of Ferromagnetic Target Localization". en. In: *IEEE Transactions on Instrumentation and Measurement* 66.7 (July 2017), pp. 1743–1750. ISSN: 0018-9456, 1557-9662. (Visited on 12/20/2022).

[52] Richard J. Kozick and Brian M. Sadler. "Algorithms for tracking with an array of magnetic sensors". en. In: *2008 5th IEEE Sensor Array and Multichannel Signal Processing Workshop*. Darmstadt, Germany: IEEE, July 2008, pp. 423–427. ISBN: 978-1-4244-2240-1. DOI: 10.1109/SAM.2008.4606904. URL: http://ieeexplore.ieee.org/document/4606904/ (visited on 01/25/2023).

[53] Hongfeng Pang et al. "Calibration of a fluxgate magnetometer array and its application in magnetic object localization". en. In: *Measurement Science and Technology* 24.7 (July 2013), p. 075102. ISSN: 0957-0233, 1361-6501. (Visited on 01/25/2023).

[54] Yaxin Mu et al. "A Novel Calibration Method for Magnetometer Array in Nonuniform Background Field". en. In: *IEEE Transactions on Instrumentation and Measurement* 68.10 (Oct. 2019), pp. 3677–3685. ISSN: 0018-9456, 1557-9662. DOI: 10.1109/TIM.2018.2880079. (Visited on 12/20/2022).

[55] Rong Zhu and Zhaoying Zhou. "A real-time articulated human motion tracking using tri-axis inertial/magnetic sensors package". en. In: *IEEE Transactions on Neural Systems and Rehabilitation Engineering* 12.2 (June 2004), pp. 295–302. ISSN: 1534-4320, 1558-0210. (Visited on 12/22/2022).

[56] Xianggang Zhang et al. "A Human Motion Capture System Based on MEMS Inertial Measurement". en. In: *2022 2nd International Conference on Intelligent*

Technology and Embedded Systems (ICITES). Chengdu, China: IEEE, Sept. 2022, pp. 148–154. ISBN: 978-1-66545-104-8. (Visited on 01/18/2023).

[57] Guanglie Ouyang and Karim Abed-Meraim. "A Survey of Magnetic-Field-Based Indoor Localization". en. In: *Electronics* 11.6 (Mar. 2022), p. 864. ISSN: 2079-9292. DOI: 10.3390/electronics11060864. URL: https://www.mdpi.com/2079-9292/11/6/864 (visited on 12/20/2022).

[58] D Willner, CB Chang, and KP Dunn. "Kalman filter configurations for multiple radar systems". In: *NASA STI/Recon Technical Report N* 77 (1976), p. 13312.

[59] D. Welsh et al. "Investigations of single-wire-pair to twisted-wire-pair crosstalk". In: *IEEE International Symposium on Electromagnetic Compatibility*. 1990, pp. 478–482. DOI: 10.1109/ISEMC.1990.252813.